

AFIT/GEO/ENP/95D-02

TWO-WAVELENGTH NEODYMIUM-BASED LASERS

THESIS

Scott Hugh McCracken
Captain, USAF

AFIT/GEO/ENP/95D-02

1996 0118 037

DTIC QUALITY INSPECTED 3

Approved for public release; distribution unlimited

The views expressed in this thesis are those of the author and do not reflect the official policy or position of the Department of Defense or the U. S. Government.

AFIT/GEO/ENP/95D-02

TWO-WAVELENGTH NEODYMIUM-BASED LASERS

THESIS

Presented to the Faculty of the School of Engineering
of the Air Force Institute of Technology

Air University

In Partial Fulfillment of the
Requirements for the Degree of
Master of Science in Electrical Engineering

Scott Hugh McCracken, B.S.

Captain, USAF


December, 1995

Approved for public release; distribution unlimited

TWO-WAVELENGTH NEODYMIUM-BASED LASERS

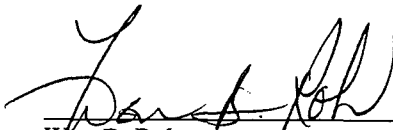
Scott H. McCracken, B.S.
Captain, USAF

Approved:




Jeffrey W. Grantham, Captain, USAF
Chairman, Advisory Committee

14 Nov 95



Won B. Roh
Member, Advisory Committee

14 Nov 95



Kenneth M. Dinndorf, Captain, USAF
Member, Advisory Committee

21 Nov 95

Acknowledgements

This work would not have been possible without the funding and support provided by the Laser Radar Research Branch of Wright Laboratory's Munitions Directorate, WL/MNGS. I would like to thank my advisor, Capt J. Grantham, for helping me overcome some of the fundamental roadblocks I encountered. I would also like to thank Capt K. Dinndorf from the Laser Radar Research Branch for sharing some of his expertise and insight into the physics of solid state laser materials. I am indebted to Capt E. Silbaugh and Capt S. Salbergh for helping to make the text of this document more readable and to Rick Patton for helping with the many details of constructing, assembling and modifying hardware. Finally, I wish to thank my wife Stacy for her help with this text and also for the support and understanding she has shown during all of those evenings, and weekends I was tied up with school work.

Scott Hugh McCracken

Table of Contents

	Page
Acknowledgements	ii
List of Figures	vi
List of Tables	viii
Abstract	x
 I. Introduction	 1-1
1.1 Background	1-1
1.1.1 Laser radar application	1-1
1.1.2 Review of laser cavity designs	1-3
1.2 Problem	1-5
1.3 Scope	1-6
1.4 Approach	1-7
 II. Laser Theory	 2-1
2.1 Population inversion and gain in neodymium (Nd) based crystals	 2-1
2.2 CW laser theory	2-5
2.3 Q-switched laser theory	2-8
2.4 General figure of merit for dual wavelength laser perfor- mance	 2-13
 III. Material Characterization	 3-1
3.1 Absorption measurements	3-5
3.2 Fluorescence measurements	3-7
3.3 Lifetime measurements	3-8

	Page
IV. Experimental results & analysis	4-1
4.1 Experimental setup	4-1
4.1.1 Nd:YAG setup	4-1
4.1.2 Nd:YLF setup	4-2
4.1.3 Nd:SVAP setup	4-3
4.2 Optical component characterization	4-3
4.2.1 High reflector	4-4
4.2.2 Laser Crystal	4-4
4.2.3 Dichroic beamsplitter	4-7
4.2.4 Q-switches	4-8
4.2.5 Output couplers	4-10
4.2.6 Diagnostic optics	4-10
4.3 CW laser Performance	4-11
4.4 Single wavelength Q-switched results	4-19
4.5 Analysis of 1.06 μ m Nd:YAG Q-switched results	4-26
4.6 Dual wavelength Q-switched results	4-36
4.6.1 Energy Crossover	4-40
4.6.2 Cavity length comparison	4-42
4.6.3 Material comparison	4-45
4.7 Error analysis	4-49
4.7.1 Uncertainty in the pump power absorbed in the laser crystal	4-49
4.7.2 Uncertainty calculation for the laser pulse energy	4-50
V. Conclusions & Recommendations	5-1
5.1 Conclusions	5-1
5.2 Recommendations	5-2

	Page
Appendix A. Laser system set up	A-1
A.1 Setup for the Ti:Sapphire Pump source	A-1
A.1.1 Ti:Sapphire laser	A-1
A.1.2 Laser crystal mount	A-3
A.2 Alignment of the dual wavelength laser cavity	A-3
Appendix B. Model	B-1
B.0.1 analyze.m	B-9
B.0.2 qspulse.m	B-13
B.0.3 runge.m	B-19
B.0.4 coup_dif.m	B-20
B.0.5 cr_spot.m	B-21
B.0.6 qsw_rise.m	B-23
B.0.7 threshld.m	B-26
Vita	VITA-1

List of Figures

Figure	Page
1.1. Tomaschke's laser cavity configuration for simultaneous wavelength output (pulsed).	1-6
2.1. Energy band diagram for neodymium in YAG.	2-2
2.2. Simple end-pumped cavity configuration.	2-5
2.3. Simple Q-switched cavity configuration.	2-8
2.4. Population inversion, threshold population level, and photon number as a function of time.	2-10
2.5. Extraction efficiency as a function of the inversion ratio $\frac{n_i}{n_{th}}$	2-12
3.1. Polarized absorption spectrum for Nd:YAG, Nd:YLF, and Nd:SVAP.	3-6
3.2. Fluorescence measurement setup.	3-7
3.3. Fluorescence spectra for Nd:YAG, Nd:YLF, and Nd:SVAP in the vicinity of $1.06\mu\text{m}$	3-9
3.4. Fluorescence spectra for Nd:YAG, Nd:YLF, and Nd:SVAP in the vicinity of $1.32\mu\text{m}$	3-10
3.5. Relative system response of the setup used to measure the fluorescence spectra from each laser crystal.	3-11
3.6. Experimental setup for lifetime measurements	3-12
3.7. Lifetime measurement of Nd:YAG	3-13
3.8. Lifetime measurement of Nd:YLF	3-14
3.9. Lifetime measurement of Nd:SVAP	3-15
4.1. Optical setup for the laser system.	4-2
4.2. Setup for the transmission measurements of the laser crystals.	4-5
4.3. Setup for the absorptance measurements of the laser crystals.	4-6
4.4. Transmission of the dichroic beamsplitter in the vicinity of $1.06\mu\text{m}$	4-8

Figure	Page
4.5. Reflectivity of the dichroic beamsplitter in the vicinity of $1.32\mu\text{m}$	4-9
4.6. Power conversion measurements for $1.06\mu\text{m}$	4-14
4.7. Power conversion measurements for $1.32\mu\text{m}$	4-15
4.8. Power conversion measurements for Nd:YAG at $1.06\mu\text{m}$	4-17
4.9. Power conversion measurements measurements for Nd:YAG at $1.06\mu\text{m}$ for two different output couplers.	4-19
4.10. Power conversion measurements for Nd:YLF at $1.047\mu\text{m}$ with two different output couplers.	4-20
4.11. Measurement setup for the Q-switched results.	4-21
4.12. Q-switched measurements made with Nd:YAG at 1.06 microns. .	4-23
4.13. Measurement results for Nd:YAG operating only at $1.34\mu\text{m}$. . .	4-24
4.14. Measured results for Nd:YLF operating only at $1.05\mu\text{m}$	4-28
4.15. Measured results for Nd:YLF operating only at $1.32\mu\text{m}$	4-29
4.16. Model results for pulse width and pulse energy as functions of pulse repetition frequency	4-32
4.17. Model results for pulse width and pulse energy as functions of pulse repetition frequency for different spot sizes.	4-34
4.18. Model results for pulse width and pulse energy as functions of pulse repetition frequency for different values of absorbed power.	4-35
4.19. Timeline showing the control sequence for the operation of the dual wavelength cavity.	4-37
4.20. Pulse shape of the $1.06\mu\text{m}$ and $1.32\mu\text{m}$ pulses from the Nd:YAG output.	4-38
4.21. Example output of the dual wavelength cavity.	4-39
4.22. Dual wavelength operation of Nd:YLF.	4-41
4.23. Dual wavelength operation of Nd:YLF showing energy crossover.	4-43
4.24. Dual wavelength operation of Nd:YAG comparing the results from two different cavity lengths.	4-46
4.25. Dual wavelength operation of Nd:YLF compared with Nd:YAG .	4-48

List of Tables

Table	Page
3.1. Published spectroscopic data for Nd:YAG	3-2
3.2. Published spectroscopic data for Nd:YLF	3-2
3.3. Published spectroscopic data for Nd:YVO ₄	3-3
3.4. Published spectroscopic data for Nd:GdVO ₄	3-3
3.5. Published spectroscopic data for Nd:SVAP	3-3
3.6. Published spectroscopic data for Nd:SFAP	3-3
3.7. Refractive Indices for several laser crystal materials @ 1064nm. .	3-4
3.8. Sum of the σ_{SETf} product from both the $^4F_{3/2} - ^4I_{11/2}$ and $^4F_{3/2} - ^4I_{13/2}$ transitions.	3-5
4.1. Transmission of the cavity high reflector for the different wave-lengths.	4-4
4.2. Reflectivity of laser crystals at the appropriate pump wavelength.	4-5
4.3. Absorptance of laser crystals at the appropriate pump wavelength.	4-7
4.4. Transmission of the long pass filter at the laser wavelengths . . .	4-10
4.5. CW Laser threshold and wavelength data	4-12
4.6. Estimates for $2\eta_{efficiency}l_g\sigma_{SETf}/h\nu_L V_{00}$ and residual cavity loss (L)	4-12
4.7. Nd:YAG laser threshold measurements	4-18
4.8. Q-switched Nd:YAG single wavelength performance at 1.06 μ m. .	4-22
4.9. Q-switched Nd:YAG single wavelength performance at 1.32 μ m. .	4-22
4.10. Cavity configuration for the Q-switched Nd:YAG data -long cavity.	4-23
4.11. Q-switched Nd:YLF single wavelength performance at 1.047 μ m	4-27
4.12. Q-switched Nd:YLF single wavelength performance at 1.32 μ m. .	4-27
4.13. Cavity configuration for the Q-switched Nd:YLF data-long cavity.	4-28
4.14. Q-switched Nd:YLF dual wavelength measurements- short cavity.	4-42

Table	Page
4.15. Q-switched Nd:YAG dual wavelength measurements—short cavity.	4-44
4.16. Cavity configuration for the dual-wavelength Q-switched Nd:YAG data —short cavity.	4-44
4.17. Q-switched Nd:YAG dual wavelength measurements—long cavity.	4-45
4.18. Cavity configuration for the dual-wavelength Q-switched Nd:YLF data —short cavity.	4-46
4.19. Q-switched Nd:YLF dual wavelength measurements—short cavity.	4-47

Abstract

A dual wavelength Q-switched laser cavity has been successfully designed and assembled to evaluate the new neodymium (Nd) based materials. Initial characterization has been achieved for Nd:YAG and Nd:YLF. The results indicate that for a fixed pulse repetition frequency, the delay time can be used to adjust the relative energy between the $1.06\mu\text{m}$ and $1.32\mu\text{m}$ pulses. Any deficiency in the performance of one transition can be made up by performance in the other simply by changing the relative amount of time the population inversion is allowed to build up for each pulse.

The best performance was obtained using a 13cm cavity length, the shortest possible cavity with the available equipment. The gain in the Nd:YLF $1.047\mu\text{m}$ cavity was so high, the diffraction efficiency of the acousto-optic Q-switch was insufficient to hold off lasing with a 5% output coupler. The transmission of the $1.047\mu\text{m}$ output coupler used for dual wavelength operation of Nd:YLF was 30% whereas the transmission of the $1.06\mu\text{m}$ output coupler necessary to achieve dual wavelength operation in Nd:YAG was 5%. At a pulse repetition frequency for each wavelength of 2kHz, and with 820mW of absorbed pump power, Nd:YLF produced pulse energies of $40\pm 2\mu\text{J}$ and $15.3\pm 0.6\mu\text{J}$, and pulse lengths of $44\pm 1\text{ns}$, and $410\pm 10\text{ns}$ at the wavelengths of $1.047\mu\text{m}$ and $1.32\mu\text{m}$ respectively. Nd:YAG produced pulse energies of $33\pm 1\mu\text{J}$ and $27\pm 1\mu\text{J}$, and pulse widths of $32\pm 0.4\text{ns}$ and $183\pm 1\text{ns}$ at the wavelengths of $1.06\mu\text{m}$ and $1.34\mu\text{m}$ respectively. A separate set of dual wavelength data is also presented for Nd:YLF at 5.0kHz.

TWO-WAVELENGTH NEODYMIUM-BASED LASERS

I. Introduction

1.1 Background

1.1.1 Laser radar application. The basic concept of a laser radar involves sending a laser pulse out to a target and sensing the reflected energy. There are a number of different measurements which can be made using a laser radar including the intensity image of a scene (which is the equivalent to using the laser as a flood-light), the range from the sensor to the target, and depending on the type of laser system, even the target's velocity. The application that this work is directed toward, involves both measuring an intensity image and the range to the target. Using a single pulse to build the entire image of a target at a long range requires a large laser which can produce high energy pulses. An alternative to the single pulse method uses a step-stare technique where the laser system focuses down on a small portion of the target and measures the reflected energy and range on just that small portion. Building the image is done by scanning over the entire scene. The amount of energy required for this last technique is much less than would be required to build the image with a single pulse. The pixel registered range information from this step-stare image can be used by an automated system to distinguish between different types of targets such as trees, missile launchers, tanks, and trucks.

One laser imaging application of interest to the Air Force is detecting targets which are either camouflaged or buried in background, with a sensor system mounted on the front of a smart munition. This type of munition is typically designed to be autonomous which means the system's electronics would have to process the data from the sensor package in order to find and track the target. Automatically

processing this tremendous amount of image data efficiently requires some target feature which the system can use to distinguish the target from its surroundings. One possible feature is reflectivity in the near infra-red (IR). It has been shown that the reflectivity of natural objects tends to decrease as the wavelength increases whereas the reflectivity of man made objects remains relatively constant or increases with wavelength (1:95; 2:41). Comparing two images made at the different wavelengths, natural objects appear relatively darker in the longer wavelength image, whereas man made objects appear relatively the same or brighter.

An imaging sensor for a smart munition could take advantage of these properties to extract man made objects from the natural background. The design of the laser system for such a sensor must consider several factors. The laser needs to produce two wavelengths in order to accomplish the discrimination, but the pulse repetition rate must be very fast to achieve the necessary image frame rate for both wavelengths. The image frame rate needs to be fast enough to update the relative position of the target during terminal homing so the munition can accurately steer for an intercept. Increasing the pulse repetition rate too far causes the pulse energy to decrease (3:623) which in turn decreases the maximum range of the sensor. However, the sensor must be able to image out to long ranges because a munition has only limited maneuverability, and so large course corrections need to be made a long time before target impact.

Increasing the pulse repetition rate also increases the pulse length of the laser, but short pulse lengths are needed to make accurate range measurements for target recognition purposes. A range precision on the order of one foot is needed to make an accurate measurement of the shape of a target. This range precision, which is a measurement of the difference in range between two adjacent pulses, requires a laser pulse length on the order of 10 nanoseconds.

The design of a sensor for the front of a smart munition must be very compact and efficient. To meet the stringent size and efficiency constraints, the ideal laser

design would use a single laser to produce both wavelengths. The difficulty is finding a suitable laser crystal which can produce two wavelengths.

The maturity of the technology plays an important role when selecting a laser crystal. At present, the most mature laser technology which can be packaged into the size requirements necessary for an autonomous sensor are crystals doped with the rare earth ion, neodymium (Nd). These crystals can be diode pumped and lasers have been constructed with this technology which are under three inches long and produce average powers of three Watts (5:89).

1.1.2 Review of laser cavity designs. As pointed out earlier, short laser pulse lengths are needed to make accurate three-dimensional measurements of a target. Considerable progress has been made in recent years to develop lasers based on neodymium which can produce short pulses. The applications currently driving this development are laser communications and laser imaging which need pulse lengths on the order of a few nanoseconds or less. Pulse lengths this short have been produced in several neodymium based materials pumped with laser diodes with much success (3:622; 20:1131; 21:6616; 22:885).

One particular group of workers from Lightwave Electronics, Inc. has made significant advances in producing short pulses, and the account of their progress is detailed in a series of articles which began in 1990. In the first article, they outline a patented laser cavity design which has a very high gain and a very short photon lifetime(3:622) – two characteristics essential for producing short pulses (23:2044). This group achieved a short photon lifetime by having a very short cavity which is less than an inch long. What makes this group's achievements all the more interesting is that they use an acousto-optic modulator to Q-switch their laser.

An acousto-optic device deflects light by sending an acoustic wave through a quartz or glass crystal. Acousto-optic devices are less expensive than electro-optic devices, which are the only other alternative for applications needing controllable Q-

switching. Besides cost, electro-optic devices also require high voltages to operate. The disadvantage of acousto-optic Q-switches is that they take longer to switch which often results in longer pulses. The pulse lengths the authors were able to achieve were on the order of 5-8ns at a wavelength of $1.06\mu\text{m}$ and 25-40ns at a wavelength of $1.32\mu\text{m}$.

The second article from this group, published in 1991 (22:885), outlines how they achieved pulse lengths of 2.7ns at repetition rates of up to 10kHz in Nd:YLF (neodymium yttrium lithium fluoride) with a laser cavity about a quarter inch long. These pulse lengths are on the same order needed to make range measurements with a range resolution on the order of one foot.

The group's last article was published in 1993 (21:6616) and describes work with the same cavity design as the one used in 1990 but with an additional laser crystal material, Nd:YVO₄ (neodymium yttrium orthovanadate). The technical achievement they highlight in this article as being crucial to their success was an acousto-optic Q-switch that had a switching time of 18ns. Using their design, they were able to achieve 0.6ns pulses at a repetition rate of 1kHz.

Although all of these short-pulse lasers produced relatively low powers, a different group, Bear et al. (20:1131), has developed a method for producing much higher powers using an alternate cavity design. They report the highest efficiency ever in a diode-pumped solid-state laser operating in the TEM₀₀ mode. Using the materials Nd:YAG (neodymium yttrium aluminum garnet) and Nd:YLF, they were able to achieve pulse lengths of 5ns at pulse repetition frequencies of 1kHz. Recently, working at Spectra-Physics, Bear has produced a Nd:YVO₄ laser which produces 5-6 Watts of average power. The pulse repetition frequency for this laser is 20kHz with pulse lengths on the order of 7-8ns (9). In order to apply their advances to the laser of interest, a method for producing two wavelengths with their cavity design is required.

All of the lasers discussed above which produce short pulse lengths are single wavelength devices. In order to change wavelengths, it is necessary to also change the optics. There are, however, several cavities already developed which can produce two wavelengths from the same crystal. Simultaneous lasing at both $1.06\mu\text{m}$ and $1.34\mu\text{m}$ wavelengths has been reported in several neodymium doped crystals including Nd:YAG, Nd:YLF, Nd:BEL, Nd:YAP (24:2315; 25:746; 26:2588; 27:444) and most recently Nd:SFAP (32). The work in this area has been driven by an application which needs simultaneous pulses at both wavelengths for sum harmonic frequency generation. An imaging laser radar would benefit from simultaneous pulses because any tracking error would be essentially eliminated allowing the reflectivities for a single target pixel to be compared. Pulses separated in time may require extra processing to ensure that the intensities being compared correspond to the same point on the target. If two pulses of different wavelengths were sent out to a target simultaneously, a method of separating them in the receiver would be necessary to process the information they contain. The work in this area relevant to the laser of interest is the "Y"-cavity laser cavity design (see Figure 1.1) developed by Tomaschke et al. (33:252) for producing two wavelengths from a single crystal. A dichroic beamsplitter is used to separate the two wavelengths by reflecting one wavelength and transmitting the other into different legs, each containing an acousto-optic Q-switch. The authors develop a model for this system but it is only applicable for simultaneous wavelength pulses, not alternating pulses.

1.2 Problem

There is an ongoing quest for the ultimate host material for neodymium which will yield a combination of high pumping efficiency, high gain, thermal stability, and good optical quality (12:387). This quest has generated a number of attractive crystals. The difficulty arises in choosing the best laser crystal for this dual wavelength laser radar application. A numerical analysis to choose the best crystal would have

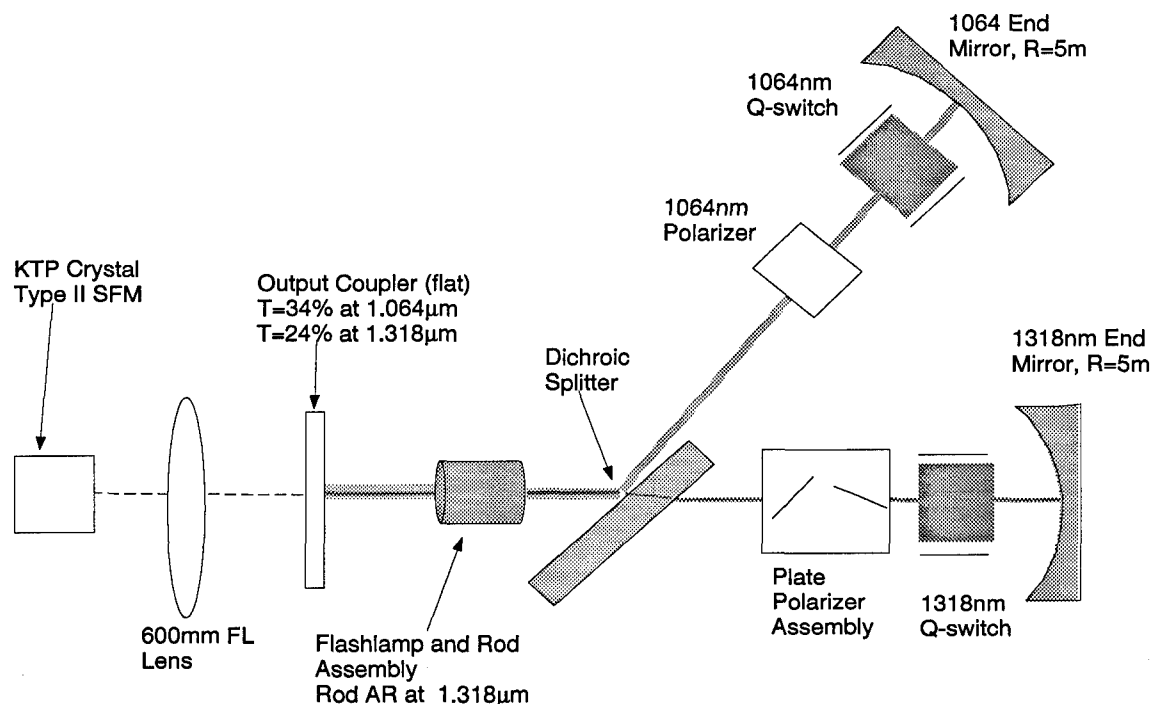


Figure 1.1 Tomaschke's laser cavity configuration for simultaneous wavelength output (pulsed).

to rely on the published data for the different material parameters of each of the available laser crystals. Unfortunately, either these reported values vary tremendously, or the values have not been published. The only way to draw meaningful conclusions about the relative performance of these available crystals is to measure their performance in an identical laser setup.

1.3 Scope

Equations describing continuous (CW) and Q-switched laser performance are presented and a general figure of merit is discussed for choosing the best laser material based on published data. A dual-wavelength Q-switched laser is designed and constructed which has a "Y" shaped cavity. The performance of the system is characterized for two different laser crystals, Nd:YAG and Nd:YLF. Both CW and

Q-switched measurements were made. The CW measurements include laser pump threshold and slope efficiency. The Q-switched measurements were made for both single and dual wavelength operation, and include the laser pulse energy and pulse length as a function of three variables: 1) pump power, 2) pulse repetition frequency, and 3) the delay time between the two pulses. A numerical model is fitted to the data from the $1.06\mu\text{m}$ results.

1.4 Approach

In Chapter II, a description of the lasing mechanism in Nd:YAG provides the foundation for presenting the equations describing both CW and Q-switched laser performance. Using these concepts, a figure of merit is discussed for choosing the most promising material from data in the published literature.

Laser crystals made from Nd:YAG, Nd:YLF, Nd:YVO₄, Nd:GdVO₄ (neodymium gadolinium orthovanadate), and Nd:SVAP (neodymium strontium fluorovanadate) were purchased for the system but only Nd:YAG, Nd:YLF, and Nd:SVAP arrived in time for evaluation. In Chapter III, measurements of the polarized absorption spectra of each material in the range from 790 nm out to 815 nm are presented, and the measurements indicate the best wavelength for pumping in the $^4\text{H}_{9/2}$ to $^4\text{F}_{5/2}$ band.

A "Y" shaped cavity was constructed which allows Q-switched operation at alternating wavelengths (see Figure 1.1). Initial laser measurements include finding the CW laser threshold for both the nominal $1.06\mu\text{m}$ and $1.32\mu\text{m}$ transitions in each sample. The change in threshold caused by inserting each component was used to calculate an estimate of the intra-cavity loss caused by each component at the lasing wavelength.

Q-switched laser performance measurements include the pulse energy and pulse length (FWHM) as functions of pulse repetition frequency. These measurements were made for two different cavity lengths. After comparing these results against

theoretical predictions from the model, both the measurement and model results are used to draw conclusions about the best material and cavity configuration for the laser imager application.

II. Laser Theory

2.1 Population inversion and gain in neodymium (Nd) based crystals

Figure 2.1 shows the energy band diagram for Nd in YAG (yttrium aluminum garnet) (6:49). Although the details of this diagram change when Nd is placed in different host crystals, the basic electronic transitions which produce lasing remain the same. A pump photon from a laser diode with a wavelength around 808nm can cause an electron in the $^4I_{9/2}$ ground state to transition to the band of allowed states between the $^4H_{9/2}$ and the $^4F_{5/2}$ states. The width of this band determines the absorption bandwidth, the range of pump wavelengths that can be used to pump the laser. High power laser diode arrays experience relatively large differences in the wavelength from the many elements which make up the arrays and so wider absorption bandwidths allow increased absorption of the pump energy (8:571; 10:999; 15:298). The most likely decay route from this band of allowed states between the $^4H_{9/2}$ and the $^4F_{5/2}$ levels is into the $^4F_{3/2}$ state via a non-radiative relaxation process where the energy is given up into lattice vibrations. The $^4F_{3/2}$ state is the upper energy level for both the transitions which produce the $1.06\mu\text{m}$ and $1.32\mu\text{m}$ wavelengths. The average amount of time that electrons spend in this state is referred to as the upper state lifetime, τ_f .

If an electron in the upper laser energy level transitions down to the $^4I_{11/2}$ state, a photon with a wavelength of $1.06\mu\text{m}$ will be emitted. If this emitted photon interacts with another neodymium ion which has an electron in the upper laser transition level, it could induce that electron to transition to the $^4I_{11/2}$ state, causing another $1.06\mu\text{m}$ photon to be emitted. This process is called stimulated emission. A measure of the probability that this stimulated emission process will take place is the stimulated emission cross section, σ_{SE} .

A related process is called stimulated absorption. This process also has an associated cross section, σ_{Ab} . Absorption can occur when a photon encounters an

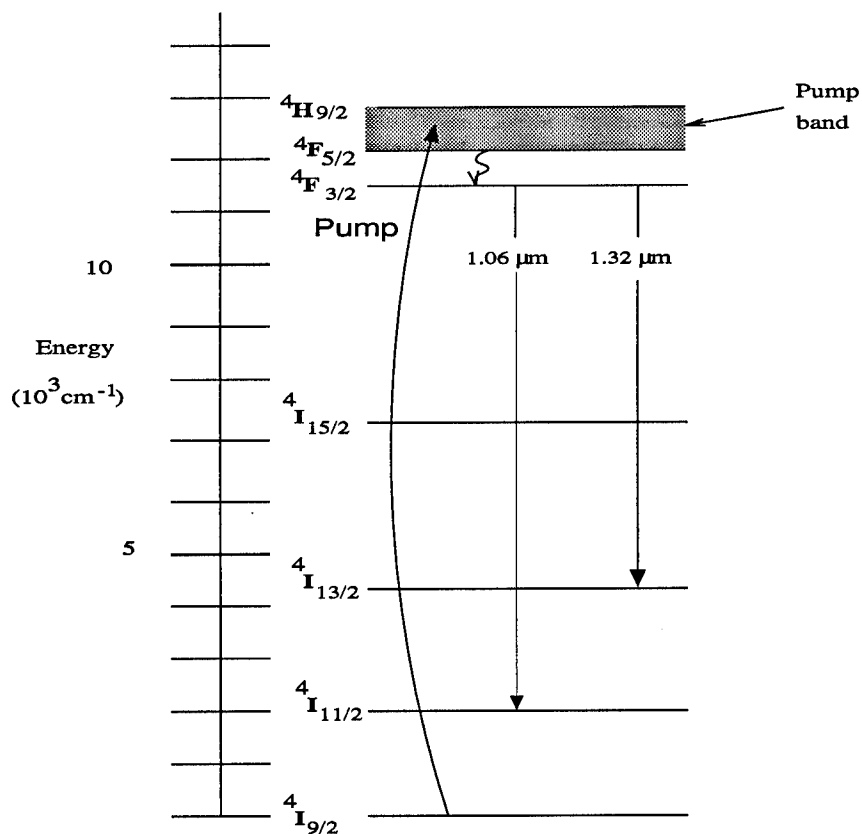


Figure 2.1 Energy band diagram for neodymium in YAG.

ion with an electron in the lower $^4I_{11/2}$ energy level. The ion absorbs the energy in the photon causing a transition to the upper energy level.

Population inversion occurs when the number of electrons in the $^4F_{3/2}$ level exceeds the number in the lower energy level. This situation implies that a photon traversing the laser crystal is more likely to encounter an electron in the upper energy level than it is to encounter an electron in the lower laser energy level. Stimulated emission is then more probable in this case than absorption, and so for a single pass through the material, a spontaneously emitted photon will see a net gain. At room temperature in thermal equilibrium, most of the electrons reside in the $^4I_{9/2}$ state. The situation where more electrons reside in the upper energy state is not a natural occurrence and thus a pumping mechanism is required to achieve it.

A laser crystal being pumped with a constant source has a gain per unit length in the gain medium given by(35:183)

$$\gamma_0 = \sigma_{SE} \left(N_2 - \frac{g_2}{g_1} N_1 \right) \quad (2.1)$$

where σ_{SE} is the stimulated emission cross section for the lasing transition, N_2 is the population density of the upper energy state, N_1 is the population density of the lower energy state for the lasing transition, and g_2 and g_1 are the degeneracies of the upper and lower laser energy levels respectively. The gain coefficient is positive for the case where $N_2 > \frac{g_2}{g_1} N_1$. When $N_2 < \frac{g_2}{g_1} N_1$ the gain coefficient is negative, and a spontaneously emitted photon experiences a net loss.

In the absence of any feedback, the population density in state 2 builds according to (35:191)

$$N_2(t) = R_2 \tau_f \left(1 - \exp \left(-\frac{t}{\tau_f} \right) \right), \quad (2.2)$$

where R_2 is the pumping rate per unit volume. The expression for R_2 is given by

$$R_2 = \frac{\eta_{Abs} P_{Pump}}{h\nu_p V_{00}}, \quad (2.3)$$

where P_{Pump} is the pump power in Watts, h is Plank's constant, ν is the frequency of the pump radiation, η_{Abs} is the probability that the incident photons are converted to useful upper level population, and V_{00} is the pumped volume in the gain medium. The value for η_{Abs} in this expression includes the fraction of incident pump photons absorbed by the gain medium multiplied by the fraction that actually relax into the upper energy level for the lasing transition. The spatial profile of the pump beam is modeled as a Gaussian and so the expression for V_{00} is given by (35:118)

$$V_{00} = \frac{\pi \omega^2}{2} l_g \quad (2.4)$$

where ω is the spot size of the laser beam inside the laser crystal.

Assuming both steady state conditions $\frac{\partial}{\partial t} = 0$, and that the lower energy state decays infinitely fast such that $N_1 = 0$, the population inversion is just equal to the population in state 2. The lifetime of the lower energy level for the ${}^4F_{3/2} - {}^4I_{11/2}$ transition has been measured in Nd:YAG and Nd:YLF(7:1987). Nd:YAG has a lower level lifetime of 0.225ns and Nd:YLF has a lifetime of 20ns. Given this data, the approximation that $N_1 = 0$ is valid for Nd:YAG for pulse lengths over 0.225ns and for Nd:YLF for pulse lengths over 20ns. The shortest pulse 1.06 μ m lengths achieved in this work were 35ns long (see Chapter IV) and so the assumption that $N_1 = 0$ is valid for this particular set up. Using these assumptions, substituting Eq (2.3) and Eq (2.2) into the expression for the small signal gain in Eq (2.1) yields

$$\gamma_0 = \sigma_{SE} \tau_f \frac{P_{pump}}{h\nu_p} \frac{\eta_{Abs}}{V_{00}} \quad (2.5)$$

From the dependence of the gain on the upper state lifetime illustrated in Eq (2.5), it can be seen that materials with longer upper state lifetimes are better at storing the pump energy. When the pulse repetition rate is below $\frac{1}{\tau_f}$, materials with longer lifetimes can achieve higher gain, given a constant pump rate (3:623).

Eq (2.5) also shows the dependence of the gain on the stimulated emission cross section, a larger cross section means less feedback is needed to cause lasing to occur and it also means that shorter pulses are possible. The value for the stimulated emission cross section applies to a single transition in a particular material. Some of the published values for this cross section in Nd:YAG at 1.064 μ m vary up to $\pm 30\%$.

The expression for the gain also illustrates the dependence on the size of the pumped volume in the laser crystal. Focusing the pump down into a smaller spot size increases the gain.

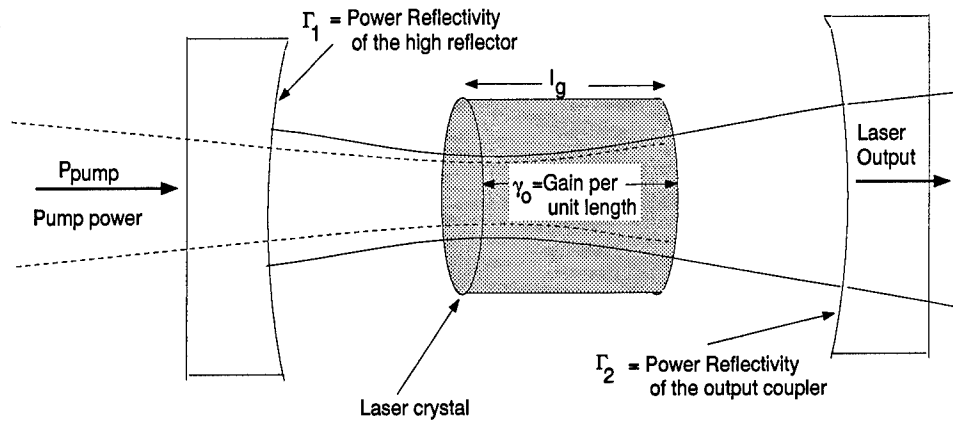


Figure 2.2 Simple end-pumped cavity configuration.

2.2 CW laser theory

If a population inversion is created in a laser crystal and feedback is provided to the stimulated emission process, the number of photons produced rises rapidly. This feedback can be created by placing the laser crystal inside a Fabry Perot cavity. Figure 2.2 shows some of the basic parameters for a simple laser cavity. In order for laser oscillation to occur, the round trip gain must be greater than the round trip losses. This requirement means that the gain coefficient must be greater than a threshold given by (35:184)

$$\gamma_{th} = \frac{1}{2l_g} \ln \left(\frac{1}{\Gamma_1 T_{Comp}^2 \Gamma_2} \right) \quad (2.6)$$

where l_g is the length of the gain medium, Γ_1 and Γ_2 represent the reflectivity of the cavity end mirrors, and T_{Comp} represents the single pass transmission of the various

optical components inside the laser cavity including the laser crystal itself. Combining Eq (2.1) for the gain coefficient and Eq 2.6 for the threshold gain coefficient yields an expression for the threshold population inversion n_{th} which is given by (35:257)

$$n_{th} = \frac{1}{2l_g\sigma_{SE}} \ln \left(\frac{1}{\Gamma_1 T_{Comp}^2 \Gamma_2} \right) V_{00} \quad (2.7)$$

After the population inversion exceeds the threshold, the general equation which describes the output characteristics of a CW laser is given by (6:96)

$$P_{out} = \sigma_S (P_{pump} - P_{Threshold}) \quad (2.8)$$

where P_{pump} is the incident pump power, $P_{Threshold}$ is the threshold pump power, and σ_S is the slope efficiency of the output power vs the input power. The expression for the slope efficiency is given as (6:100).

$$\sigma_S = \frac{(1 - \Gamma_2)\eta_{efficiency}}{\left[1 + \sqrt{\frac{\Gamma_2}{\Gamma_1 T_{Comp}^2}} \right] [1 - \sqrt{\Gamma_1 \Gamma_2 T_{Comp}^2}] \lambda_L} \quad (2.9)$$

where Γ_1 is the power reflectivity of the cavity high reflector, Γ_2 is the power reflectivity of the output coupler, T_{comp} is the one way transmission of the components within the cavity including the laser crystal itself, $\eta_{efficiency}$ is the pumping efficiency, and λ_L is the wavelength of the lasing transition. The expression for the pumping efficiency is given by

$$\eta_{efficiency} = \eta_B \eta_{Abs} \frac{\lambda_p}{\lambda_L} \quad (2.10)$$

where η_B is the beam overlap efficiency which is inserted to include only the gain which is within the mode volume, and λ_p is the wavelength of the pump source. The laser cavity shown in Figure 2.2 shows an end-pumped scheme. The size of the pump beam relative to the size of the oscillating laser mode effects the pumping efficiency because the portion of the gain medium outside the laser mode volume does not need

to be pumped. The optimum design condition is when the pump beam size and the laser beam size match inside the laser crystal. If Gaussian pump and laser profiles are assumed, the beam overlap efficiency can be calculated from (6:92)

$$\eta_B = \frac{2\omega^2}{\omega_p^2 + \omega^2} \quad \text{for } \omega_p > \omega \quad (2.11)$$

and

$$\eta_B = 1 \quad \text{for } \omega_p \leq \omega \quad (2.12)$$

where ω is the spot size (radial distance from the center of the beam to the $\frac{1}{e^2}$ intensity point) of the laser mode in the gain medium and ω_p is the spot size of the pump beam in the gain medium. Eq (2.12) indicates that the overlap efficiency is 100% when $\omega_p \leq \omega$.

The expression for the amount of pump power to reach threshold, $P_{Threshold}$, is given by (6:100)

$$P_{Threshold} = \frac{-V_{00}h\nu_L \ln \left(\sqrt{\Gamma_2 \Gamma_1 T_{comp}^2} \right)}{\sigma_{SE} \tau_f \eta_{efficiency} l_g} \quad (2.13)$$

where V_{00} is the laser mode volume in the crystal, h is Planck's constant, ν_L is the optical frequency of the laser radiation, Γ_2 is the reflectivity of the output coupler, Γ_1 is the reflectivity of the high reflector, σ_{SE} is the stimulated emission cross section, τ_f is the fluorescence lifetime, l_g is the length of the gain medium, and $\eta_{efficiency}$ is the probability that an incoming photon is converted to useful population inversion.

By measuring the threshold pump power with different output coupler reflectivities, an estimate of the round trip cavity loss and the pumping efficiency can be estimated by plotting the natural log of the output coupler reflectivity against the threshold pump power. The equation describing this plot is (6:101)

$$-\ln(\Gamma_2) = 2 \frac{\sigma_{SE} \tau_f \eta_{efficiency} l_g}{V_{00} h \nu_L} P_{Threshold} - L \quad (2.14)$$

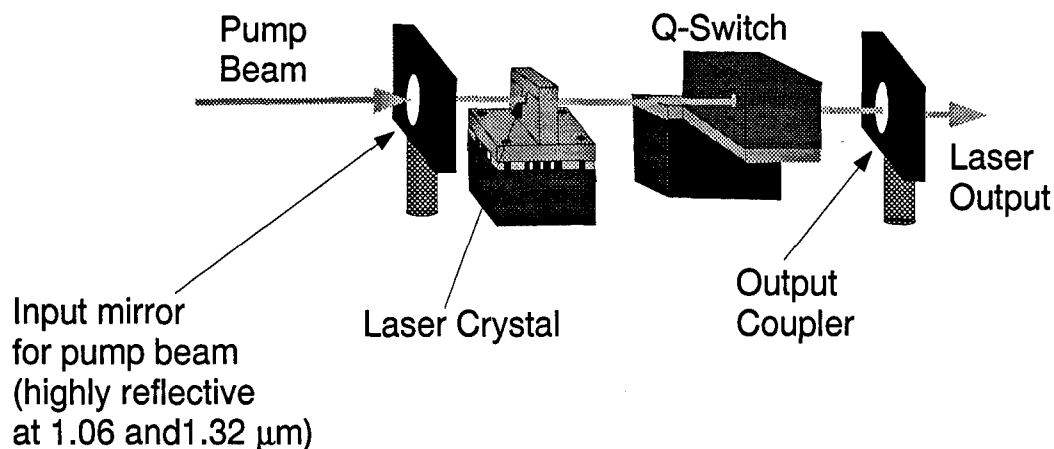


Figure 2.3 Simple Q-switched cavity configuration.

where L is the total loss in the cavity other than the output coupler

$$L = 1 - \Gamma_1 T_{comp}^2 \quad (2.15)$$

2.3 Q-switched laser theory

Q-switching a laser cavity is the process of increasing the cavity loss to the point where no lasing can take place. Under continuous pumping, this causes a large population inversion to be created. Then the loss in the cavity is reduced very quickly, causing feedback to the gain medium to increase. The stimulated emission process quickly escalates, resulting in a large number of photons emitted from the laser in a short pulse, all with roughly the same wavelength.

The diagram for a simple Q-switched cavity configuration is shown in Figure 2.3. For this analysis the pump is treated as a CW optical beam from another laser. The Q-switch element provides additional loss in the cavity, this additional loss causes the threshold population level to increase according to Eq (2.7). If this increased threshold level is high enough, the actual population inversion remains below this threshold and the cavity does not lase. Under this situation of CW pumping

and high Q-switch loss, the population builds up according to Eq (2.2). After the Q-switch returns to low loss, the photon number N_{phot} and the population inversion n change according to the two coupled nonlinear differential equations (35:253)

$$\frac{dN_{phot}}{dT} = \left(\frac{n}{n_{th}} - 1 \right) N_{phot} \quad (2.16)$$

$$\frac{dn}{dT} = -\frac{n}{n_{th}} N_{phot} \quad (2.17)$$

where T is time normalized to units of photon lifetime, and n_{th} is the threshold population inversion. The expression for the photon lifetime is given by

$$\tau_{phot} = \frac{\tau_{rt}}{1 - \Gamma_1 \Gamma_2 T_{Comp}^2} \quad (2.18)$$

where τ_{rt} is the round trip time for a photon in the cavity.

The two differential equations which describe the change in the number of photons circulating in the cavity (Eq (2.16)), and the change in the total population inversion (Eq (2.17)), assume that the effect of the pumping mechanism is negligible over the duration of the pulse and that the Q-switch has essentially a zero turn-on time. These equations were implemented in a software model (see Appendix B) and Figure 2.4 on page 2-10 shows an example of the population inversion and the photon number as functions of time. The threshold population level in the upper plot changes because the Q-switch is modeled as having a non-zero switching speed, and the additional loss caused by the Q-switch causes a change in the threshold.

The initial photon number and initial population level used to initiate these equations have a significant effect on the results. The photons which exist in the cavity prior to lasing that have wavelengths corresponding to the lasing transition, are a result of spontaneous emission. The initial number of these photons has an indirect impact on the amount of energy calculated in the pulse and the pulse width by effecting on how fast the pulse builds up after the threshold population level drops

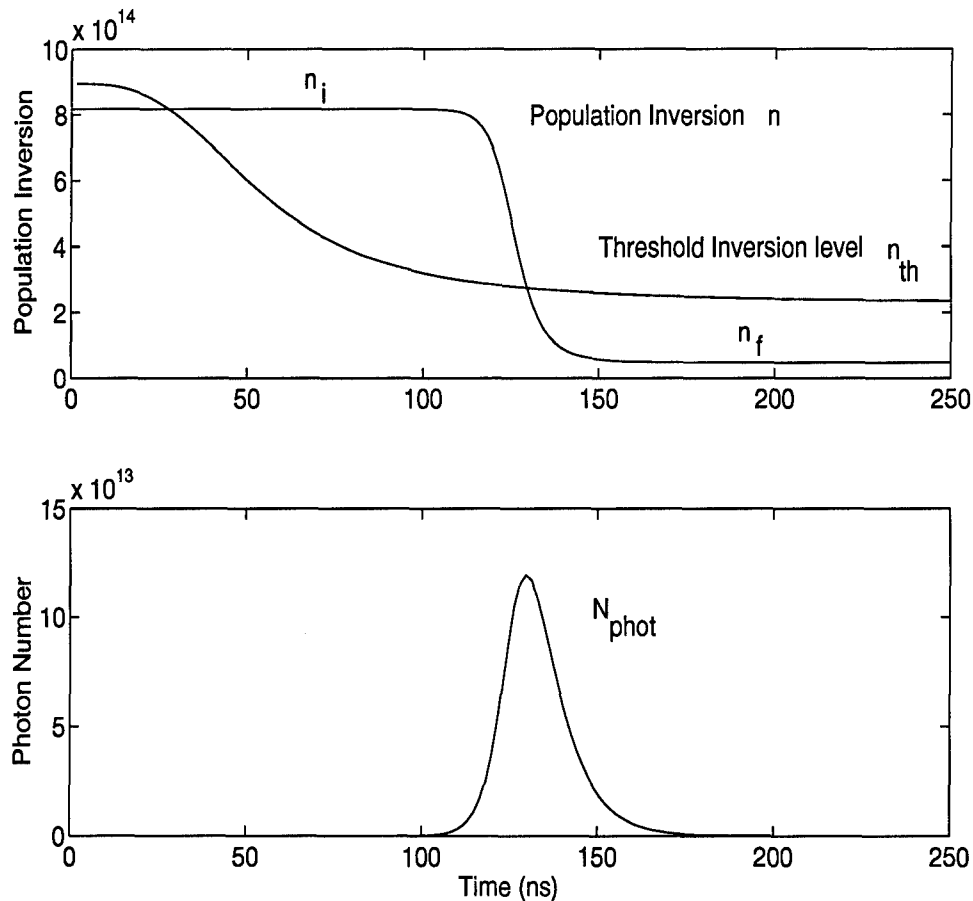


Figure 2.4 Population inversion, threshold population level, and photon number as a function of time.

below the initial population inversion level. When the Q-switch is modeled as taking a finite time to switch from high loss to low loss, as it is here, a large initial photon number causes the pulse to build up earlier while the Q-switch is still switching from high to low loss. This overlap of the Q-switch transition with the emerging pulse causes a decrease in the amount of energy in the pulse and an increase in the pulse length. A lower initial photon number causes the pulse to build up later when the Q-switch is almost fully transmissive and has no significant effect on the pulse.

The total energy in the output pulse shown in the bottom portion of Figure 2.4 is calculated from the change in the inversion level which is shown in the top portion of Figure 2.4. The expression for the laser output energy is given by (23:2042)

$$W_{out} = (n_i - n_f) h\nu_L \frac{\alpha_{ext}}{\alpha_{total}} \quad (2.19)$$

where n_i and n_f are the initial and final population inversions respectively, α_{ext} is the portion of loss which is extracted from the cavity as useful output, and α_{total} is the total loss in a round trip of the cavity. The expression for α_{total} is given by

$$\alpha_{total} = \ln \left(\frac{1}{\Gamma_1 \Gamma_2 T_{Comp}^2} \right) \quad (2.20)$$

where again, Γ_1 is the power reflectivity of the high reflector, Γ_2 is the power reflectivity of the output coupler, and T_{Comp} is the total one way transmission of all of the various components in the cavity. The expression for α_{ext}

$$\alpha_{ext} = \ln \left(\frac{1}{\Gamma_2} \right) \quad (2.21)$$

A relationship exists between the initial population level at the start of the pulse, the threshold level, and the fraction of energy which is extracted from the population inversion. The initial, final, and threshold inversion levels are related through the expression (35:255)

$$\frac{n_f}{n_i} = \exp \left[- \left(\frac{n_i - n_f}{n_{th}} \right) \right] \quad (2.22)$$

The fraction of the initial inversion which is converted to photons is typically defined as an extraction efficiency

$$\eta_{extrn} = \frac{n_i - n_f}{n_i} \quad (2.23)$$

The relationship of this value to the inversion ratio, the ratio of initial population inversion n_i to threshold inversion n_{th} is shown in Figure 2.5. From this relationship,

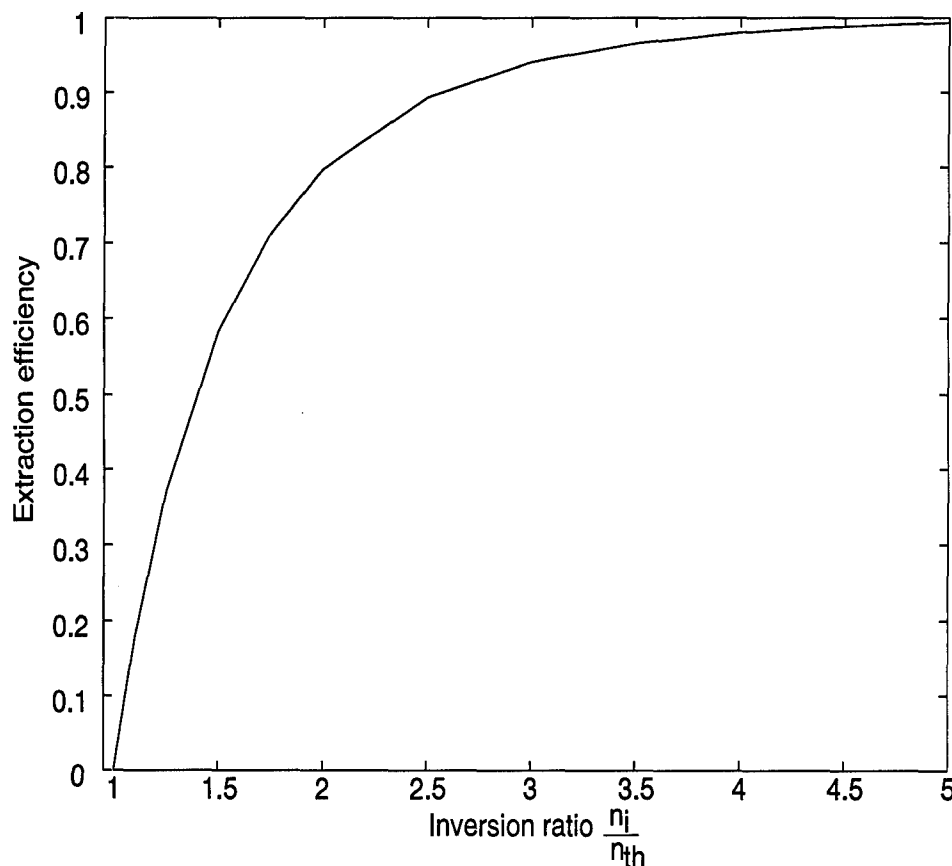


Figure 2.5 Extraction efficiency as a function of the inversion ratio $\frac{n_i}{n_{th}}$.

it becomes evident that the percentage of the energy extracted from the initial population inversion is a strong function of the inversion ratio. For a Q-switched pulse, the initial population level is very important. According to Eq (2.2), it depends on the pump rate per unit volume, the fluorescence lifetime, and the amount of time the population is allowed to build up. In a repetitively Q-switched laser, another factor to consider is the residual population inversion from the previous pulse. This leftover population, depending on how efficiently the last pulse swept out the gain region, can be significant. In order to properly model the laser's behavior, this number must be taken into account by calculating an equivalent pumping time. The equivalent

pumping time is the amount of time that it would take to reach this final population level at the given pumping rate and it can be calculated by using the final population inversion n_f from the last pulse in Eq (2.2) and solving for time

$$t_{equiv} = -\tau_f \ln \left(1 - \frac{n_f}{R_2 \tau_f} \right) \quad (2.24)$$

The initial population inversion is then calculated using the sum of this equivalent pumping time with $\frac{1}{\text{pulse rep rate}}$ in for t in Eq (2.2). A model of the Q-switched laser performance was developed using the equations in sections 2.1 - 2.3. A version of this model, written in Matlab, is presented in Appendix B.

2.4 General figure of merit for dual wavelength laser performance

The performance of a particular laser system depends on a large number of variables. Examining the expression for the threshold pump power in Eq (2.13) on page 2-7, there are a large number of factors which are based on the particular cavity. Lower threshold values can be achieved by reducing both the size of the beam in the crystal and the cavity losses. For the sake of comparing different materials, these will be assumed to be the same for all.

The significant material dependent parameters in Eq (2.13) are the absorption efficiency, stimulated emission cross section, and fluorescence lifetime. The absorption efficiency is a function of the material and the pumping mechanism. A Ti:Sapphire laser has a very narrow line width which allows this source to be a very efficient pump for most materials even when the absorption line width in the laser material is very narrow. High power laser diode arrays used for laser diode pumping exhibit some wavelength variation among the individual elements (18:560). In order to use the pump power most efficiently, the absorption line width in the material should be broader than the wavelength content from the laser diode arrays. Absorption efficiency is a complex problem dependent on the laser material, pumping

mechanism, and laser geometry. Since the total absorptance can be made equal in each of the materials by changing the length of the gain region, it will be set aside for the sake of comparison.

The remaining factor is the product of the stimulated emission and the upper state lifetime, $\sigma_{SE}\tau_f$. The values of these two parameters depends on the interaction of the neodymium ion with the surrounding crystal lattice. The larger this product is, the lower the threshold, and so this product provides a general figure of merit for comparing different materials (12:159). The performance of a laser operating at two wavelengths depends on this product from both lasing transitions. The figure of merit becomes the sum of this product from both transitions.

III. Material Characterization

Choosing a laser crystal for the two wavelength laser radar application which has the optimum combination of large absorption bandwidth, large stimulated emission cross section, and long upper state lifetime is difficult, in part, because of the large number of possible materials. These materials are the result of an ongoing quest for the ultimate host material for neodymium which will yield a combination of high pumping efficiency, high gain, thermal stability, and good optical quality (12:387). A numerical analysis to choose the best crystal from among those available must rely on the published data for the material parameters for each crystal. Unfortunately, these reported values either vary tremendously, as shown in Tables 3.1 - 3.5, or the values have not been published. So, the only way to draw meaningful conclusions about the relative performance of these available crystals is to measure their performance in an identical laser setup.

The cross sections given in Tables 3.1 - 3.5 are effective laser cross sections. The effective stimulated-emission cross section is the spectroscopic cross section multiplied by the occupation of the upper laser level relative to the entire $^4F_{3/2}$ manifold (6:50).

Table 3.1 shows the values for Nd:YAG. This crystal is probably the most commonly used laser material for lasers at $1.06\mu\text{m}$, and it is often used as the standard against which new materials are compared. Nd:YLF is attractive as a laser material because it has a long upper state lifetime (see Table 3.2). Nd:YVO₄ has been studied recently because of its large peak absorption cross section and broad absorption bandwidth in the pump region, as well as its large stimulated emission cross section at both $1.06\mu\text{m}$ and $1.32\mu\text{m}$ (14:5546; 15:298). The drawbacks of Nd:YVO₄ are the nonavailability of high quality crystals and the short upper state lifetime, which indicates that it does not store the pump energy as well as the other materials with longer lifetimes. Nd:GdVO₄ (neodymium gadolinium orthovanadate) is a relatively

Table 3.1 Published spectroscopic data for Nd:YAG (neodymium yttrium aluminum garnet). The stimulated emission cross sections are the effective cross sections, which take into account the Boltzmann distribution of the electrons within the two Stark sub-levels of the $^4F_{3/2}$ manifold.

Reference	% doping	τ_f (μs)	$\lambda = 1.064\mu m$ $\sigma_{SE} 10^{-19} cm^2$	$\lambda = 1.34\mu m$ $\sigma_{SE} 10^{-19} cm^2$
(18:561)		244	3.4	
(29:3067)	1.0	245	3.2	
(8:572)		230	6.5	
(11:1443)	1	244	3.4	0.9
(17:376)	1.1		2.1	
(5:90)	1	220	2.8	
(14:5547)	1		2.8	
(28:6375)	1.1	240	2.8	
(30:1869)	1.0	272 ± 12		
(31:1314)	1.0	237 ± 10		
this work	1.0	237		

Table 3.2 Published spectroscopic data for Nd:YLF (neodymium yttrium lithium fluoride).

Reference	% doping	τ_f (μs)	$\lambda = 1.047\mu m$ $\sigma_{SE} 10^{-19} cm^2$	$\lambda = 1.313\mu m$ $\sigma_{SE} 10^{-19} cm^2$
(18:561)		480	3.7	
(8:572)		480	3.2	
(11:1443)		480	3.7	0.6
(28:6375)	1.1	500	1.9	
this work	1.0	504		

Table 3.3 Published spectroscopic data for Nd:YVO₄ (neodymium yttrium orthovanadate).

Reference	% doping	τ_f (μ s)	$\lambda = 1.064\mu\text{m}$ $\sigma_{SE} 10^{-19} \text{ cm}^2$	$\lambda = 1.3\mu\text{m}$ $\sigma_{SE} 10^{-19} \text{ cm}^2$
(18:561)	1.0	98	6.2	
(29:3067)	1.0	97	9.84 ± 1.4	
(15:298)				7 ± 2
(8:572)		98	20.1	
(5:90)	1	100	15.6	
(28:6375)	1.1	100	15.6	
(13:43)		115	10.7	

Table 3.4 Published spectroscopic data for Nd:GdVO₄ (neodymium gadolinium orthovanadate).

Reference	% doping	τ_f (μ s)	$\lambda = 1.064\mu\text{m}$ $\sigma_{SE} 10^{-19} \text{ cm}^2$	$\lambda = 1.3\mu\text{m}$ $\sigma_{SE} 10^{-19} \text{ cm}^2$
(17:376)	1.2	90	7.6	1.8
(5:90)	1	94	7.6	
(13:43)		≈ 100	> 7.6	

Table 3.5 Published spectroscopic data for Nd:SVAP (neodymium strontium fluorovanadate).

Reference	% doping	τ_f (μ s)	$\lambda = 1.064\mu\text{m}$ $\sigma_{SE} 10^{-19} \text{ cm}^2$	$\lambda = 1.3\mu\text{m}$ $\sigma_{SE} 10^{-19} \text{ cm}^2$
(5:90)	0.4	220	5.0	
(13:43)		215	5	
(28:6375)	0.38	230	5	
this work		216		

Table 3.6 Published spectroscopic data for Nd:SFAP (neodymium strontium fluorapatite). The stimulated emission cross sections are the effective cross sections.

Reference	% doping	τ_f (μ s)	$\lambda = 1.064\mu\text{m}$ $\sigma_{SE} 10^{-19} \text{ cm}^2$	$\lambda = 1.3\mu\text{m}$ $\sigma_{SE} 10^{-19} \text{ cm}^2$
(32:43)		298	5.4	2.4

Table 3.7 Refractive Indices for several laser crystal materials @ 1064nm.

	n_o	n_e	
Nd:YAG	1.81633	N.A.	(35:318)
Nd:YLF	1.4481	1.4704	(6:60)
Nd:SVAP	1.824	1.809	(13:43)
Nd:YVO ₄	1.958	2.168	(13:43)
Nd:SFAP	1.629	1.624	(13:43)

new material which is receiving a lot of attention recently because it exhibits similar spectroscopic properties to that of Nd:YVO₄ (16:1071; 10:999; 17:373). What makes it even more interesting is that high quality crystals are easier to manufacture because of the closeness in size between the neodymium atom and the gadolinium atom it displaces in the crystal lattice (17:373).

Nd:SVAP and Nd:SFAP both have cross sections at 1.06 μ m which are approximately twice the values published for Nd:YAG. The lifetime of Nd:SVAP is only around 10% below the values published for Nd:YAG whereas the lifetime for Nd:SFAP is approximately 20% higher. The values for Nd:SFAP indicate that it will have much higher gain than Nd:YAG for a similar amount of pump power.

The final section in Chapter II outlined a general figure of merit for choosing the best material for the dual wavelength laser application. Table 3.8 on page 3-5 shows the calculation of this metric for some of the most promising laser crystals. The values used to calculate the metric for each material were drawn from the most recently published values in Tables 3.1 - 3.5. There is no entry in Table 3.8 due to the lack of a published cross section for the ⁴F_{3/2} - ⁴I_{13/2} transition. Based on the information in Table 3.8, Nd:SFAP is the optimum material for a dual wavelength laser system. This conclusion should be supported with appropriate experimental measurements. Also, this conclusion disregards issues such as beam quality, thermal lensing, and other material and system related issues.

Table 3.8 Sum of the $\sigma_{SE}\tau_f$ product from both the $^4F_{3/2} - ^4I_{11/2}$ and $^4F_{3/2} - ^4I_{13/2}$ transitions.

	$\sigma_{SE(1.06\mu m)}\tau_f + \sigma_{SE(1.3\mu m)}\tau_f$ ($10^{-17}\mu s\text{ cm}^2$)
Nd:YAG	10.5
Nd:YLF	20.6
Nd:GdVO ₄	8.5
Nd:YVO ₄	17.0
Nd:SFAP	23.2

3.1 Absorption measurements

The measurements of the polarized absorption for Nd:YAG, Nd:YLF, and Nd:SVAP in the wavelength region of interest for laser diode pumping are shown in Figure 3.1. Nd:YAG is an optically isotropic crystal and so there is no polarization dependence on the absorption. Nd:YLF and Nd:SVAP are both uniaxial crystals and exhibit different absorption characteristics for incident radiation polarized along the optic axis ($E||c$) versus perpendicular to it ($E\perp c$). The peak absorption wavelength for Nd:SVAP occurs at 808.5nm for both polarizations; however, the peak absorption is stronger for $E||c$. The peak absorption for Nd:YLF occurs at 792nm with the electric field polarized parallel to the optic axis, however, the absorption at 792nm for $E\perp c$ is relatively small. In order for a pump source to be efficient at this wavelength, it must linearly polarized, and the polarization must be carefully aligned to the optic axis of the crystal.

The absorptance shown in each plot in Figure 3.1 is the total fraction of incident pump power absorbed as a function of wavelength. Both the Nd:YAG and Nd:YLF sample were 0.5cm long whereas the Nd:SVAP sample was only 0.3cm long. Even with this shorter length, the peak absorptance in Nd:SVAP is comparable to the peak in Nd:YAG and Nd:YLF indicating that it has a very high absorption cross section at the pump wavelength. The wavelength accuracy of the Perkin Elmer Lambda 9 Spectrophotometer which measured the absorption data is $\pm 0.8\text{nm}$.

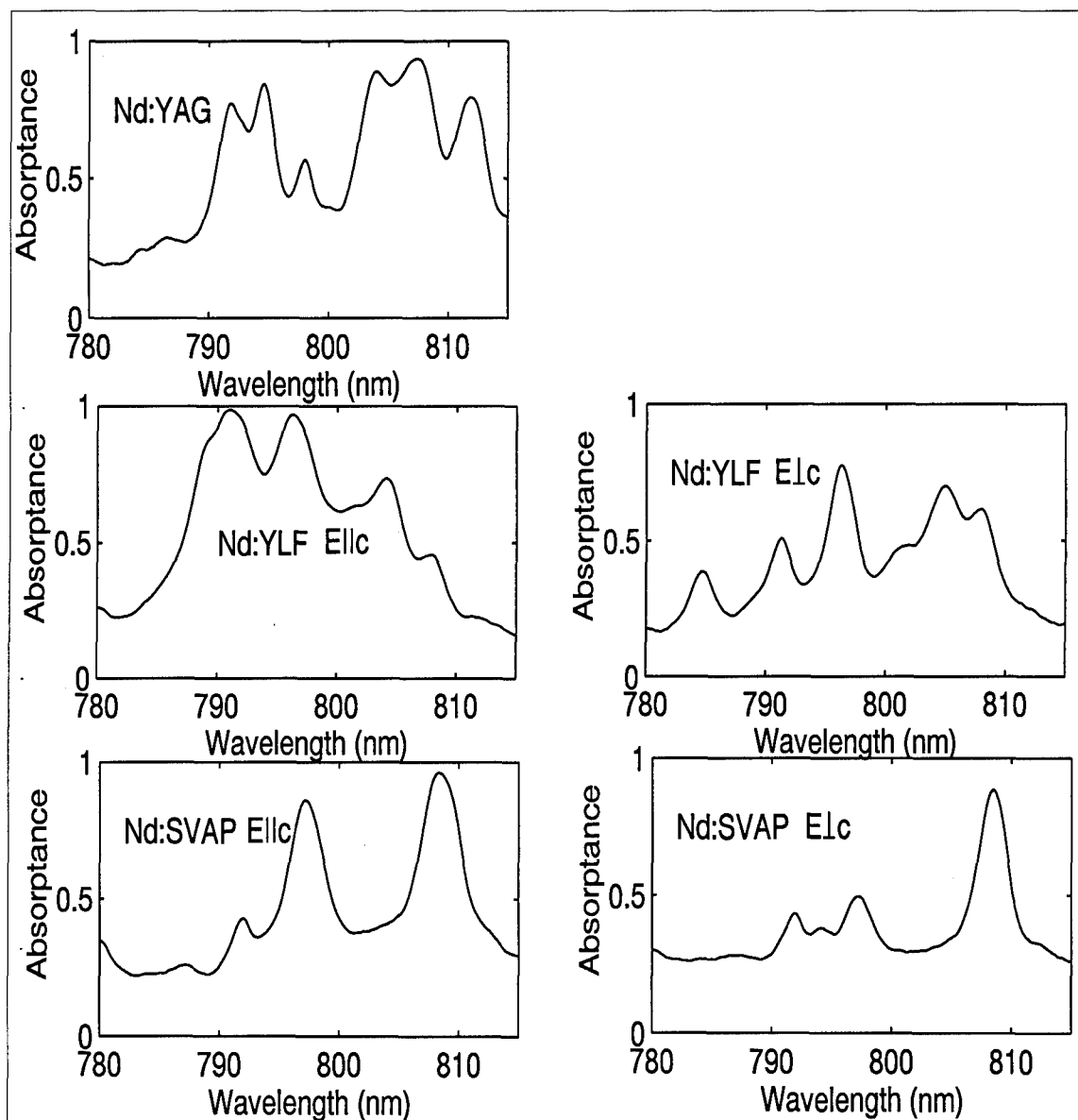


Figure 3.1 Polarized absorption spectrum for Nd:YAG, Nd:YLF, and Nd:SVAP.

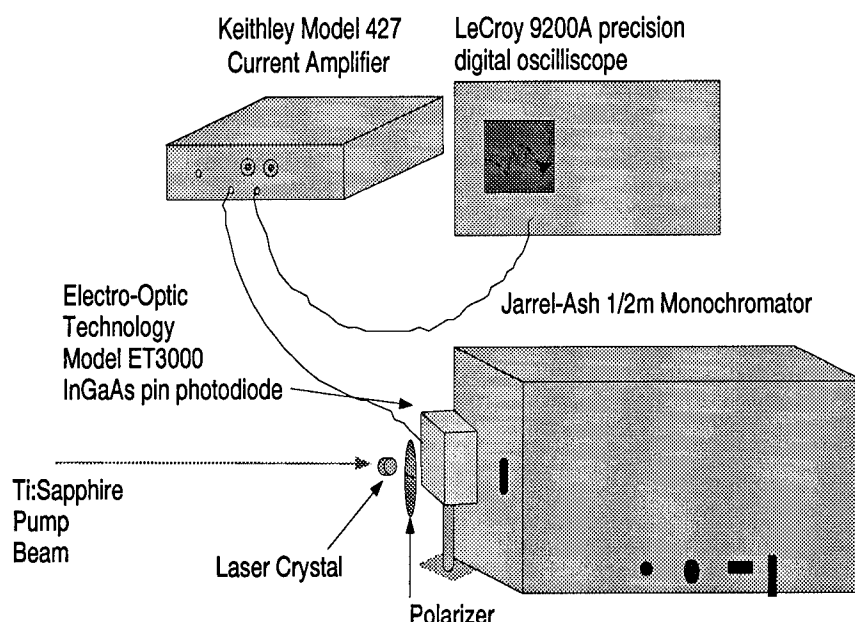


Figure 3.2 Fluorescence measurement setup. The Ti:Sapphire pumped laser crystal was replaced with a black body source for the measurement of the relative wavelength response.

3.2 Fluorescence measurements

Using the peak absorption wavelength for each laser crystal as indicated in Figure 3.1 for a pump source, the polarization-dependent fluorescence was analyzed. The measurements were made with the experimental setup shown in Figure 3.2 on page 3-7. The 0.5 meter Jarrel-Ash monochromator contained a grating blazed for $1.37\mu\text{m}$. The measurement results are shown in Figure 3.3 and 3.4 and they indicate the wavelengths where each crystal will lase. These results also give an indication about the number of transitions that are possible and their relative strength.

The multiple wavelengths present in the Nd:YAG and Nd:YLF emission are in part due to the splitting of the $^4F_{3/2}$ and $^4I_{11/2}$ multiplets. This splitting is present in Nd:SVAP, but the Stark splitting is unusually large and so the emission is dominated by a single transition. This transition is stronger than in Nd:YAG because it occurs from the heavily populated lower level. This lower level is more heavily populated

than the equivalent levels in Nd:YAG due to the Boltzmann distribution of the excited ions in the $^4F_{3/2}$ multiplet (13:44; 17:376).

The fluorescence spectra have been corrected for the relative wavelength response of the measurement setup. The wavelength response was measured by placing a calibrated blackbody source at a temperature of 1000°C in front of the aperture. This source was directed straight into the monochromator with no reflections. The system's relative response, shown in Figure 3.5 on page 3-11, was calculated by dividing the measurement of the output of the blackbody source by the theoretical radiance from a blackbody. The spectrum for each material was essentially corrected by dividing the measured spectrum by the relative response.

Since there was no detector available which could measure both the 1.32 μ m emission from the laser crystal and the output from a calibration lamp, calibration of the wavelength scale in the emission measurements was a two-step process. The monochromator counter reading was calibrated using a neon lamp. The location of the lines in the second and third order of the grating were used to calibrate the counter in the vicinity of 1.06 μ m and 1.32 μ m. During a spectrum measurement, the output of the detector was amplified using a current amplifier and then recorded using the LeCroy 9200A oscilloscope. This recorded output was matched to the monochromator dial setting by passing a bright light over the detector when the monochromator dial passed through specific points before and after the wavelength regions of interest. The measured detector trace then contained two spikes which corresponded to specific dial settings on the monochromator allowing the calculation of dial settings for each point in the trace. The dial settings were then converted to actual wavelengths from the earlier calibration using a neon lamp.

3.3 *Lifetime measurements*

The fluorescence lifetime, the lifetime of the $^4F_{3/2}$ energy state, was measured in Nd:YAG, Nd:YLF, and Nd:SVAP with the setup shown in Figure 3.6. The results

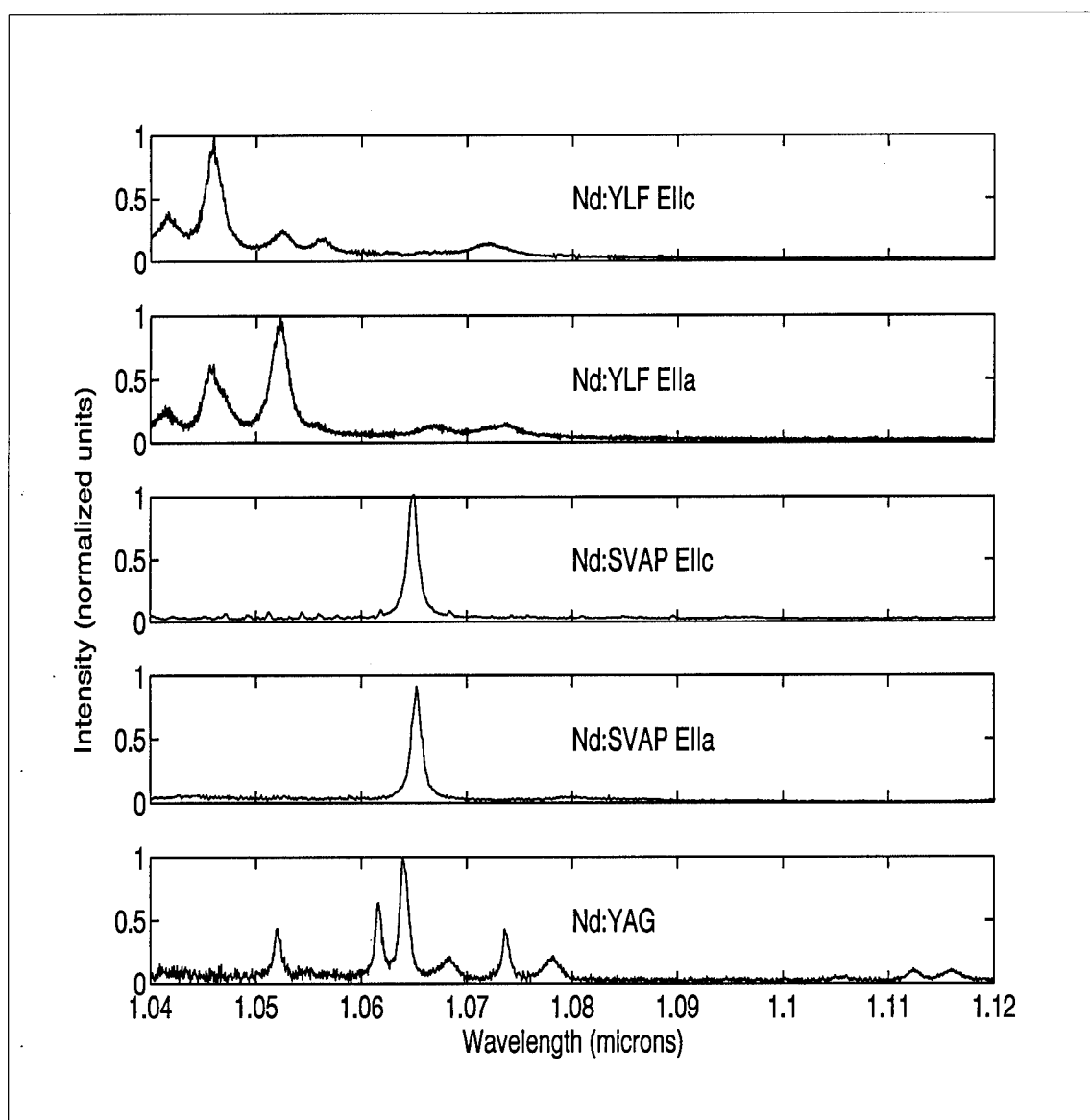


Figure 3.3 Fluorescence spectra for Nd:YAG, Nd:YLF, and Nd:SVAP in the vicinity of $1.06\mu\text{m}$.

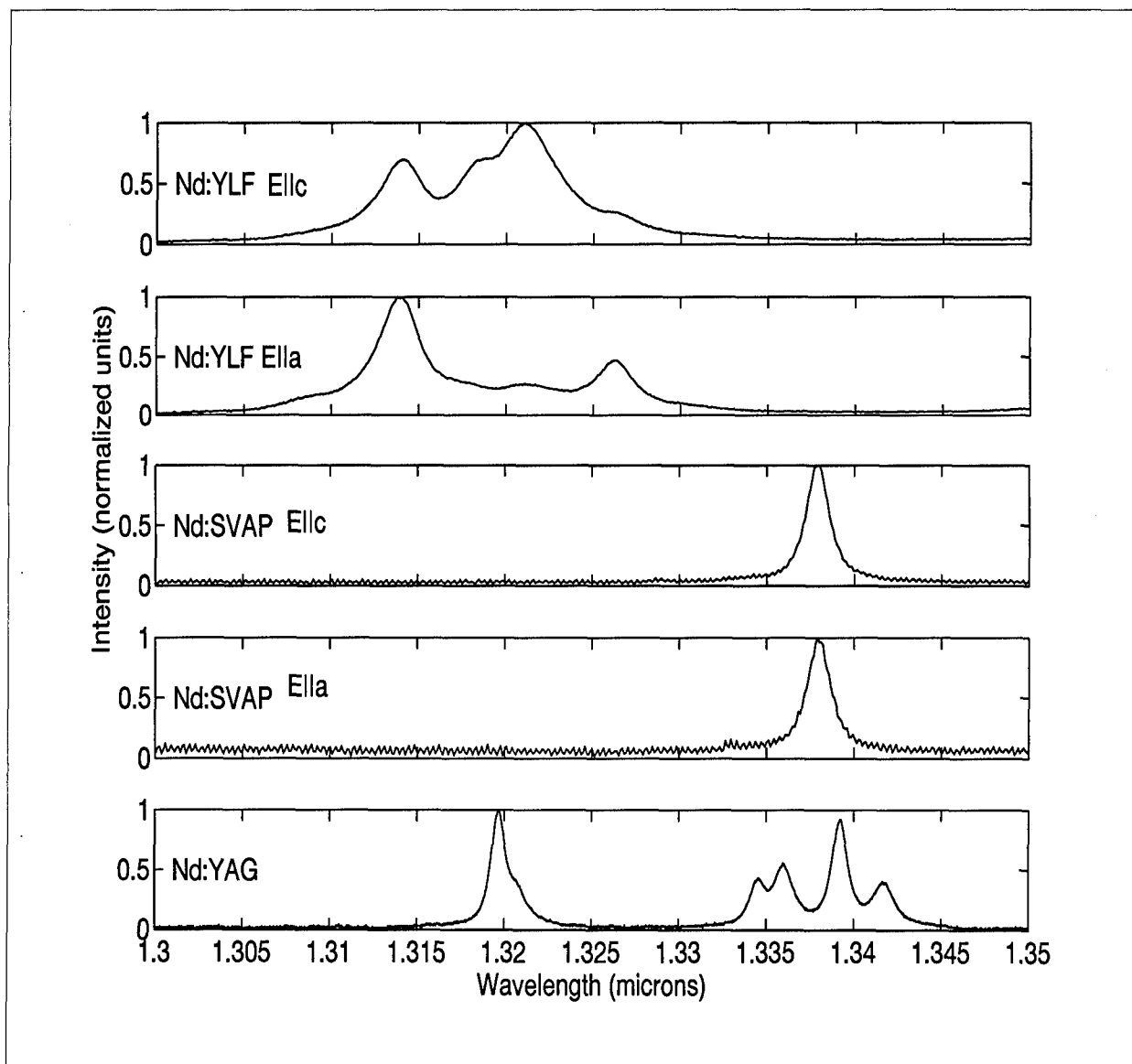


Figure 3.4 Fluorescence spectra for Nd:YAG, Nd:YLF, and Nd:SVAP in the vicinity of $1.32\mu\text{m}$.

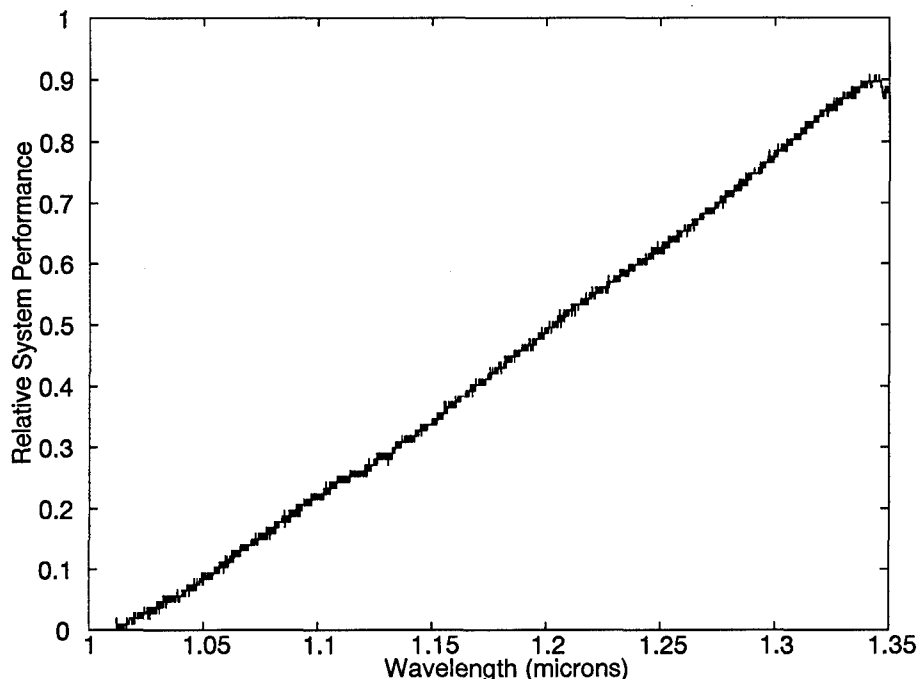


Figure 3.5 Relative system response of the setup used to measure the fluorescence spectra from each laser crystal.

are plotted on a log scale in Figures 3.7-3.9. The measured lifetimes for Nd:YAG and Nd:SVAP are within 1.5% of the published values. The measured lifetime for Nd:YLF which was $504\mu\text{s}$, however, is 5% higher than the typical published value of $480\mu\text{s}$ but is still under the value of $520\mu\text{s}$ quoted by Dallas as typical (28:6374) (I have not found any other publications which support his value). One possible explanation for this larger measured value is radiation trapping. The lifetime of $^4\text{I}_{11/2}$ energy level in Nd:YLF is 20ns, three orders of magnitude larger than the 225ps in Nd:YAG. The population residing in this lower energy state is available for reabsorption - re-emission causing the lifetime to appear longer than it actually is.

The measured decay signal was corrected by subtracting the zero-offset bias from the detector signal and finding the best straight line to the log of the intensity

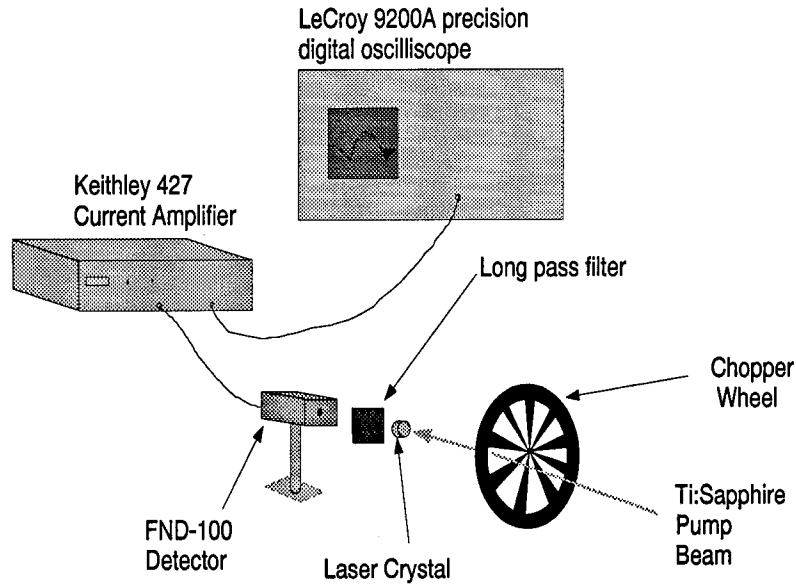


Figure 3.6 Experimental setup for measuring the fluorescence lifetime of Nd:YAG, Nd:YLF, and Nd:SVAP

versus time. With the pump beam blocked, the intensity is assumed to decay as:

$$I(t) = I_o \exp\left(-\frac{t}{\tau_f}\right) \quad (3.1)$$

where τ_f is the fluorescence lifetime, the lifetime of the upper population level. Taking the natural logarithm of the above equation yields a straight line with a slope equal to the fluorescence lifetime. The displayed curve for Nd:YAG is the result of averaging 100 traces on the digital oscilloscope; the curves for Nd:YLF and Nd:SVAP are the average of 200 traces. The error from the curve fit was less than $1 \mu\text{s}$ for each lifetime measurement.

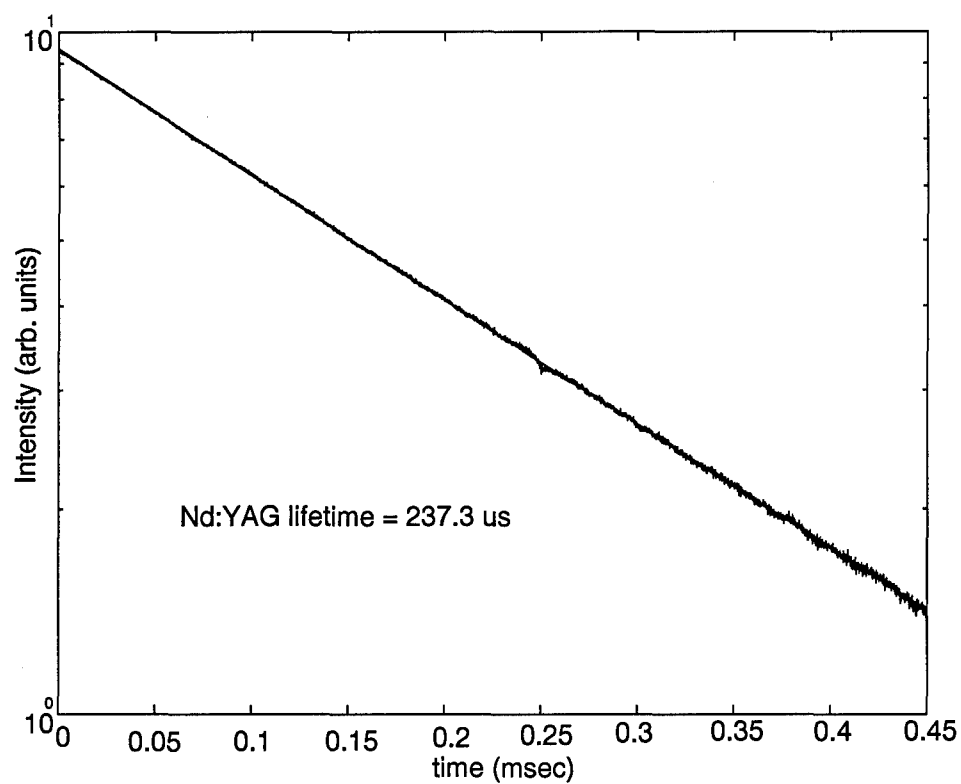


Figure 3.7 Lifetime measurement of Nd:YAG. Both best fit as well as the measured decay curve are shown (they overlap). The displayed data is the average of 100 traces taken with the oscilloscope. The chopper speed used in this measurement was 2394 Hz.

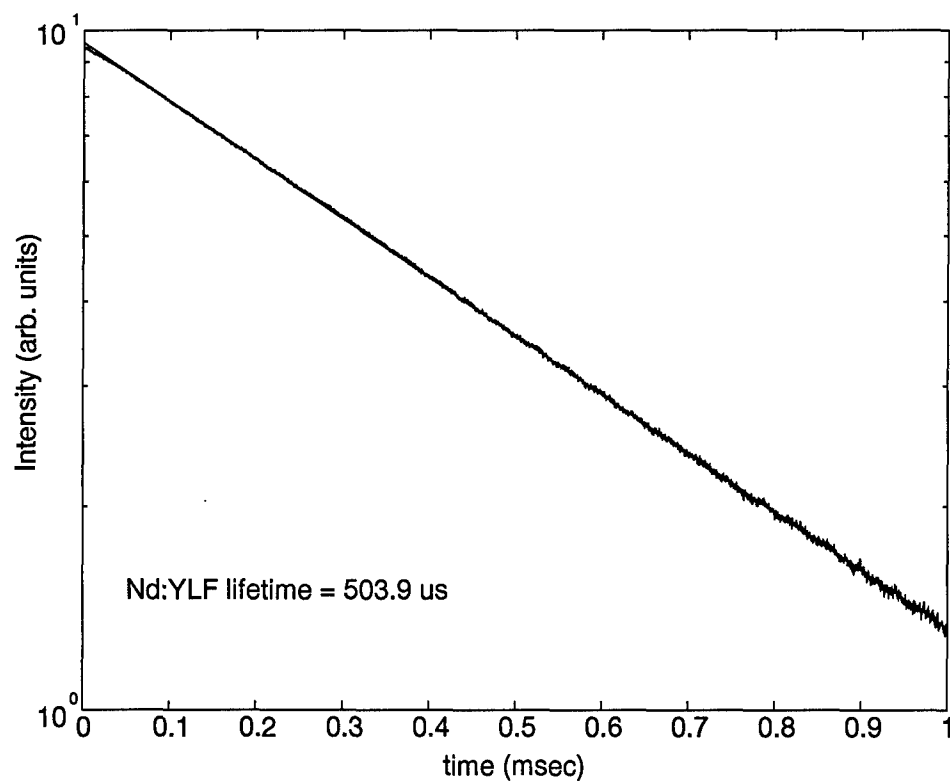


Figure 3.8 Lifetime measurement of Nd:YLF. Both best fit as well as the measured decay curve are shown (they overlap). The displayed data is the average of 200 traces taken with the oscilloscope. The chopper speed used in this measurement was 1104 Hz.

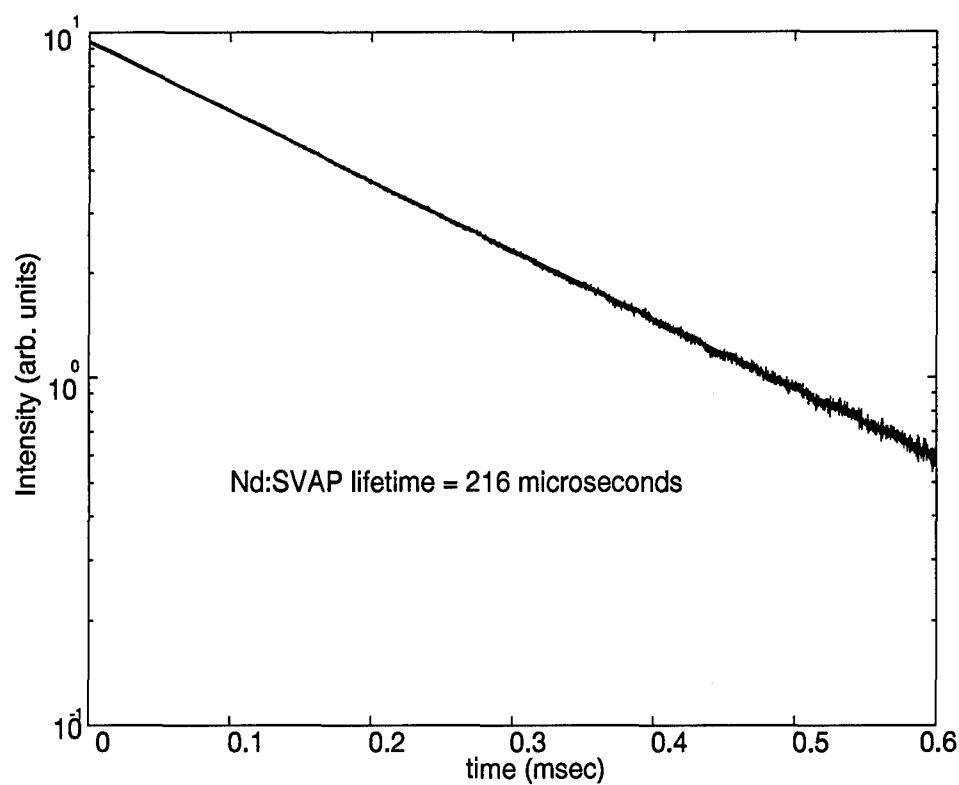


Figure 3.9 Lifetime measurement of Nd:SVAP. Both best fit as well as the measured decay curve are shown (they overlap). The displayed data is the average of 200 traces taken with the oscilloscope. The chopper speed used in this measurement was 2112 Hz.

IV. *Experimental results & analysis*

4.1 *Experimental setup*

A perspective view of the optical setup is shown in Figure 4.1 and it shows the Burleigh Wavemeter used to monitor the wavelength of the Ti:Sapphire pump beam. This setup proved extremely convenient for accurately tuning the wavelength of the Ti:Sapphire to the wavelength of peak absorption in each crystal. The neutral density filter wheel was used to vary the incident pump power into the cavity. The alignment of the Ti:Sapphire pump beam and the calculation of the position of the 30cm focusing lens is covered in Appendix A. The dichroic beamsplitter in the "Y" cavity configuration is used to separate the two different wavelengths. Since the dichroic beamsplitter reflects the $1.3\mu\text{m}$, the $1.3\mu\text{m}$ cavity is "L" shaped. The dichroic beamsplitter allows the $1.06\mu\text{m}$ beam to travel through so the $1.06\mu\text{m}$ cavity is straight.

Using thermo-electric coolers, the temperature of the laser crystal was maintained at $19.5\pm 0.5^\circ\text{C}$ for all of the laser materials. Due to the high humidity in the laboratory, water started to condense on the mount if the temperature was dropped more than 5°C below room temperature. This prohibited any investigations into the temperature sensitivity of the laser performance.

4.1.1 Nd:YAG setup. The Nd:YAG crystal was a cylindrical rod 4mm in diameter and 5mm long. The absorption curve in Figure 3.1 indicated that the best pump wavelength was 808nm. The Ti:Sapphire was tuned to this wavelength and focused down into the laser rod. After the cavity was lasing at $1.06\mu\text{m}$, the wavelength was tuned to the point where maximum power was achieved. This wavelength was found to be $808.54\pm 0.6\text{nm}$ as measured with the Burleigh wavemeter. When setting up for Q-switched operation, the optimum angle of the dichroic surface normal with the incident beam was found to be $41.8\pm 0.3^\circ$ for maximum $1.06\mu\text{m}$ output power.

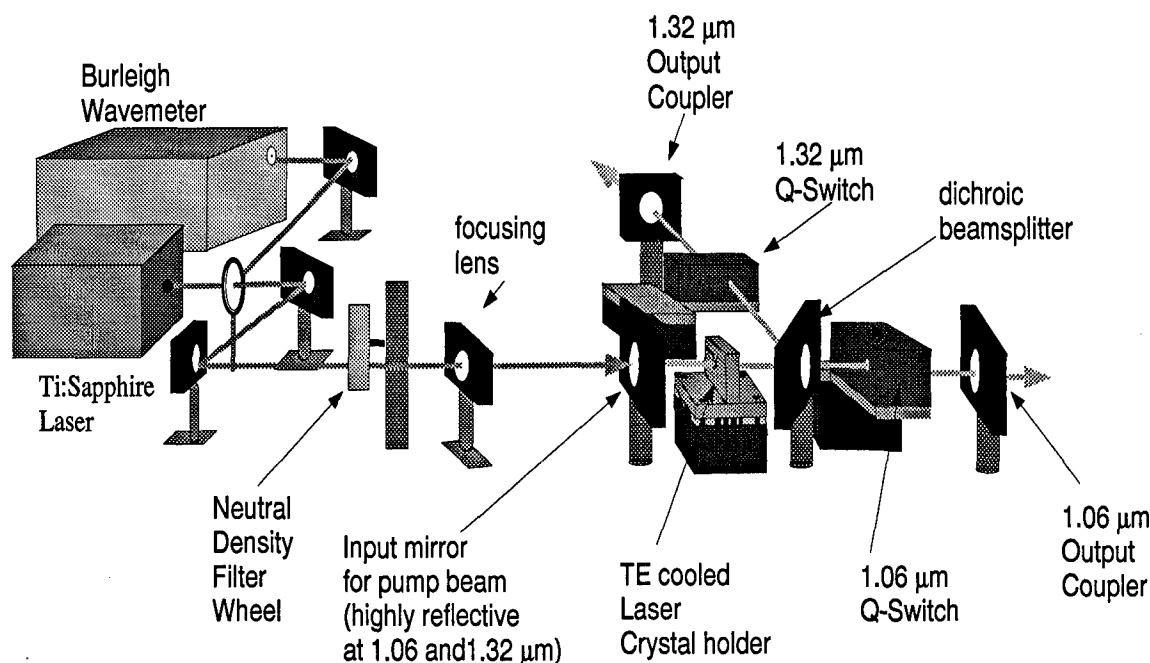


Figure 4.1 Optical setup for the laser system.

4.1.2 Nd:YLF setup. The setup for Nd:YLF proved to be a bit more involved than for Nd:YAG. The Nd:YLF was also a cylindrical rod 4mm in diameter and 5mm long. Nd:YLF, however, is a uniaxial crystal and this particular crystal was an “a-cut” crystal meaning that both polarizations could be accessed. The output from the Ti:Sapphire was linearly polarized with the polarization horizontal to the surface of the optical table. The first step in setting up the cavity for Nd:YLF was to tune the wavelength of the Ti:Sapphire to the peak absorption wavelength of 792nm, as indicated in Figure 3.1. This beam was focused down into the laser rod using the 30cm focal length lens. A protected silver mirror was placed on the other side of the rod to reflect the residual pump beam into a power meter. The rod was then rotated until this transmitted power was minimized. The mirror was removed and the cavity was aligned. Once the 1.047μm cavity was lasing, the wavelength of the Ti:Sapphire was adjusted to achieve maximum power out of the Nd:YLF laser. When setting up for Q-switched operation, the optimum angle of the dichroic surface

normal with the incoming beam for Nd:YLF was found to be $45.0 \pm 0.5^\circ$ for maximum $1.047 \mu\text{m}$ output power.

4.1.3 Nd:SVAP setup. The Nd:SVAP crystal was a 3mm cube and it was also an "a-cut" uniaxial crystal. The brass mount for this crystal was made with the sample 5mm too low. This meant that the top of the high reflector needed to be tilted towards the crystal, the result was that the pump beam had a higher transmission through the high reflector for this location and tilt angle.

This crystal underwent catastrophic failure during the setup for the Q-switch measurements. The amount of incident pump power was approximately 1.0 Watt and the beam diameter in the crystal was $270 \pm 10 \mu\text{m}$. Visually, the damage appeared to be faint fracture lines internal to the crystal.

The failure of the Nd:SVAP crystal brings to light one aspect of the laser material which had not been investigated – manufacturability and durability. The crystal itself was originally to be a 4mm by 4mm crystal but, because of imperfections, was cut down to a 3mm cube. Manufacturers of this type of crystal have found that they tend to fracture during the cutting process so they tend to have a poor yield which contributes to a relatively high cost(12:51).

4.2 Optical component characterization

This next section steps through each component and presents the important transmission measurements for the cavity components and diagnostic optics. To understand and accurately predict the behavior of a laser system, the characteristics of the components which make up that system must be known. As seen in Eq (2.13), predicting the pump power necessary to achieve lasing threshold requires two important values; the amount of loss that each component causes at the laser wavelength, and the percentage of the pump power incident onto the cavity which is actually absorbed in the laser gain medium.

Table 4.1 Transmission of the cavity high reflector for the different wavelengths.

Laser crystal	T_{HR} Transmission	Wavelength (nm)
Nd:YAG	0.74 ± 0.01	808.1nm 0° angle of incidence
Nd:YLF	0.791 ± 0.006	792.1nm
Nd:SVAP	0.821 ± 0.001	808.5nm 20° angle of incidence

4.2.1 High reflector. For all of the laser measurements, the power in the incident pump beam was measured after the 30cm focusing lens. Traveling to the right toward the laser crystal, the pump beam initially passes through the high reflector. The transmission measurements of the high reflector η_{HR} at the pump wavelengths for the various laser crystals are shown in Table 4.1.

The high reflector is also the first element in both laser cavities. The reflectivity of this element at $1.06\mu\text{m}$ was measured to be

$$\Gamma_{HR} = 0.9998 \pm 0.0001$$

where the reflectivity Γ was calculated from the transmission using $\Gamma = 1 - T$ (this assumes no absorption loss). The uncertainty was derived from the standard deviation of multiple measurements.

4.2.2 Laser Crystal. After passing through the high reflector, the pump beam is incident onto the front face of the laser crystal. The amount of pump power which is reflected from this surface was measured using the setup shown in Figure 4.2. The uncertainties in the reflectivity values came from the standard deviation of multiple measurements. The reflectivity measurements of the different crystals are shown in Table 4.2.

After passing through the bulk of the laser crystal, the pump beam exits the back face, which is assumed to have the same power reflectivity as the front face. Two

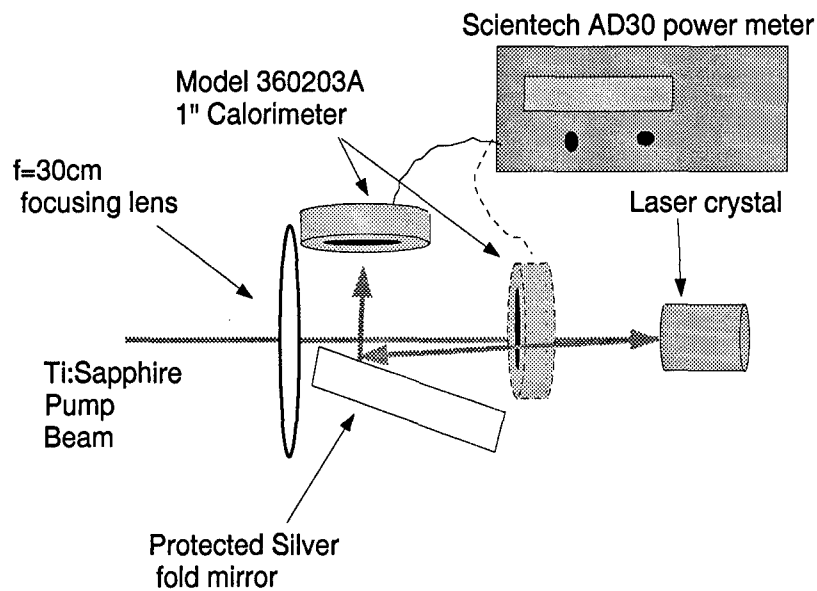


Figure 4.2 Setup for the transmission measurements of the laser crystals.

Table 4.2 Reflectivity of laser crystals at the appropriate pump wavelength.

Laser crystal	Γ_{LC} Reflectivity	Wavelength (nm)
Nd:YAG	0.0498 ± 0.0002	808.1nm
Nd:YLF	0.0050 ± 0.0008	792.1nm
Nd:SVAP	0.042 ± 0.001	808.5nm

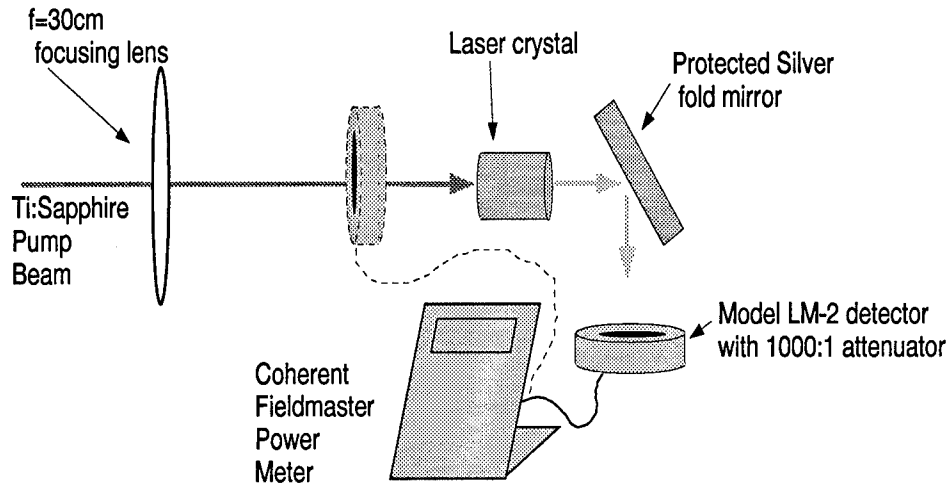


Figure 4.3 Setup for the absorptance measurements of the laser crystals.

values of power were used to calculate the transmission at the pump wavelength. The locations where they were measured are shown in Figure 4.3. The power measured after the crystal must be corrected for the percentage reflected off of the back face in order to accurately calculate, η_{Abs} . The fraction of incident power actually absorbed in the crystal is given by

$$\eta_{Abs} = \frac{P_{incident} (1 - \Gamma_{LC}) - \frac{P_{transmitted}}{(1 - \Gamma_{LC})}}{P_{incident}}$$

The average absorptance of each laser crystal was measured at its pump wavelength using the experimental setup shown in Figure 4.3 on page 4-6. The results are shown in Table 4.3 on page 4-7. The expression for calculating the amount of pump power absorbed in the laser crystal from the value of the pump power measured before the high reflector becomes

$$P_{Absorbed} = \eta_{Abs} \eta_{HR} P_{incident} \quad (4.1)$$

Table 4.3 Absorptance of laser crystals at the appropriate pump wavelength.

Laser crystal	η_{Abs} Absorptance	Wavelength
Nd:YAG	0.88 ± 0.01	808.1nm
Nd:YLF	0.996 ± 0.001	792.1nm
Nd:SVAP	0.923 ± 0.009	808.5nm

4.2.3 *Dichroic beamsplitter.* The transmission of the dichroic beamsplitter measured at $1.064\mu\text{m}$ using the unpolarized output of the Nd:YAG laser was

$$T_{Dichroic(Nd:YAG)} = 0.90 \pm 0.02$$

The amount of power reflected by the dichroic was measured while it was lasing in the Nd:YLF cavity at the optimum angle. The amount of $1.047\mu\text{m}$ output power was back propogated into the cavity to calculate the amount of power traveling to the left and right in the cavity just on the other side of the output coupler. The amount of power reflected by the output coupler was calculated from the reflectivity of the output coupler and the output power. This reflected power was used as the incident value onto the dichroic beamsplitter. The transmission, calculated by comparing this value with the power reflected by the dichroic beamsplitter, was

$$T_{Dichroic(Nd:YLF)} = 0.982 \pm 0.002$$

The wavelength and polarization dependent transmission of the dichroic beamsplitter was also measured using a Perkin Elmer Lambda 9 Spectrophotometer. These results are shown for $1.06\mu\text{m}$ in Figure 4.4. These curves tended to shift horizontally in wavelength as the incident angle was changed. This effect caused the dichroic beamsplitter to have a different optimum angle in the cavity than Nd:YLF.

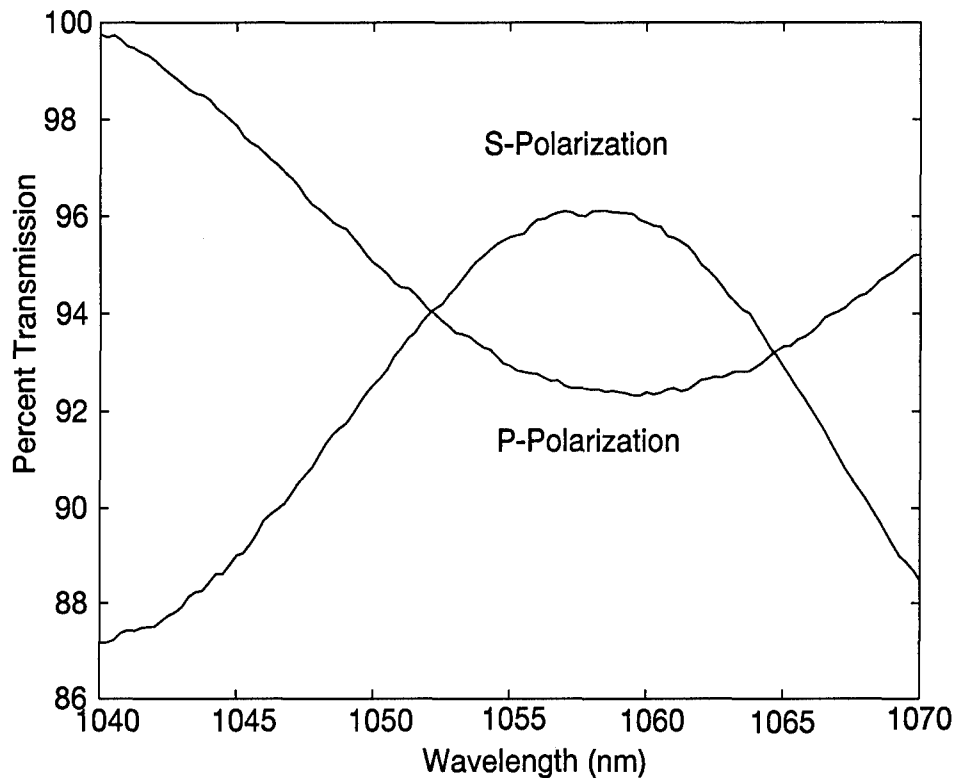


Figure 4.4 Transmission of the dichroic beamsplitter in the vicinity of $1.06\mu\text{m}$ at 45° angle of incidence. These curves demonstrate the relative transmission levels at different wavelengths and were taken with a Perkin Elmer Lambda 9 UV/VIS/NIR Spectrophotometer.

The transmission was also measured in the vicinity of $1.3\mu\text{m}$ with the values converted to a reflectivity using $\Gamma=1-T$; the results are shown in Figure 4.5 on page 4-9.

4.2.4 *Q-switches.* The transmission of the $1.06\mu\text{m}$ Q-switch was measured with the output of the Nd:YAG laser and found to be

$$T_{106QS} = 0.95 \pm 0.02$$

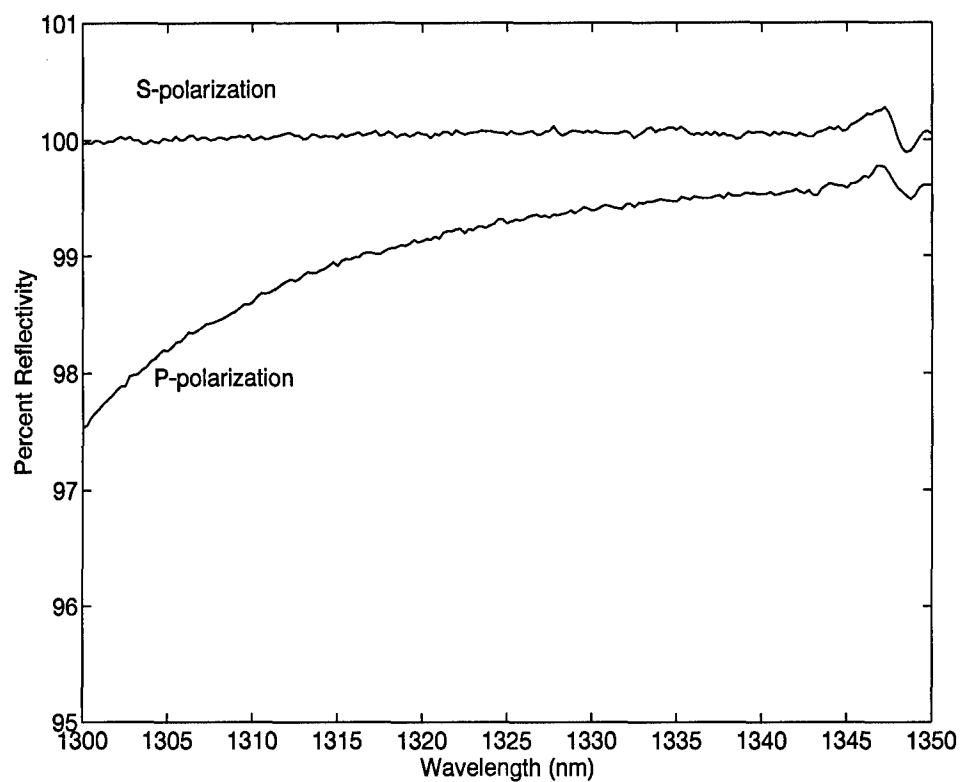


Figure 4.5 Reflectivity of the dichroic beamsplitter in the vicinity of $1.32\mu\text{m}$ at 45° angle of incidence. These measurements were made with a Perkin Elmer Lambda 9 UV/VIS/NIR Spectrophotometer.

Table 4.4 Transmission of the long pass filter at the laser wavelengths

λ	Transmission T_{LP}
$1.047\mu\text{m}$	0.58 ± 0.01
$1.064\mu\text{m}$	0.636 ± 0.006
$1.32\mu\text{m}$	0.856 ± 0.005

The transmission of both Q-switches was also measured with the Perkin Elmer Lambda 9 Spectrophotometer and the results were

$$T_{106QS} = 0.98 \pm 0.5$$

and

$$T_{132QS} = 0.98 \pm 0.8$$

4.2.5 Output couplers. The reflectivities of the two $1.06\mu\text{m}$ output couplers were measured as

$$\Gamma_{95\%} = 0.95 \pm 0.01$$

$$\Gamma_{70\%} = 0.700 \pm 0.008$$

4.2.6 Diagnostic optics. To filter out the pump wavelength the output of each laser was passed through a long pass filter made from Schott RG-1000 glass. The transmission of this optic at the laser wavelengths was measured and the results are shown in Table 4.4.

The reflectivity of the protected silver fold mirrors, used to direct the laser beam into the power meter, was measured at an incident angle of 45° to be

$$\Gamma_{fold} = 0.953 \pm 0.005$$

where the uncertainty is derived from multiple measurements.

4.3 CW laser Performance

This section presents the results from measurements made with the laser cavity lasing in CW mode. The results are used to verify the amount of loss caused by each element in the laser cavity and to estimate the pumping efficiency. Both the pumping efficiency and the cavity loss values are necessary to accurately model the Q-switched laser performance.

The first set of CW measurements were made with only the laser crystal in the laser cavity. These measurements can be used to estimate the combined loss from the high reflector and from the laser crystal. Eq (2.14) on page 2-7 gives an equation for determining the cavity loss from measurements of the laser pump threshold for different output coupler reflectivities. Two output coupler reflectivities, 95% and 70% were available for $1.06\mu\text{m}$ measurements but only one, 96%, at $1.3\mu\text{m}$. Threshold measurement results using the available output couplers are shown in Table 4.5. The wavelength measurements at $1.06\mu\text{m}$ were made with the Burleigh Wavemeter, and the wavelength measurements at $1.32\mu\text{m}$ were made with the Jarrel-Ash monochromator. The $1.3\mu\text{m}$ CW output of both Nd:YAG and Nd:YLF contained two wavelengths, which is common for Nd-based lasers operating in the $1.3\mu\text{m}$ region (34:52). Figure 3.4 on page 3-10 shows the measured emission spectra for these materials. Both materials have two dominant energy level transitions that are on the same order of magnitude.

Table 4.5 CW Laser threshold and wavelength data

Output Coupler (% Reflectivity)	λ_p (nm)	Material	λ_L (μm)	$P_{\text{Threshold}}$ (mW)
95	808.1	Nd:YAG	1.064	109 \pm 3
70	808.1	Nd:YAG	1.064	670 \pm 20
96	808.1	Nd:YAG	1.338/1.318	490 \pm 10
95	792.1	Nd:YLF	1.047	78 \pm 2
70	792.1	Nd:YLF	1.047	620 \pm 20
96	792.1	Nd:YLF	1.313/1.321	270 \pm 10
95	808.5	Nd:SVAP	1.065	82 \pm 2
96	808.5	Nd:SVAP	1.337	280 \pm 10

Table 4.6 Estimates for $2\eta_{\text{efficiency}}l_g\sigma_{SE\tau_f}/h\nu_L V_{00}$ and residual cavity loss (L)

Material	$\frac{2\eta_{\text{efficiency}}l_g\sigma_{SE\tau_f}}{h\nu_L V_{00}}$	L
Nd:YAG	0.545	0.011 \pm 0.003
Nd:YLF	0.561	-0.005 \pm 0.002

The two threshold values at 1.06 μm for Nd:YAG and at 1.047 μm for Nd:YLF were used in Eq (2.14) to determine a value for the total cavity loss for each crystal. The results of these calculations are shown in Table 4.6. The total cavity loss (excluding the output coupler) for both crystals is extremely small. The value for Nd:YLF is less than zero, which implies gain. Since this is not possible, there must be some uncertainty in the threshold pump powers that is not evident from the measurements.

The next set of CW measurements were power conversion measurements (output laser power versus input pump power), and these were also made using the simple cavity configuration. The data from these measurements is plotted in Figures 4.6 and 4.7. As expected, the increased fluorescence lifetime in Nd:YLF produces a lower threshold and higher output for a given pump power than Nd:YAG – but not as high

as would be predicted from a material with over twice the fluorescence lifetime. The poor slope efficiency performance of Nd:SVAP at $1.06\mu\text{m}$ is unexpected because it has a higher stimulated emission cross section-fluorescence lifetime product for the $1.06\mu\text{m}$ transition than Nd:YAG but less than that of Nd:YLF. This relative performance is reflected in the $1.3\mu\text{m}$ results. Although there is no published cross section for Nd:SVAP at $1.3\mu\text{m}$, based on the results shown in Figure 4.7 and the threshold measurement results in Table 4.5, the cross section should be much larger than both Nd:YAG and Nd:YLF. Comparing the threshold pump power of Nd:SVAP with Nd:YLF from Table 4.5, shows the threshold for Nd:SVAP is only 4mW higher in the identical cavity. Since the threshold pump power is inversely proportional to the product of the stimulated emission cross section and fluorescence lifetime and since the lifetime of Nd:YLF is over twice that of Nd:SVAP, the conclusion is that Nd:SVAP has a much higher cross section.

The $1.05\mu\text{m}$ output of the Nd:YLF crystal was found to be polarized at least 1000:1, which was based on measurements with a calcite polarizer. This polarization was along the optic axis of the crystal oriented horizontal to the table. This orientation was required in order to be aligned with the polarization of the Ti:Sapphire pump laser (as described in subsection 4.1.2).

The last set of CW measurements focus on only the Nd:YAG cavity and were designed to provide an additional measurement of the intracavity loss caused by each component. Table 4.7 shows the measured slope efficiencies and power thresholds when different components are placed in the cavity. These values correspond to the laser output power vs absorbed pump power curves shown in Figure 4.8 on page 4-17. The pump threshold values were calculated from the curves by extrapolating them to the horizontal axis. Figure 4.8 shows the increase in threshold pump power as each element is added to the cavity. The cavity containing both the Q-switch and the dichroic beamsplitter is identical to the one used to make the Q-switch

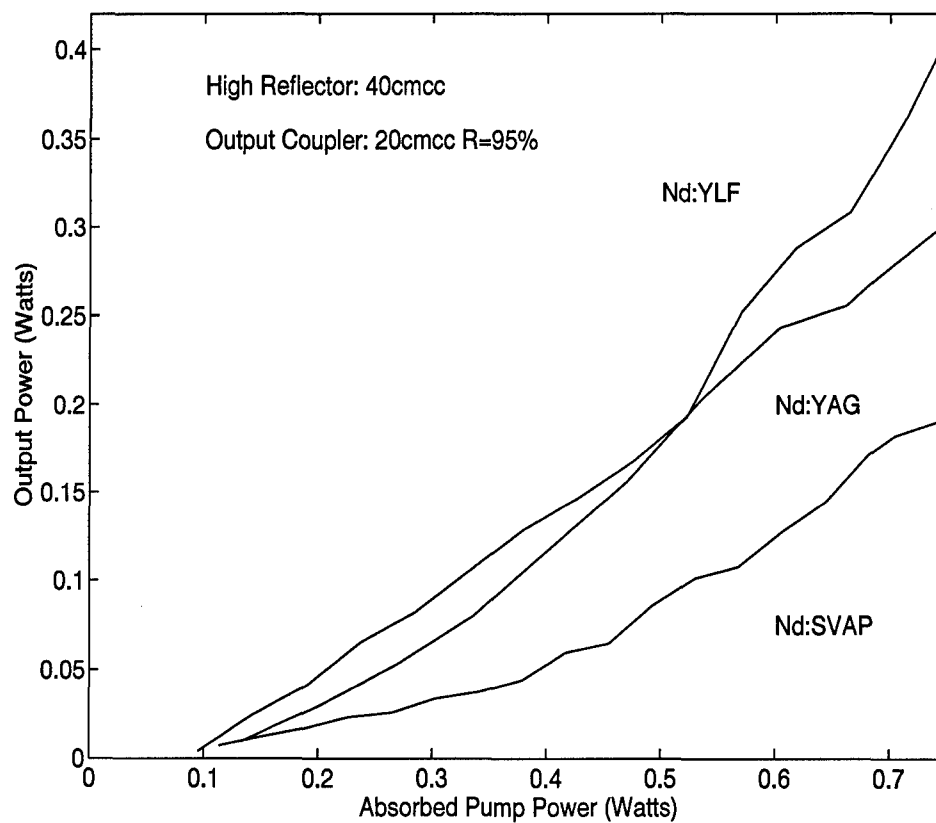


Figure 4.6 Power conversion measurements for $1.06\mu\text{m}$. The same cavity was used for each material.

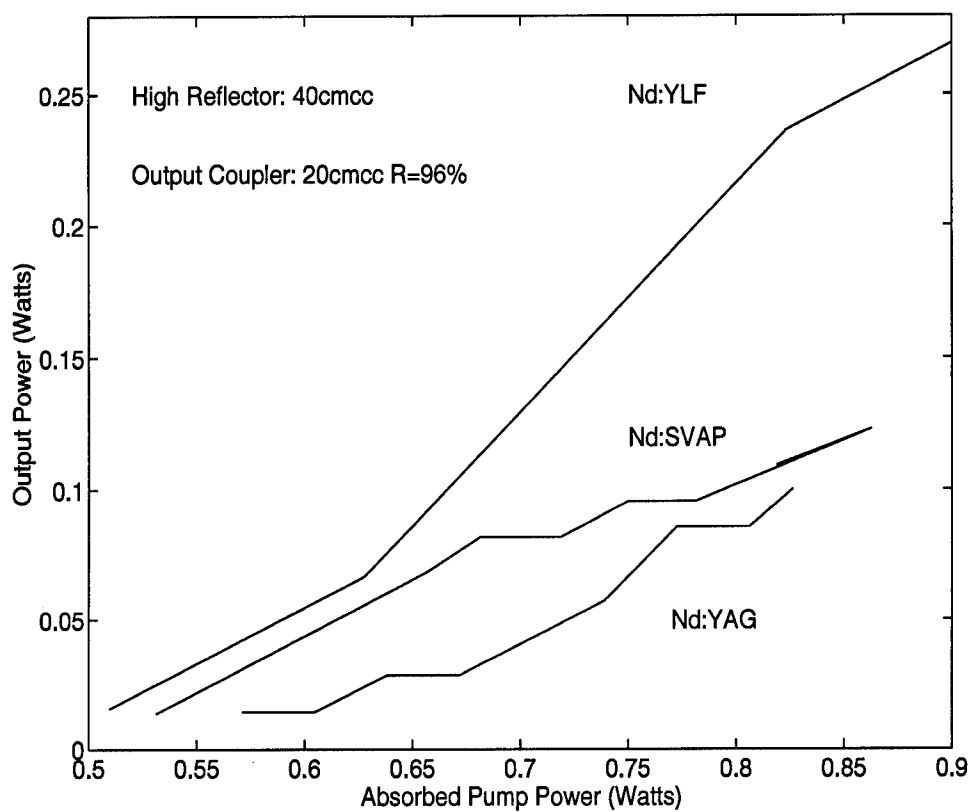


Figure 4.7 Power conversion measurements for $1.32\mu\text{m}$. The same cavity was used for each material.

measurements, and so a measurement of the loss in this cavity is useful in predicting the Q-switched laser performance.

The equation for the CW laser threshold in Eq (2.13) can be used to determine the unknown loss caused by a cavity element. The equation for the threshold pump power when all of the cavity losses are known is given by

$$P_{Thresh_1} = \frac{-V_{00}h\nu_L \ln \left(\sqrt{\Gamma_2 \Gamma_1 T_{Known}^2} \right)}{\sigma_{SE} \tau_f \eta_{efficiency} l_g} \quad (4.2)$$

where T_{Known} is the known one way transmission of the components in the cavity. The threshold pump power for a cavity containing an unknown loss is

$$P_{Thresh_2} = \frac{-V_{00}h\nu_L \ln \left(\sqrt{\Gamma_2 \Gamma_1 T_{Unknown}^2 T_{Known}^2} \right)}{\sigma_{SE} \tau_f \eta_{efficiency} l_g} \quad (4.3)$$

where $T_{Unknown}$ is the unknown one way transmission of the added component(s). Taking the ratio of these two equations and solving for $T_{Unknown}$ yields

$$T_{Unknown} = \frac{\exp \left\{ \frac{P_{Thresh_2}}{P_{Thresh_1}} \ln \left(\sqrt{\Gamma_1 \Gamma_2 T_{Known}^2} \right) \right\}}{\sqrt{\Gamma_1 \Gamma_2 T_{Known}^2}} \quad (4.4)$$

This expression was used to calculate the transmission values of the different components presented in Table 4.7. The value for the transmission of the dichroic calculated from the lasing threshold of the Nd:YAG laser is within the experimental uncertainty of the value measured with the unpolarized Nd:YAG output as a source (see subsection 4.2.3 on page 4-6). The value for the transmission of the 1.06 μ m Q-switch calculated from the threshold change (Table 4.7) is 4% higher than the value measured in subsection 4.2.4. There are two possible explanations. The first is a problem that plagued measurements throughout this work, and that is contamination. When the beam sizes are on the order of less than a millimeter, the dust particles in the air have a significant impact on power measurements. A small dust

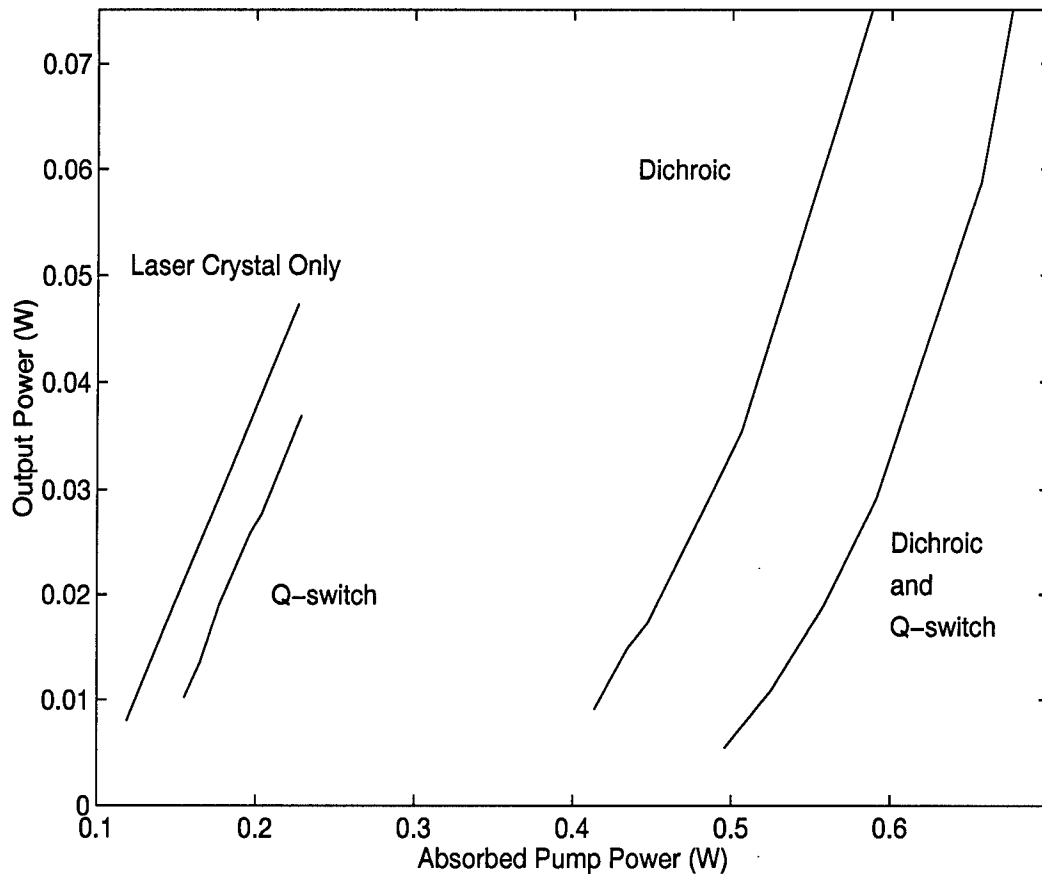


Figure 4.8 Power conversion measurements for Nd:YAG at $1.06\mu\text{m}$ with different combinations of components in the cavity.

particle on either face of the dichroic could significantly effect the transmission and cause it to be lower than actual. The second possible explanation is that by placing the Q-switch into the cavity, with its refractive index on the order of 1.68, it caused the effective cavity length to decrease. Decreasing the effective cavity length causes the cavity to become more stable, it also increases the effective spot size of the laser mode in the laser crystal. If the pump beam size was larger than the laser mode in the laser crystal, increasing the laser mode size would increase the beam overlap efficiency according to Eq (2.10) on page 2-6.

Figures 4.9 and 4.10 show the change in the output power curve for Nd:YAG and Nd:YLF, respectively, when the output coupler reflectivity is changed from 70%

Table 4.7 Nd:YAG laser threshold measurements with different combinations of components in the cavity.

Components in the cavity	Wavelength (μm)	Slope Efficiency %	Threshold Pump Power (W)	Transmission of element(s) %
Laser crystal only	1.06	36.4 ± 0.09	0.1041 ± 0.0002	99.2 (Table 4.6)
Dichroic	1.06	29.0 ± 1	0.40 ± 0.006	91.9
Q-switch	1.06	36.4 ± 0.8	0.134 ± 0.001	99.2
Q-switch and Dichroic	1.06	33 ± 4	0.502 ± 0.008	89.3
Dichroic	1.32	$81 \pm 3.$	0.640 ± 0.001	
Q-switch	1.32	75 ± 0.2	0.699 ± 0.002	99.8

to 95%. Examining the curves, the slope efficiency does not change between the output coupler values. The reason for this is found by examining the equation for the slope efficiency (Eq (2.9)), repeated here for convenience

$$\sigma_S = \frac{(1 - \Gamma_2)\eta_{efficiency}}{\left[1 + \sqrt{\frac{\Gamma_2}{\Gamma_1 T_{Comp}^2}}\right] \left[1 - \sqrt{\Gamma_1 \Gamma_2 T_{Comp}^2}\right] \lambda_L}$$

If the greatest loss is due to the output coupler and the other components in the cavity have very little loss, that is their collective transmission is close to 1, then the slope efficiency becomes

$$\sigma_S = \frac{(1 - \Gamma_2)\eta_{efficiency}}{(1 + \sqrt{\Gamma_2})(1 - \sqrt{\Gamma_2})\lambda_L}$$

Combining the two expressions in the denominator, this becomes,

$$\sigma_S = \frac{\eta_{efficiency}}{\lambda_L}$$

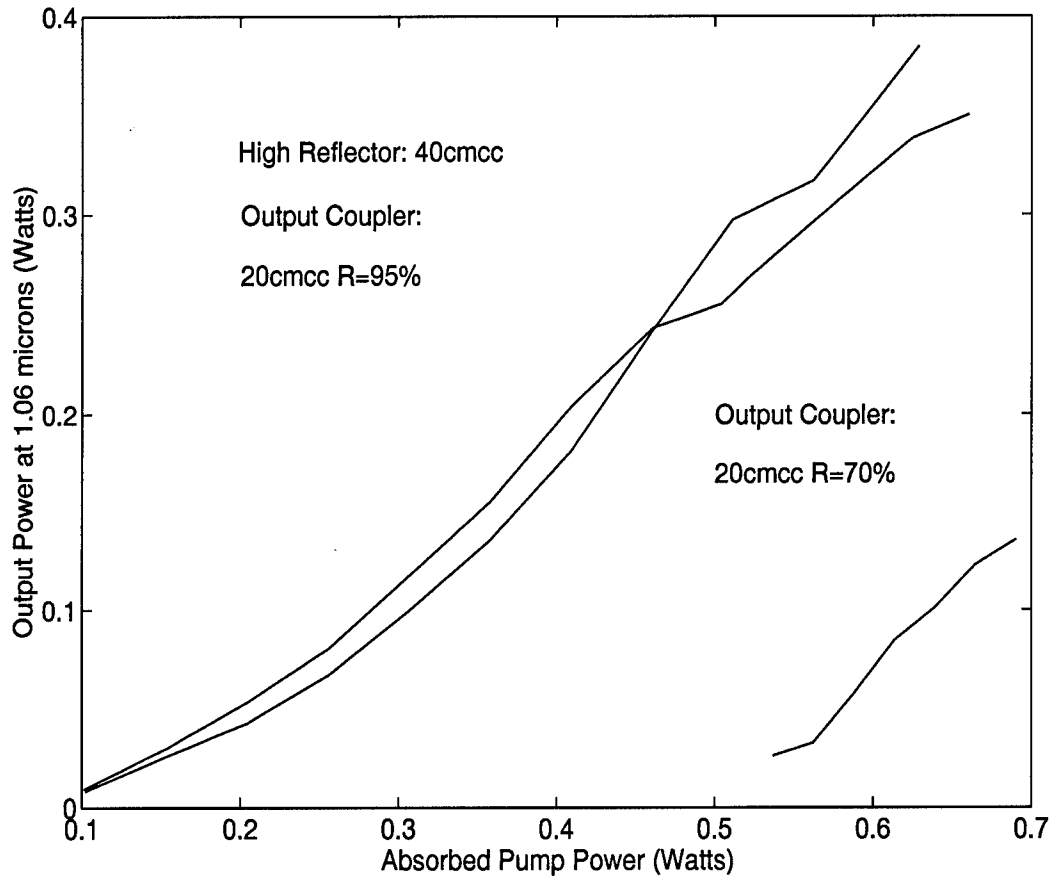


Figure 4.9 Power conversion measurements for Nd:YAG at $1.06\mu\text{m}$ for two different output couplers. The two overlapping curves on top for the 95% reflective coupler are simply repeated measurements and they demonstrate the repeatability. The curve to the right was measured using a 70% reflective output coupler.

which is independent of the output coupler reflectivity. From the similar slope efficiencies for the two output coupler values shown in Figures 4.9 and 4.10, it can be concluded that the cavity used to make these measurements was very low loss.

4.4 Single wavelength Q-switched results

This section outlines a set of Q-switched measurements made for Nd:YAG and Nd:YLF while lasing only at one wavelength. In the next section, the model output is fit to the measured results at $1.06\mu\text{m}$ for Nd:YAG using the results from the CW

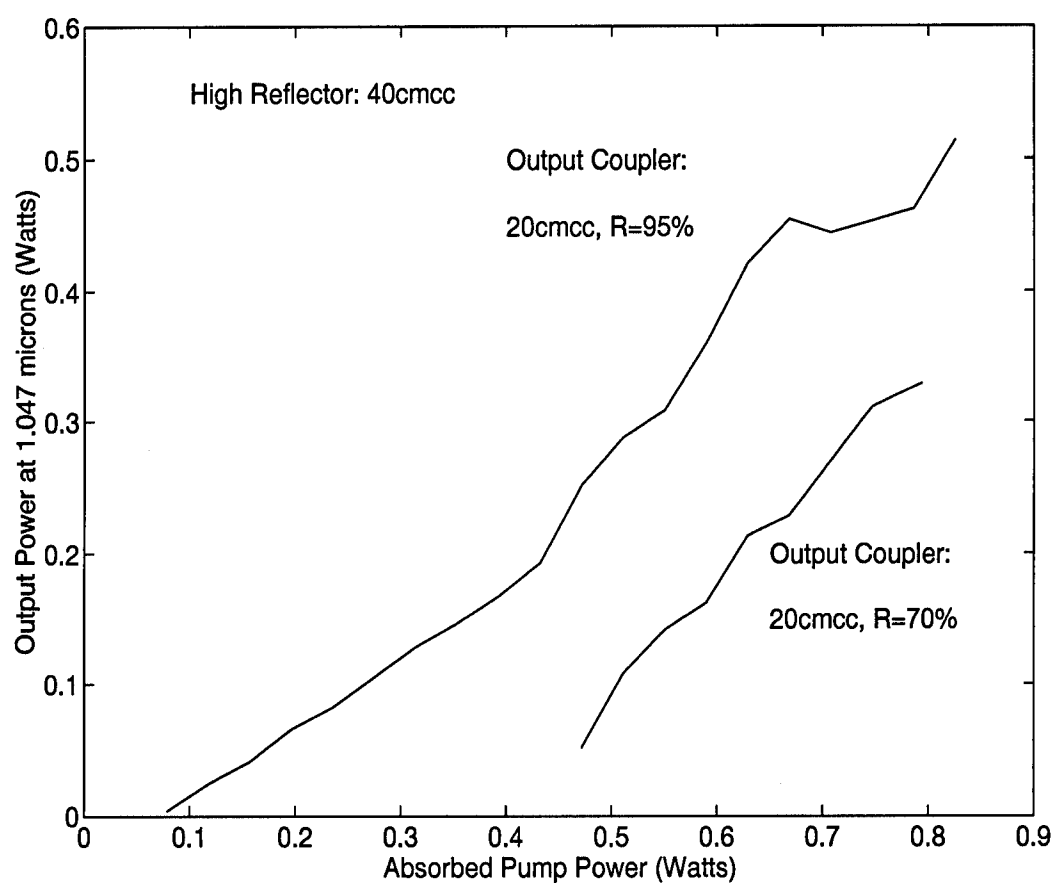


Figure 4.10 Power conversion measurements for Nd:YLF at $1.047\mu\text{m}$ with two different output coupler reflectivities.

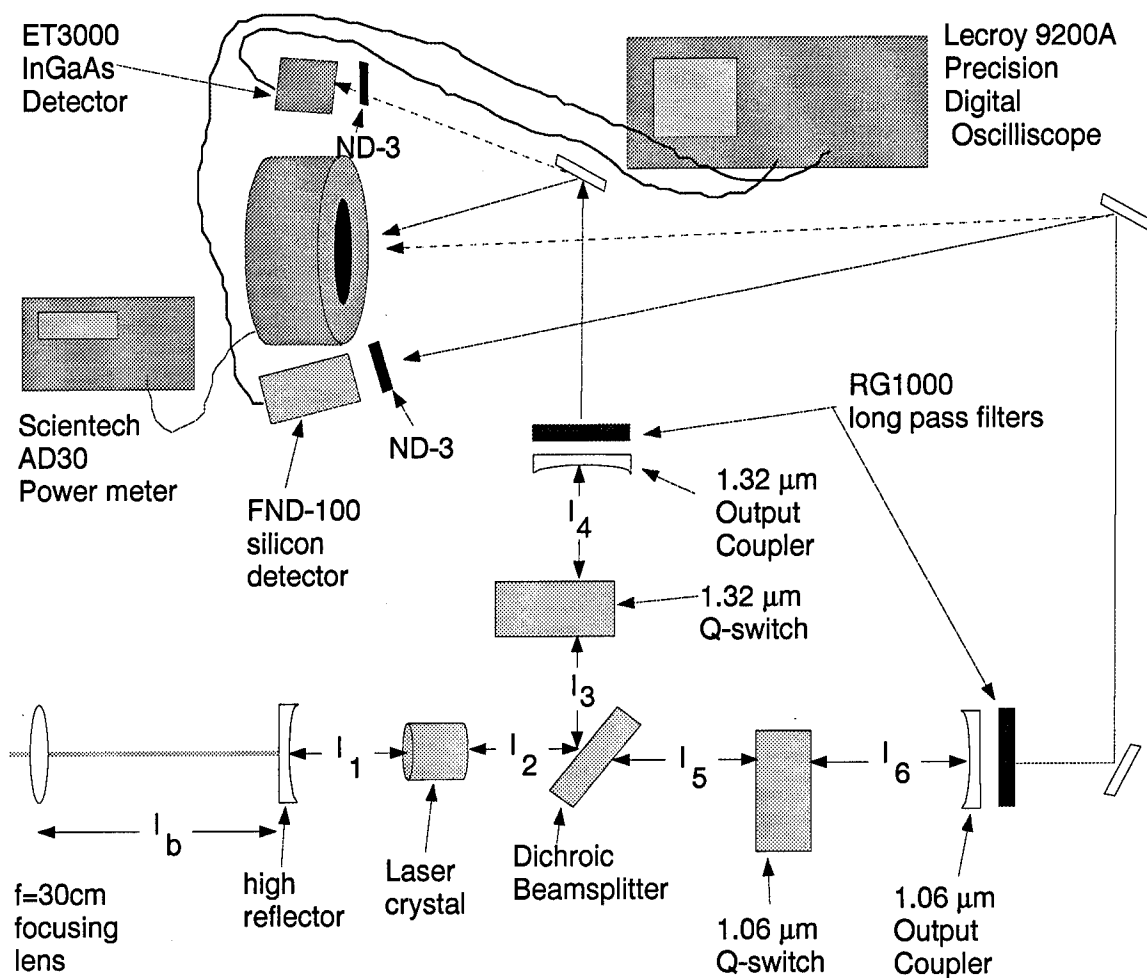


Figure 4.11 Measurement setup for the Q-switched results.

measurements outlined in the last section, the energy measurements presented in this section, and the theory developed in Chapter II. The lasing results for Nd:YAG at $1.3\text{ }\mu\text{m}$ and for Nd:YLF at both $1.047\text{ }\mu\text{m}$ and $1.3\text{ }\mu\text{m}$ are merely presented, no attempt was made to fit the model to the measured results.

Figure 4.11 shows a diagram of the general measurement setup used for all of the Q-switched results. The $1.06\text{ }\mu\text{m}$ results were obtained by placing a beam block in the $1.3\text{ }\mu\text{m}$ cavity and vice versa. The measurements for Nd:YAG at $1.064\text{ }\mu\text{m}$ are

Table 4.8 Q-switched Nd:YAG single wavelength performance at $1.06\mu\text{m}$.

Incident Pump Power (W)	Absorbed Pump Power (W)	Pulse Repetition Rate (Hz)	Pulse Energy (μJ)	Pulse Width (ns)
1.45	0.92 ± 0.03	500	55 ± 2	36.4 ± 0.2
1.45	0.92 ± 0.03	500	56 ± 2	36.3 ± 0.5
1.30	0.83 ± 0.03	500	55 ± 2	40.1 ± 0.8
1.30	0.83 ± 0.03	1000	52 ± 2	42.1 ± 0.6
1.30	0.83 ± 0.03	4000	36 ± 1	57.1 ± 0.8

Table 4.9 Q-switched Nd:YAG single wavelength performance at $1.32\mu\text{m}$.

Incident Pump Power (W)	Absorbed Pump Power (W)	Pulse Repetition Rate (Hz)	Pulse Energy (μJ)	Pulse Width (ns)
1.45	0.92 ± 0.03	500	45 ± 2	235 ± 1
1.45	0.92 ± 0.03	500	58 ± 2	228 ± 4
1.30	0.83 ± 0.03	500	37 ± 1	303 ± 3
1.30	0.83 ± 0.03	1000	35 ± 1	257 ± 5
1.30	0.83 ± 0.03	4000	21.8 ± 0.6	475 ± 4

shown in Table 4.8. Figure 4.12 shows a plot of some of these values along with the results of the model. The cavity measurements are shown in Table 4.10.

The pulse energies were calculated from an average power measurement of the output. There is no commercially available energy meter which can measure the amount of energy in each pulse at repetition rates of over 500Hz. In order to calculate an average pulse energy, the average power of the laser output is divided by the pulse repetition frequency.

Table 4.10 Cavity configuration for the Q-switched Nd:YAG data -long cavity.

$l_1=1.0\text{cm}$	$l_4=6.3\text{cm}$
$l_2=4.2\text{cm}$	$l_5=1.9\text{cm}$
$l_3=4.1\text{cm}$	$l_6=8.5\text{cm}$

	Output coupler	Cavity length
$1.32\mu\text{m}$	T=4%, 20cmcc	17.7cm
$1.06\mu\text{m}$	T=5%, 20cmcc	18.8cm

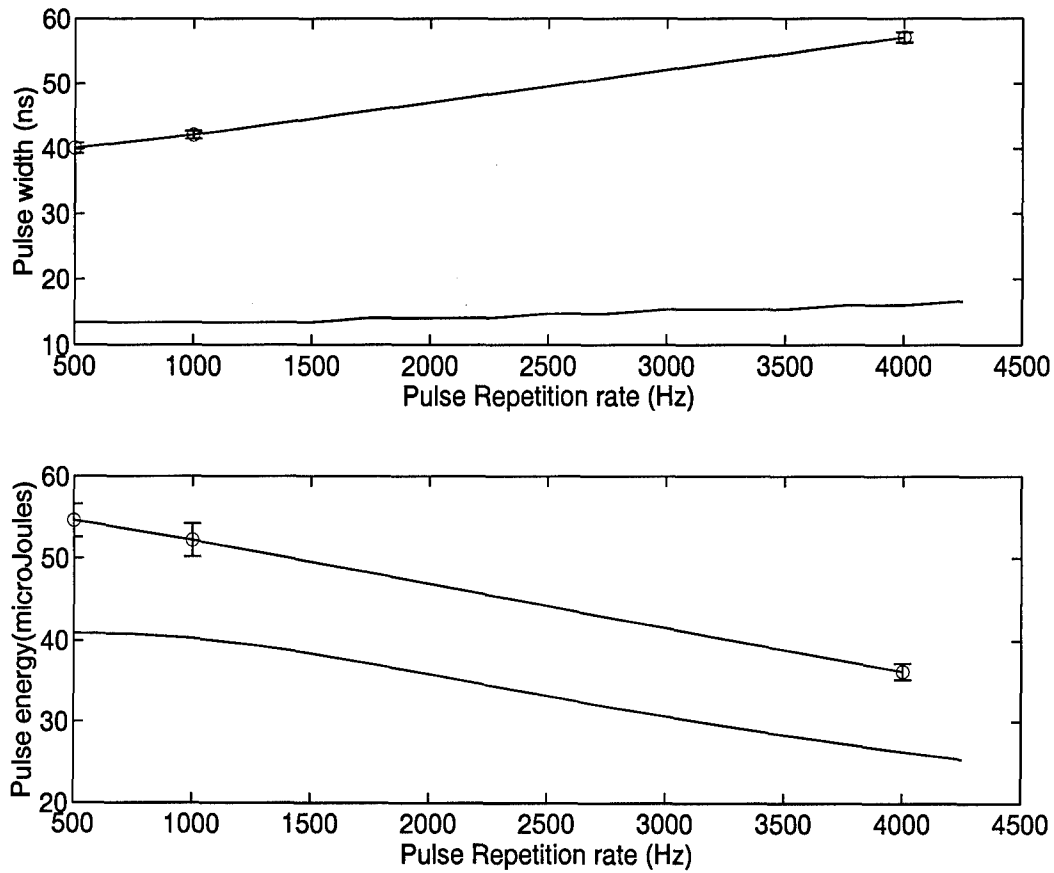


Figure 4.12 Q-switched measurements made with Nd:YAG at 1.06 microns. The model results are plotted with the solid line and the measured results are marked with "o". The absorbed pump power was 830mW.

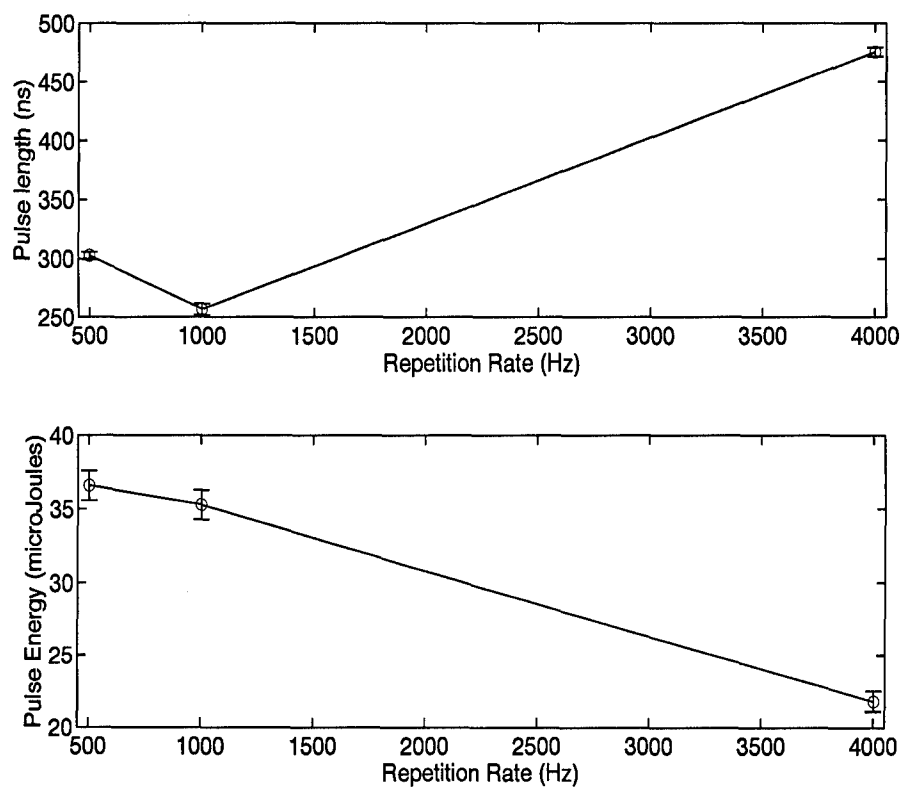


Figure 4.13 Measurement results for Nd:YAG operating only at $1.34\mu\text{m}$. The absorbed pump power was 830mW.

The Q-switched measurements of the Nd:YAG $1.32\mu\text{m}$ cavity shown in Table 4.9 and plotted in Figure 4.13. Because each plot has only three points, it is difficult to draw any conclusions with confidence. However, the pulse energy is expected to stay constant until a pulse repetition rate equal to $\frac{1}{\tau_f}$, or 4.2kHz. The plots in Figures 4.13 and 4.12 show a steady decrease in energy to this point (no data was taken beyond this) and this is probably due to the effects of thermal lensing in the laser crystal.

The measured results from Nd:YLF shown in Tables 4.11 and 4.12 are plotted in Figures 4.14 4.15 for the $1.05\mu\text{m}$ and $1.32\mu\text{m}$ cavities respectively. Similarly to Nd:YAG, the pulse energy is expected to roll off with increasing repetition rate at a rate corresponding to around $\frac{1}{\tau_f}$, which is 2.0kHz for Nd:YLF. The point where the roll off starts to occur in Figures 4.14 4.15 is 1.0kHz. This roll off does match the experimental data published by Grossman(3:623).

Figures 4.14 and 4.15 also show a decrease in pulse energy for decreasing repetition rate which is contrary to the equations. The reason for this decrease can be seen by examining the amount of energy stored in the material. The pump beam was focused down to a spot size of $135\mu\text{m}$ inside the laser crystal. Previous measurements show 99.6% of the incident pump power absorbed by the 5mm long crystal. This indicates an absorption coefficient $\alpha_{Nd:YLF}$ of

$$\alpha_{Nd:YLF} = -\frac{\ln(1 - .996)}{l_g} = 11\text{cm}^{-1}$$

The amount of power absorbed in the first 1 mm of the crystal is given by

$$P_{Abs_1mm} = P_{Inc} (1 - \exp(-(0.1\text{cm}) \alpha_{Nd:YLF}))$$

where P_{Inc} is the amount of power in the incident pump beam. This can be converted to the energy stored in the $^4F_{3/2}$ state per unit volume using Eqs (2.2) and (2.3

$$\frac{W_{stored}}{Vol_{1mm}} = P_{Inc} \frac{(1 - \exp(-0.1 \text{cm} \alpha_{Nd:YLF})) \tau_f (1 - \exp(-\frac{t}{\tau_f}))}{Vol_{1mm}} \frac{h\nu_4 F_{3/2}}{h\nu_p}$$

where t is the population build up time, and Vol_{1mm} is the volume of the pumped region in the first 1mm of the crystal.

Using the incident pump power of 1.17W used to generate the data in Figures 4.14 and 4.15, and inserting values for the other parameters yields

$$\frac{W_{stored}}{Vol_{1mm}} = 11.5 \left(1 - \exp\left(-\frac{t}{\tau_f}\right) \right) \frac{\text{Joules}}{\text{cm}^{-3}}$$

This expression is a function of the pulse repetition rate. The effect of decreasing pulse energy begins at pulse repetition rate of 1kHz which gives a stored energy of

$$\frac{W_{stored}}{Vol_{1mm}} = 9.9 \frac{\text{Joules}}{\text{cm}^{-3}}$$

This significant concentration of energy causes negative thermal lensing in Nd:YLF. This negative thermal lensing increases the effective spot size of the laser mode in the laser crystal. This increase in the spot size increases the threshold population inversion and decreases the amount of extracted energy according to Eq (2.22)

4.5 Analysis of 1.06 μm Nd:YAG Q-switched results

The model used to analyze these results was the same one used to design the initial system and is shown in Appendix B. The results shown in Figure 4.12 on page 4-23 demonstrate that the model (solid line) gives a pulse energy and a pulse width which are approximately half of the measured values.

Examining the energy per pulse first, a minimum value for the amount of absorbed pump power that is needed to produce these energies can be calculated

Table 4.11 Q-switched Nd:YLF single wavelength performance at $1.047\mu\text{m}$. The data for the cavity configuration is given in Table 4.13

Incident Pump Power (W)	Absorbed Pump Power (W)	Pulse Repetition Rate (Hz)	Pulse Energy (μJ)	Pulse Width (ns)
1.483	1.17 ± 0.04	89.9	87 ± 4	24.8 ± 0.1
1.483	1.17 ± 0.04	150.6	113 ± 4	24.3 ± 0.2
1.483	1.17 ± 0.04	1061	122 ± 4	26.1 ± 0.6
1.483	1.17 ± 0.04	2080	101 ± 4	28.4 ± 0.3
1.483	1.17 ± 0.04	3000	86 ± 3	32.6 ± 0.6
1.483	1.17 ± 0.04	4000	72 ± 3	35.9 ± 0.3
1.483	1.17 ± 0.04	5000	61 ± 2	39.8 ± 0.3
1.485	1.17 ± 0.04	10680	33 ± 1	60 ± 1
1.300	1.02 ± 0.03	10680	23.3 ± 0.8	78 ± 2
1.179	0.93 ± 0.03	10680	14.3 ± 0.5	123 ± 4

Table 4.12 Q-switched Nd:YLF single wavelength performance at $1.32\mu\text{m}$. The data for the cavity configuration is given in Table 4.13.

Incident Pump Power (W)	Absorbed Pump Power (W)	Pulse Repetition Rate (Hz)	Pulse Energy (μJ)	Pulse Width (ns)
1.485	1.17 ± 0.04	89.9	47 ± 2	143 ± 4
1.485	1.17 ± 0.04	150.6	52 ± 2	134 ± 3
1.485	1.17 ± 0.04	1009	51 ± 2	156 ± 5
1.485	1.17 ± 0.04	2000	38 ± 1	204 ± 4
1.485	1.17 ± 0.04	3000	32 ± 1	233 ± 7
1.485	1.17 ± 0.04	4000	24.8 ± 0.8	265 ± 8
1.485	1.17 ± 0.04	5000	24.0 ± 0.8	300 ± 10
1.295	1.02 ± 0.03	5000	12.4 ± 0.5	422 ± 9

Table 4.13 Cavity configuration for the Q-switched Nd:YLF data-long cavity.

$l_1=1.0\text{cm}$	$l_4=6.7\text{cm}$
$l_2=4.2\text{cm}$	$l_5=1.9\text{cm}$
$l_3=4.1\text{cm}$	$l_6=8.5\text{cm}$

	Output coupler	Cavity length
$1.32\mu\text{m}$	T=4%, 20cmcc	18.1cm
$1.06\mu\text{m}$	T=30%, 20cmcc	18.8cm

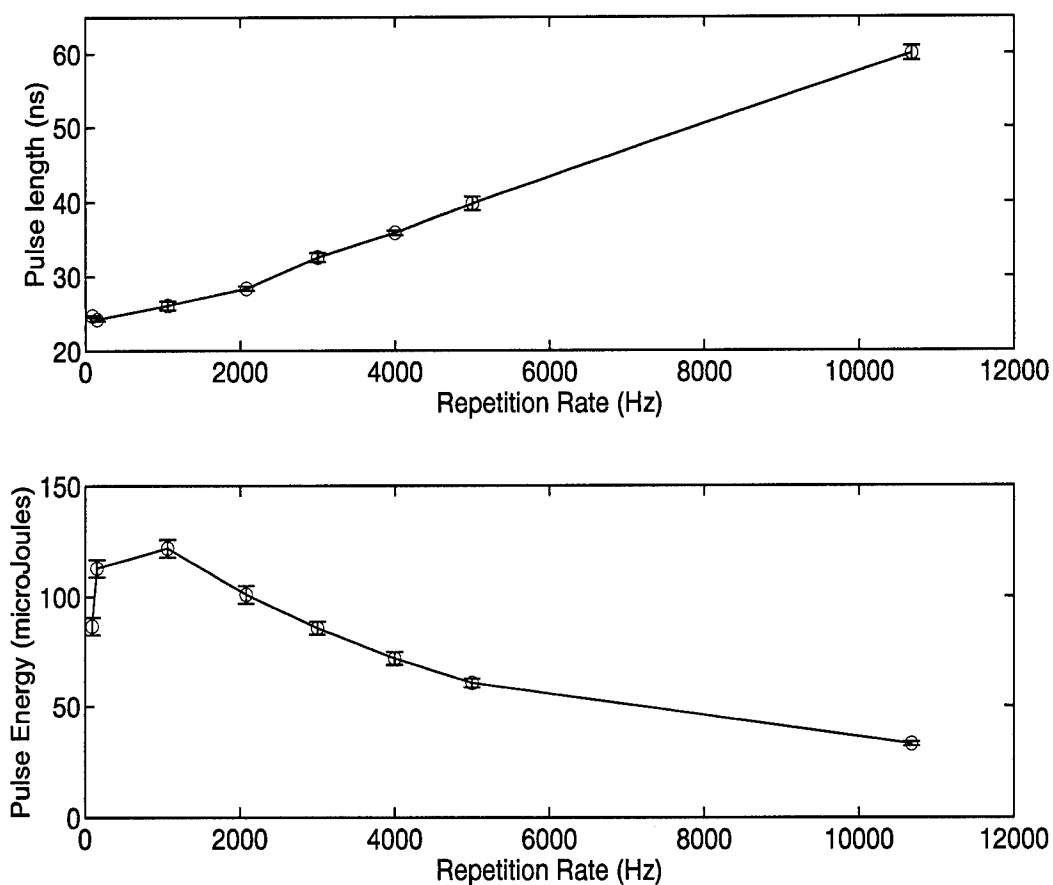


Figure 4.14 Measured results for Nd:YLF operating only at $1.05\mu\text{m}$. The absorbed pump power was 1.17W.

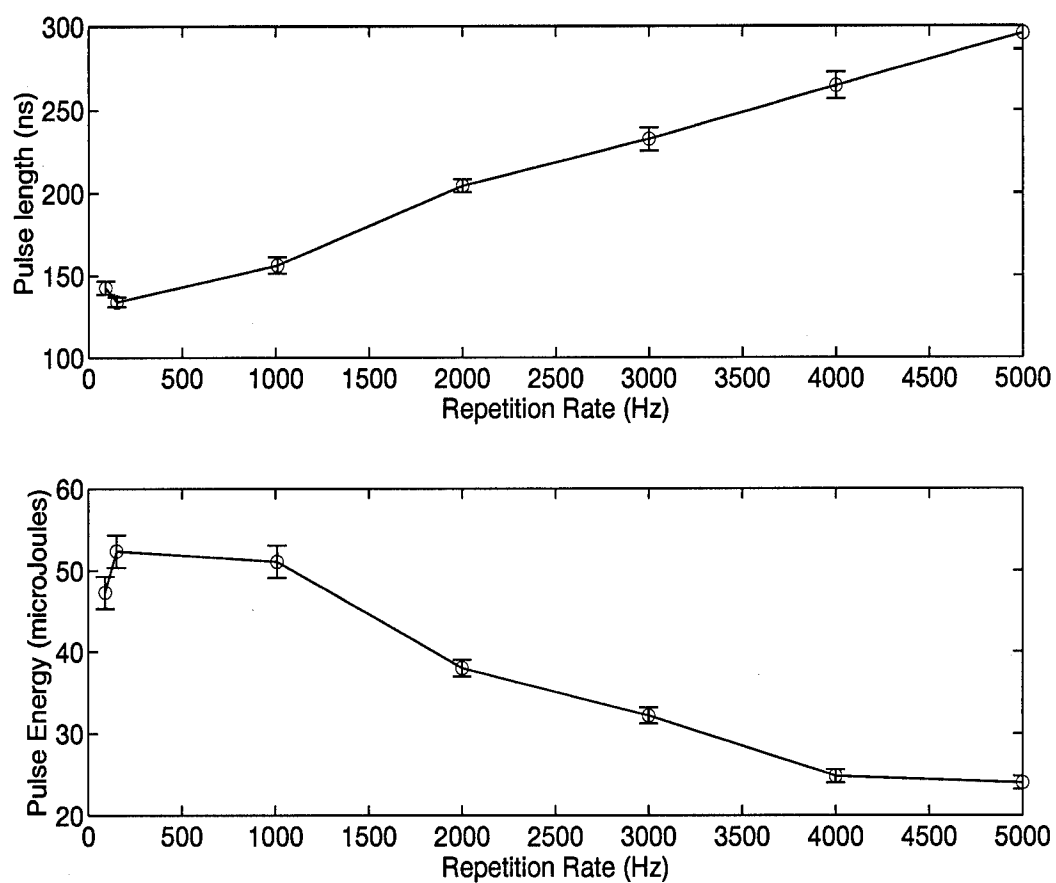


Figure 4.15 Measured results for Nd:YLF operating only at $1.32\mu\text{m}$. The absorbed pump power was 1.17W.

using these results and the theory developed in Chapter II. Table 4.8 on page 4-22 indicates a measured pulse energy of $55 \pm 2 \mu\text{J}$ for an incident pump power of 1.3W at a repetition rate of 500Hz. The expression for the pulse energy given in Eq (2.19) (repeated here for convenience) gives the pulse energy as a function of the change in population inversion.

$$W_{out} = (n_i - n_f) h\nu_L \frac{\alpha_{ext}}{\alpha_{total}}$$

Solving this equation for $(n_i - n_f)$ yields the change in the population inversion that it took to create the measured pulse energy:

$$(n_i - n_f) = \frac{\alpha_{total} W_{out}}{\alpha_{ext} h\nu_L} \quad (4.5)$$

Inserting the measured energy and the cavity loss from Table 4.7 on page 4-18 into Eq (4.5) gives $(n_i - n_f) = 1.3 \times 10^{14}$. The value for n_{th} , calculated using Eq (2.7), is $n_{th} = 4.5 \times 10^9$. Using these values in Eq (2.22) gives the fraction of population inversion left at the end of the Q-switched pulse

$$\frac{n_f}{n_i} \approx 0$$

which says that n_f is much smaller than n_i and so it is safe to approximate $(n_i - n_f)$ as just n_i or

$$n_i \approx (n_i - n_f) = \frac{\alpha_{total} W_{out}}{\alpha_{ext} h\nu_L} \quad (4.6)$$

This value can be used in the expression for the population inversion versus time given in Eq (2.2) and the pump rate given in Eq (2.3) to calculate the necessary absorbed pump power to produce this population inversion. This absorbed pump power is

$$P_{Pump} \cdot \eta_{efficiency} = 1.023 \text{ Watts}$$

This is greater than the 0.827 Watts calculated from the measured transmission values. This difference brings to light one difficulty encountered in making accurate

measurements of the transmission values used to determine the amount of absorbed pump power. At the time the measurements were made, the only power meter available with the necessary dynamic range was a Coherent Fieldmaster with a model LM-2 silicon detector which required a 1000:1 attenuator for measurements above 50mW. What made accurate, repeatable measurements difficult is that the displayed power varied by up to $\pm 30\%$ depending on the position and angle of arrival of the beam on the surface of the attenuator. This places an uncertainty on the measurements which were made absorptance of the pump beam and the transmission of the optics in the cavity, and leads to an analysis to determine their relationship from the measurements of the pulse energy.

Going back through the analysis, the two most uncertain values which have the greatest impact on both the pulse energy and the pulse length are the total internal cavity losses, α_{total} , and the absorption efficiency of the measured pump power, $\eta_{efficiency}$. The total absorption efficiency includes a number of different efficiency factors

$$\eta_{efficiency} = T_{HR}\eta_{Abs}\eta_B$$

Solving Eq (2.2), Eq (2.3), and Eq (4.5) for these two values yields a ratio given by

$$\frac{\eta_{efficiency}}{\alpha_{total}} = \frac{\nu_p}{\nu_L} \frac{W_{out}}{\alpha_{ext}\tau_f \left(1 - e^{-\frac{t}{\tau_f}}\right) P_{Pump}} \quad (4.7)$$

where t is the amount of time the population is allowed to build up ($\frac{1}{\text{pulse-rep-rate}}$ for single wavelength operation).

Calculating this ratio for the values in Table 4.8 yields

$$\frac{\eta_{efficiency}}{\alpha_{total}} = 4.6 \pm 0.2$$

Using these values in the model gives the results shown in Figure 4.16. The measured pulse energies fall within the bounds of the ratio but the calculated pulse

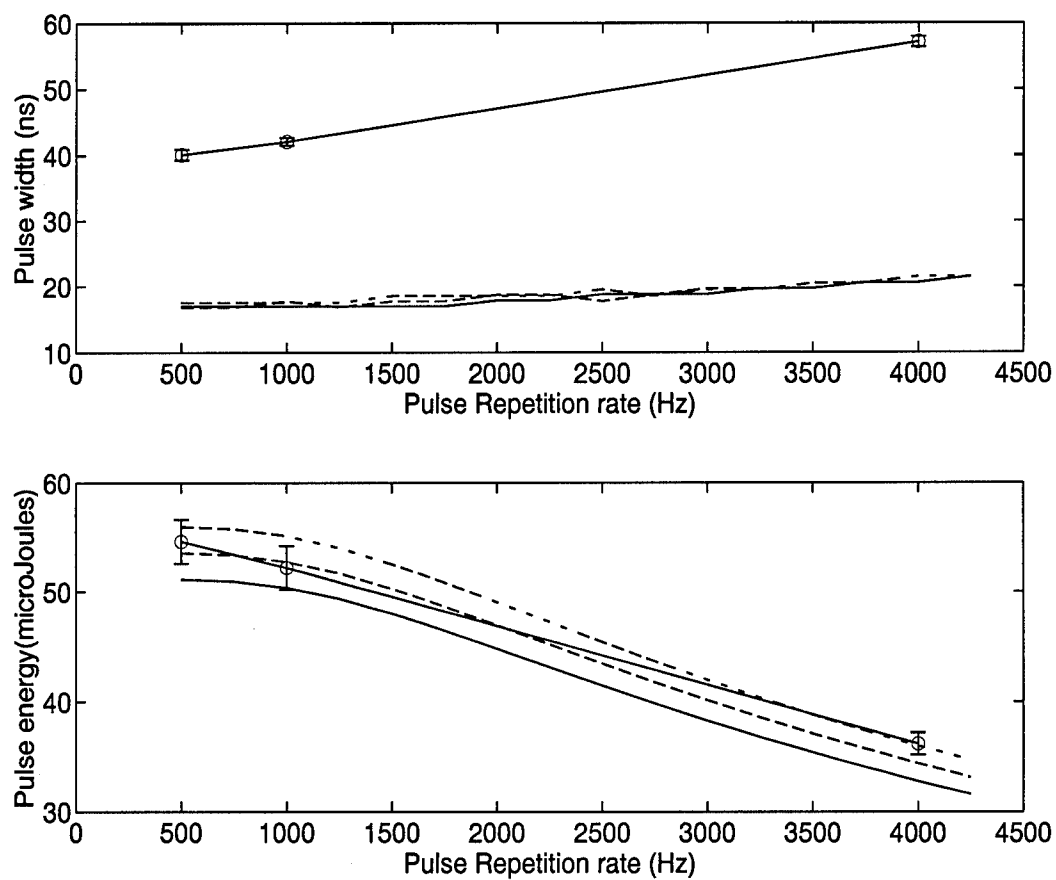


Figure 4.16 Model results for pulse width and pulse energy as functions of pulse repetition frequency. The multiple curves represent the variation in the value of the ratio of absorption efficiency to total cavity loss calculated from the data.

width is still approximately half of the measured values. One possibility is that the size of the beam in the laser cavity is larger than the TEM₀₀ spot size used in the model. Using the nominal value for the ratio and increasing the size of the beam in the crystal produced the results shown in Figure 4.17. The solid line represents the spot size in the laser crystal scaled up by a factor of 1.1 over the value calculated using the cavity configuration information. The curve shows that increasing the spot size decreases the pulse energy and increases the pulse length. An increase in the spot size increases the mode volume which intersects the laser crystal. An increase in the mode volume increases the threshold population inversion (which can be seen by examining Eq (2.7) on page 2-6). A beam size of 1.9 times larger than the value calculated from the cavity geometry produces the correct pulse lengths but the corresponding pulse energies are too low. Using this beam size, the value of the ratio $\frac{\eta_{efficiency}}{\alpha_{total}}$ was adjusted until the calculated energy matched the measured values. The value of the $\frac{\eta_{efficiency}}{\alpha_{total}}$ ratio was found to be 5.27 and the results are plotted in Figure 4.18.

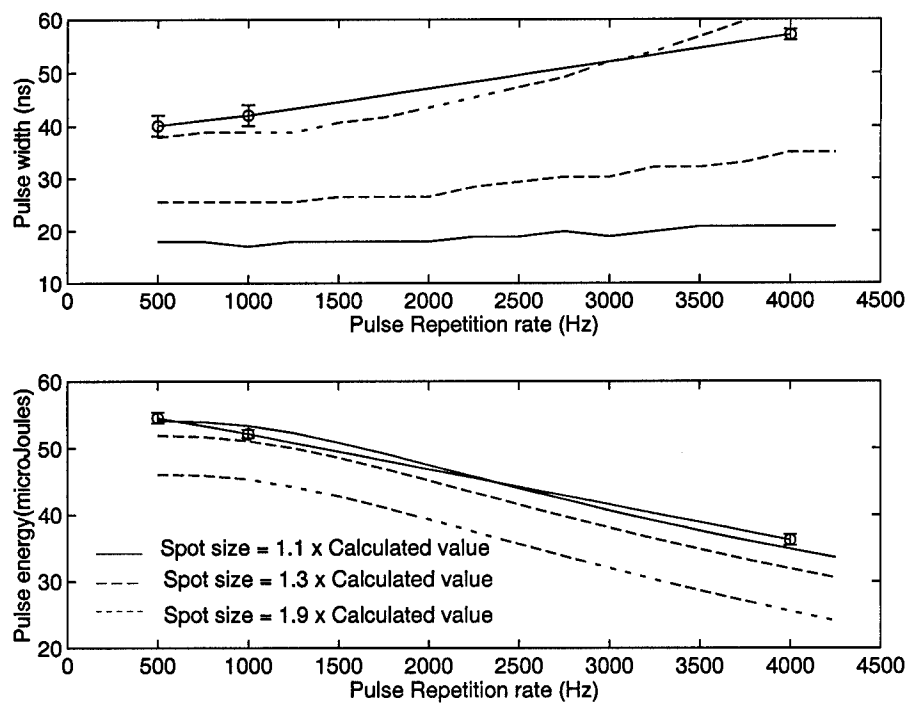


Figure 4.17 Model results for pulse width and pulse energy as functions of pulse repetition frequency. The multiple curves demonstrate the effect of changing the spot size in the crystal.

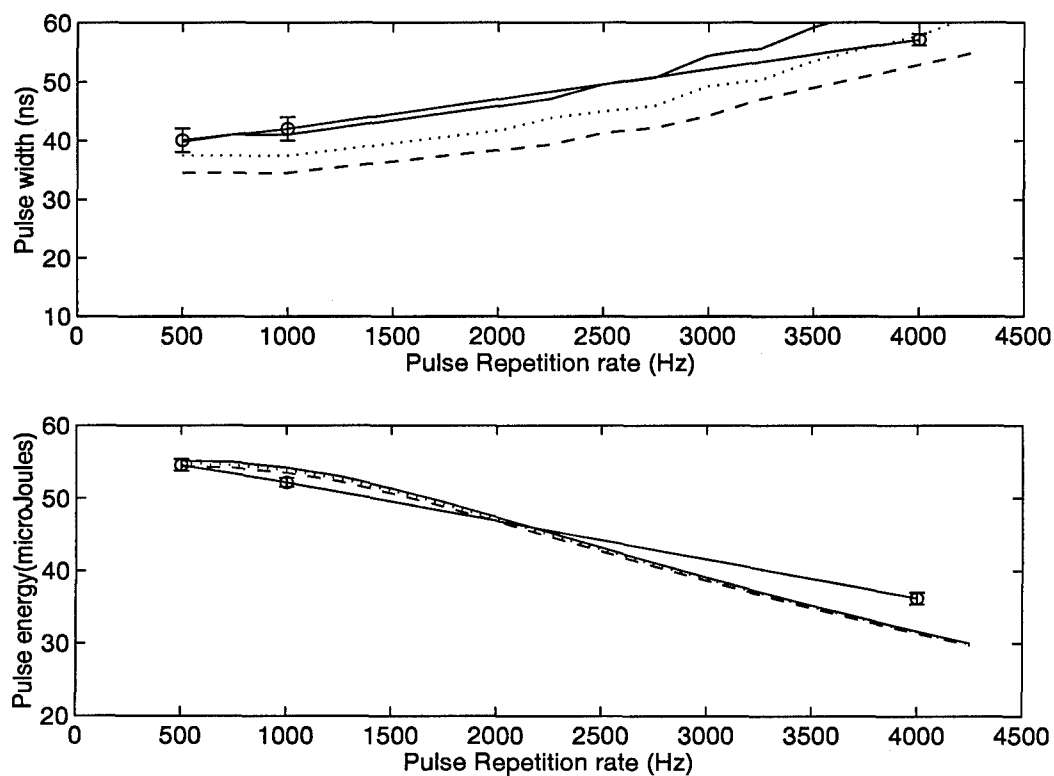


Figure 4.18 Model results for pulse width and pulse energy as functions of pulse repetition frequency. The multiple curves demonstrate the effect of changing amount of absorbed power while maintaining the same ratio of absorption efficiency to total cavity loss. The value of $\frac{\eta_{efficiency}}{\alpha_{total}}$ used to produce this plot was 5.27 (empirical).

4.6 Dual wavelength Q-switched results

This section begins by outlining the control sequence for the dual wavelength cavity. Examples of the output which reflect this control sequence are presented. Two cavity lengths were analyzed and the measurement results are presented in a series of tables. Most of the data for Nd:YAG is spread out in parameter space and the initial plan was to use this data to optimize the model which could then predict the optimum delay time, and cavity configuration. The development never reached that stage. The results do, however, illustrate some key concepts which are important for designing this type of laser for a laser radar system.

Figure 4.19 on page 4-37 shows the timeline for the control sequence as well as some of the terms used to describe the operation of the dual wavelength cavity. When power is applied to the acousto-optic Q-switches, they deflect a portion of the incident radiation making the cavity high-loss. Once a Q-switch is turned "off", it no longer deflects energy and the cavity returns to low-loss.

The experimental set up for these pulsed measurements is shown in Figure 4.11 on page 4-21 and the procedure for aligning the cavity is described in Appendix A. A plot of the shape of the $1.06\mu\text{m}$ and $1.32\mu\text{m}$ pulses is shown in Figure 4.20 on page 4-38. It should be noted that the time scales for the two plots in the figure are different. The outputs from the two detectors, showing the $1.3\mu\text{m}$ and the $1.06\mu\text{m}$ pulses are shown in Figure 4.21 on page 4-39. The figure shows the amplitude of the $1.06\mu\text{m}$ pulse, which is reflected by the dichroic beamsplitter into the $1.3\mu\text{m}$ output leg, is higher than the amplitude of the $1.3\mu\text{m}$ pulse. This highlights one design feature that needs refinement for this system to be optimized for Nd:YAG. The transmission of the dichroic beamsplitter at $1.064\mu\text{m}$ was measured to be 89.5%. This is significantly lower than the design specification of 95% for unpolarized light.

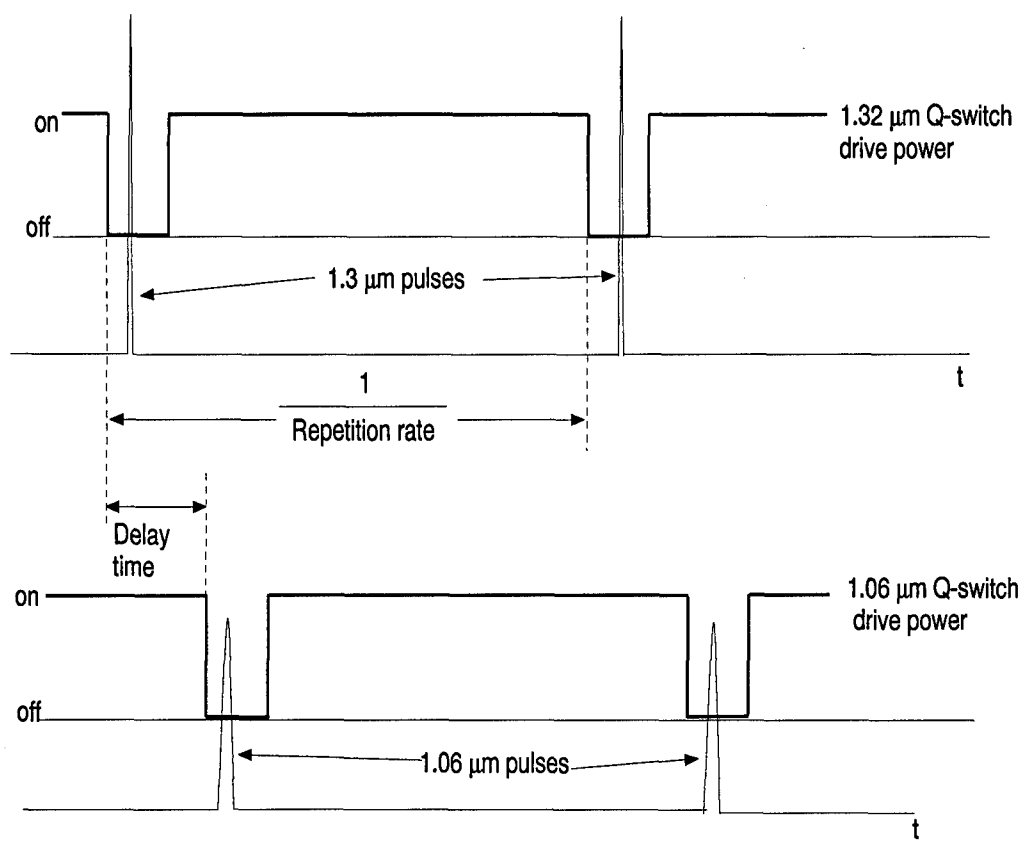


Figure 4.19 Timeline showing the control sequence for the operation of the dual wavelength cavity.

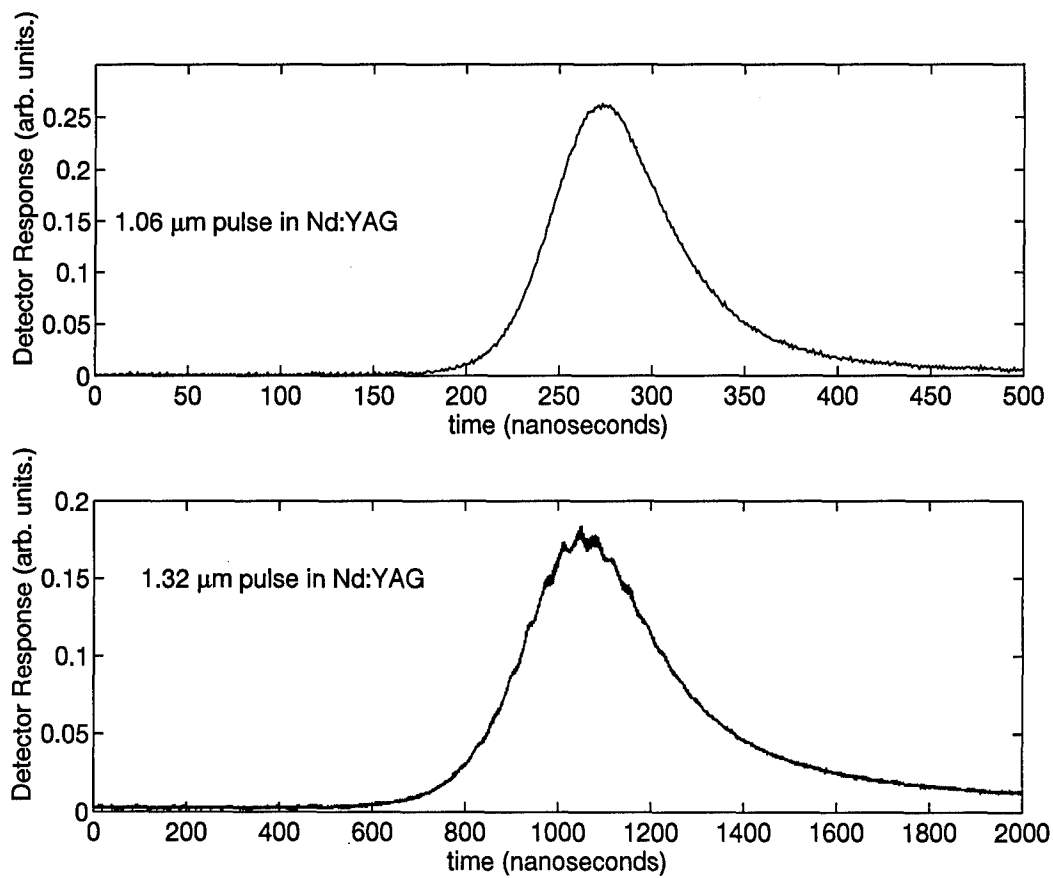


Figure 4.20 Pulse shape of the 1.06 μm and 1.32 μm pulses from the Nd:YAG output.

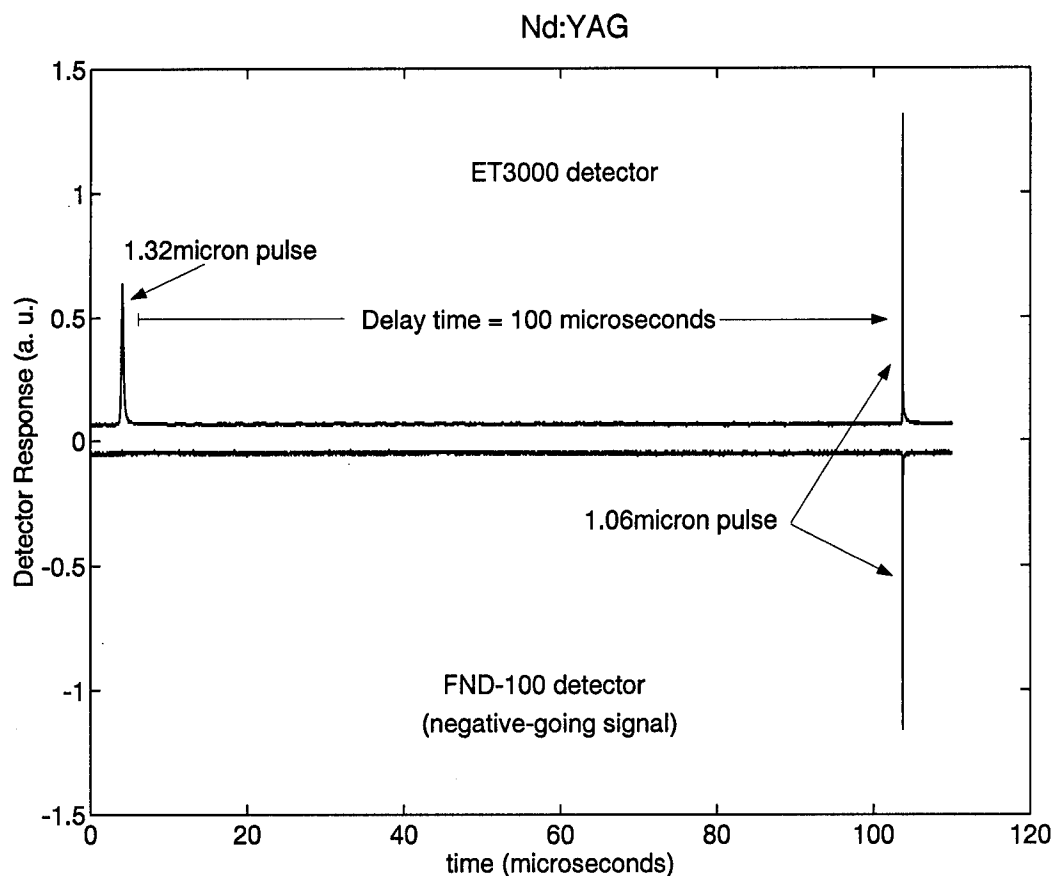


Figure 4.21 Example output of the dual wavelength cavity. The top curve shows the output of the $1.3\mu\text{m}$ cavity measured with the ET3000 detector and it shows the presence of both the $1.3\mu\text{m}$ pulse and the $1.06\mu\text{m}$ pulse which is reflected by the dichroic into the $1.3\mu\text{m}$ output leg. The bottom curve shows the output of the $1.06\mu\text{m}$ cavity measured with the FND-100 detector.

4.6.1 Energy Crossover. Table 4.14 on page 4-42 contains the results from Nd:YLF operating in the dual wavelength mode of operation. The pulse energy and pulse length data is plotted as a function of the delay time in Figure 4.22 on page 4-41. As the delay time increases, it increases the population inversion for the $1.047\mu\text{m}$ pulse and decreases it for the $1.3\mu\text{m}$ pulse. This decrease in the initial population inversion decreases the portion of initial population which is extracted according to Eq (2.22). Population left over by the inefficiency of the $1.32\mu\text{m}$ provides additional population inversion for the $1.05\mu\text{m}$ pulse which increases its extraction efficiency. By increasing the extraction efficiency of the $1.05\mu\text{m}$ pulse, the initial population inversion for the $1.32\mu\text{m}$ pulse decreases even further, and so the whole process reinforces a decrease in the amount of $1.32\mu\text{m}$ energy. In order to have a stable system which has equivalent pulse energies at $1.32\mu\text{m}$ and $1.05\mu\text{m}$, the pumping rate must be sufficient at the given pulse repetition frequency to provide enough initial population inversion relative to the threshold inversion level for the $1.32\mu\text{m}$ to efficiently extract the population inversion. The population inversion should be at least twice the threshold inversion level for the $1.3\mu\text{m}$ pulse. The relationship of the extraction efficiency to the ratio of initial population inversion to threshold inversion level (n_i/n_{th}) in Figure 2.5 on page 2-12 shows that for ratios of less than 2.0, the extraction efficiency starts dropping dramatically.

In designing a laser radar system, the energy of the two wavelengths would be adjusted to account for differences in atmospheric propagation, target reflectivity, detector responsivity, and other performance aspects considered in a system design and trade off analysis. From Figure 4.22, it is clear that for a fixed repetition rate, the amount of delay between the $1.3\mu\text{m}$ pulse and the $1.064\mu\text{m}$ pulse can be used to change the relative amount of energy in the two pulses. This can be seen more clearly in Figure 4.23 where the pulse energy from both wavelengths from Figure 4.22 are plotted on the same graph. The two plots from the two wavelengths actually cross.

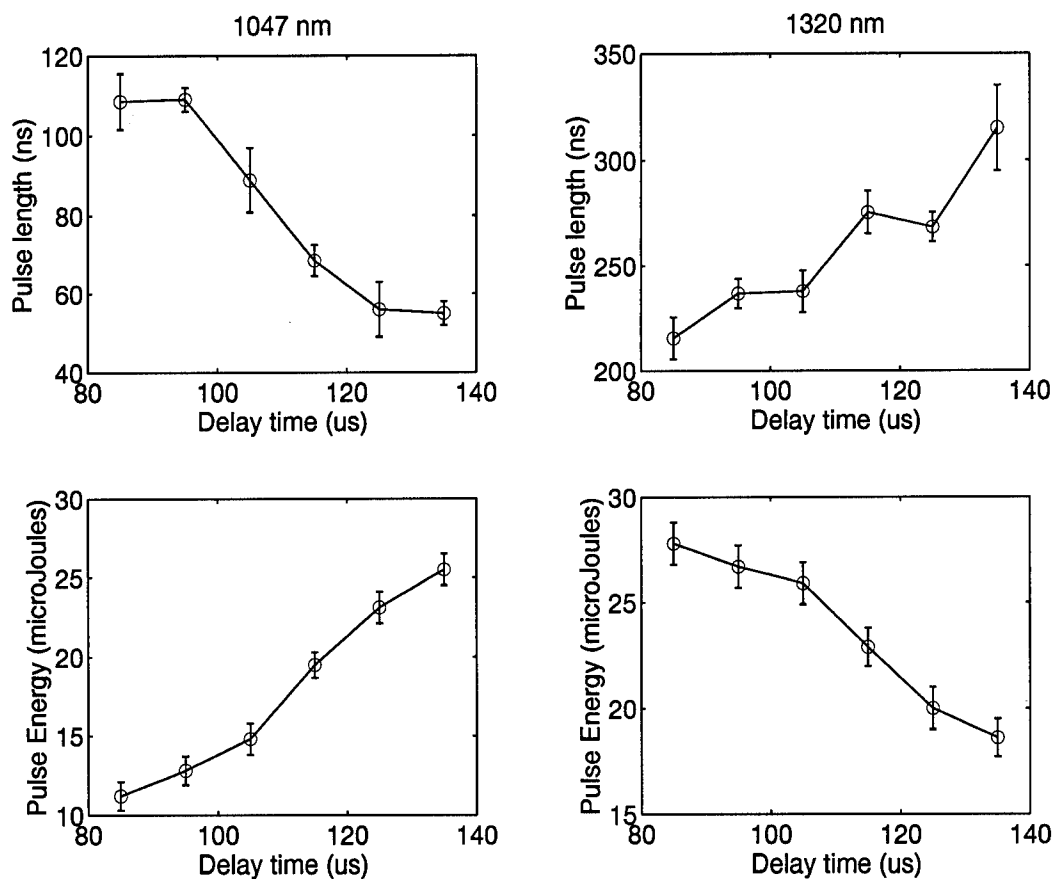


Figure 4.22 Dual wavelength operation of Nd:YLF. The repetition rate for each wavelength was fixed at 5.0kHz and the absorbed pump power was 950 mW.

Table 4.14 Q-switched Nd:YLF dual wavelength measurements- short cavity.

Pump Power Inc. (W)	Pump Power Abs. (W)	Pulse Rep. Rate (Hz)	Delay time (μ s)	1.06 μ m Pulse Energy (μ J)	1.06 μ m Pulse Width (ns)	1.34 μ m Pulse Energy (μ J)	1.34 μ m Pulse Width (ns)
0.965	0.92 \pm 0.03	5000	85	11.2 \pm 0.9	109 \pm 7	28 \pm 1	220 \pm 10
0.965	0.92 \pm 0.03	5000	95	12.8 \pm 0.9	109 \pm 3	27 \pm 1	237 \pm 7
0.965	0.92 \pm 0.03	5000	105	14.8 \pm 1	89 \pm 8	26 \pm 1	240 \pm 10
0.965	0.92 \pm 0.03	5000	115	19.5 \pm 0.8	69 \pm 4	22.9 \pm 0.9	280 \pm 10
0.965	0.92 \pm 0.03	5000	125	23.1 \pm 1	56 \pm 7	20 \pm 1	269 \pm 7
0.965	0.92 \pm 0.03	5000	135	25.5 \pm 1	55 \pm 3	18.6 \pm 0.9	320 \pm 20

Changing the delay time can compensate for the differences in stimulated emission cross section as well as losses between the two cavities. The ability to adjust the pulse energies using the delay time validates the use of the stimulated emission cross section - fluorescence lifetime product as a metric for choosing the optimum material for this dual wavelength laser. Any deficiency in the performance of one transition can be made up by performance in the other simply by changing the relative amount of time the population inversion is allowed to build up for each pulse. Different materials with comparable values of this metric would have to be evaluated for their ability to achieve higher repetition rates. The energy in the materials with the longer lifetimes will begin to drop sooner as the repetition rate is increased (3:623)

4.6.2 Cavity length comparison. Measurements were made at with the Nd:YAG crystal at two different cavity lengths. The longer cavity lengths were on the order of 18cm long and the shorter cavity lengths were on the order of 13cm long. The length of the short cavity was determined by reducing the distances between components as much as possible within the constraints of the hardware. The separation of the different components in the short cavity are shown in Table 4.16 (see Figure 4.11 on page 4-21 for the definitions) and the laser measurements are

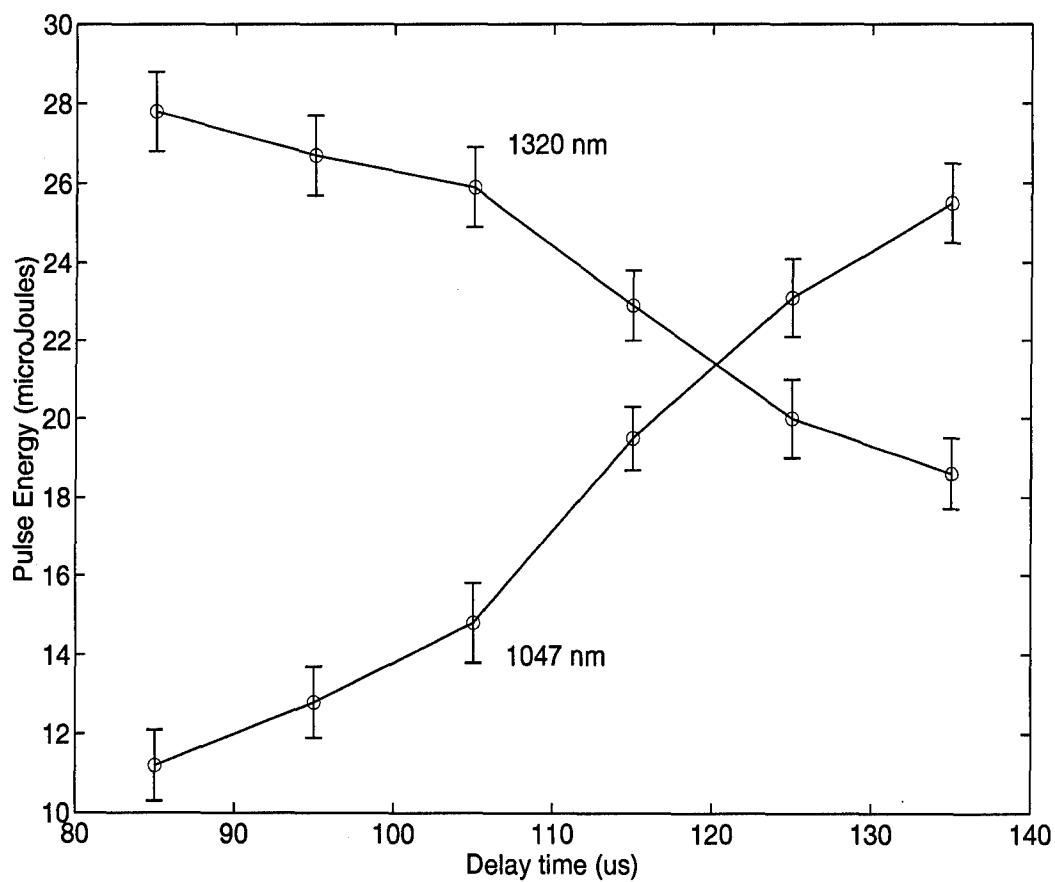


Figure 4.23 Dual wavelength operation of Nd:YLF showing energy crossover. The repetition rate for each wavelength was fixed at 5.0kHz and the absorbed pump power was 920 mW.

Table 4.15 Q-switched Nd:YAG dual wavelength measurements—short cavity.

Pump Power Inc. (W)	Pump Power Abs. (W)	Pulse Rep. Rate (Hz)	Delay time (μ s)	1.06 μ m Pulse Energy (μ J)	1.06 μ m Pulse Width (ns)	1.34 μ m Pulse Energy (μ J)	1.34 μ m Pulse Width (ns)
1.3	0.83 \pm 0.03	2000	100	33 \pm 1	31.5 \pm 0.4	26.7 \pm 0.8	183 \pm 1
1.3	0.83 \pm 0.03	2000	150	40 \pm 1	32.9 \pm 0.7	23.2 \pm 0.7	199 \pm 4
1.3	0.83 \pm 0.03	2000	225	43 \pm 1	28.2 \pm 0.6	19.3 \pm 0.6	274 \pm 5
1.3	0.83 \pm 0.03	2880	100	32 \pm 1	32.2 \pm 0.3	16.3 \pm 0.5	338 \pm 3

Table 4.16 Cavity configuration for the dual-wavelength Q-switched Nd:YAG data—short cavity.

$l_1=1.4\text{cm}$	$l_4=0.7\text{cm}$
$l_2=3.5\text{cm}$	$l_5=2.4\text{cm}$
$l_3=3.5\text{cm}$	$l_6=1.9\text{cm}$

	Output coupler	Cavity length
$1.32\mu\text{m}$	T=4%, 20cmcc	11.4cm
$1.06\mu\text{m}$	T=5%, 20cmcc	12.2cm

shown in Table 4.15. The separations of the components in the long cavity are shown in Table 4.10 back on page 4-23 and the laser measurements are shown in Table 4.17.

The effect of the changing the cavity length is shown in Figure 4.24. Shortening the cavity length from 18cm to 13cm has a dramatic impact on the pulse length. The pulse lengths for both wavelengths are reduced by a factor of two. This supports the conclusion that the shortest possible cavity is the optimum one for producing short pulses(3:622). Shortening the cavity length decreases the round trip time, and as a result, the photon lifetime is decreased also. When this happens, the photons in the cavity provide their feedback to the gain medium faster causing the pulse to build and

Table 4.17 Q-switched Nd:YAG dual wavelength measurements—long cavity.

Pump Power Inc. (W)	Pump Power Abs. (W)	Pulse Rep. Rate (Hz)	Delay time (μ s)	1.06 μ m Pulse Energy (μ J)	1.06 μ m Pulse Width (ns)	1.34 μ m Pulse Energy (μ J)	1.34 μ m Pulse Width (ns)
1.45	0.92 ± 0.03	500	100	42 ± 4	49.8 ± 0.9	40 ± 2	211 ± 2
1.45	0.92 ± 0.03	500	150	44 ± 2	43.4 ± 0.3	45 ± 1	216 ± 2
1.295	0.823 ± 0.03	500	200	47 ± 2	45.9 ± 0.5	35 ± 1	288 ± 7
1.3	0.83 ± 0.03	1000	200	45 ± 2	46.8 ± 0.5	33 ± 1	301 ± 2
1.3	0.83 ± 0.03	1000	150	42 ± 1	64.0 ± 0.4	34 ± 1	267 ± 7
1.3	0.83 ± 0.03	2000	100	38 ± 2	52.1 ± 0.5	21.7 ± 0.7	410 ± 10
1.3	0.83 ± 0.03	2000	150	38 ± 2	48.1 ± 0.6	19.2 ± 0.6	504 ± 4
1.2	0.76 ± 0.03	2000	100	36 ± 1	54 ± 1	10.5 ± 0.3	790 ± 20

sweep out the gain region faster than in a longer cavity. This increased photon flux increases the efficiency of extracting the stored energy through stimulated emission.

4.6.3 Material comparison. A set of measurements was also made with Nd:YLF in a short cavity. The cavity lengths for Nd:YAG (Table 4.16) were approximately 1cm shorter than they were in Nd:YLF (Table 4.18) because the angle of the dichroic beamsplitter was different for the two materials causing the relative position of the Q-switch mounts to change. The laser measurements for Nd:YLF are shown in Table 4.19. The measurement results for Nd:YAG were shown in the previous subsection in Table 4.15.

The Nd:YAG and Nd:YLF measurements made with the short cavity were to provide a direct comparison of the two materials using the shortest possible cavity. Unfortunately, there are several differences between the results from the two materials which make a direct comparison impossible. The analysis in section 4.4 for the 1.06 μ m cavity makes the calculation for the absorbed pump power uncertain, it indicates that the level of absorbed power for Nd:YAG might be greater than

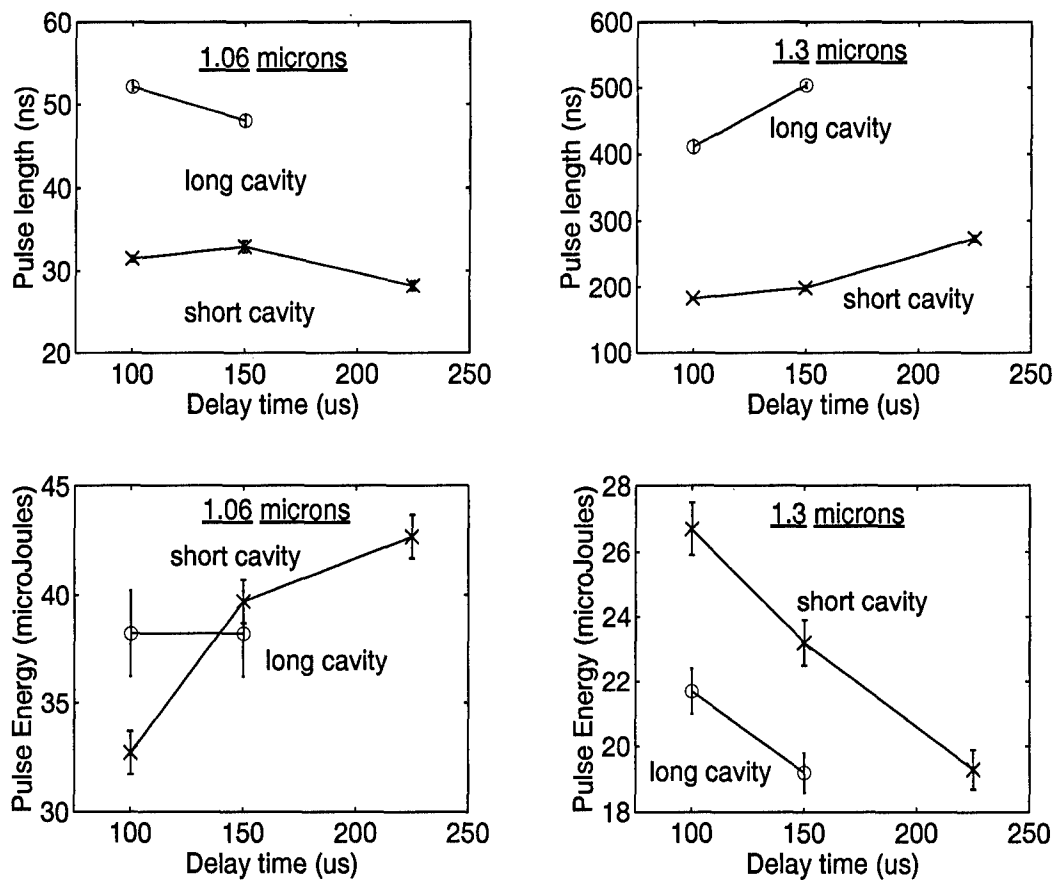


Figure 4.24 Dual wavelength operation of Nd:YAG comparing the results from two different cavity lengths. The plots on the left hand side are for the $1.06\mu\text{m}$ cavity and the plots on the right hand side are for the $1.32\mu\text{m}$ cavity. The pulse repetition frequency (for both wavelengths) is fixed at 2000Hz.

Table 4.18 Cavity configuration for the dual-wavelength Q-switched Nd:YLF data -short cavity.

	$l_1=1.4\text{cm}$	$l_4=0.7\text{cm}$
	$l_2=4.1\text{cm}$	$l_5=2.1\text{cm}$
	$l_3=4.6\text{cm}$	$l_6=2.5\text{cm}$
	Output coupler	Cavity length
$1.32\mu\text{m}$	T=4%, 20cmcc	13.1cm
$1.06\mu\text{m}$	T=30%, 20cmcc	13.0cm

Table 4.19 Q-switched Nd:YLF dual wavelength measurements—short cavity.

Power Inc. (W)	Power Abs. (W)	Rep. Rate (Hz)	Delay time (μ s)	1.047 μ m Pulse Energy (μ J)	1.047 μ m Pulse Width (ns)	1.32 μ m Pulse Energy (μ J)	1.32 μ m Pulse Width (ns)
0.959	0.76 \pm 0.02	2000	100	34 \pm 1	51 \pm 2	12.3 \pm 0.5	460 \pm 10
0.959	0.76 \pm 0.02	2000	150	39 \pm 1	44.4 \pm 0.5	9.9 \pm 0.4	666 \pm 7
0.959	0.76 \pm 0.02	2000	225	41 \pm 2	44.8 \pm 0.9	9.8 \pm 0.4	1020 \pm 40
1.046	0.82 \pm 0.03	2000	100	40 \pm 2	44 \pm 1	15.3 \pm 0.6	410 \pm 10
1.046	0.82 \pm 0.03	2000	150	48 \pm 2	45 \pm 1	13.8 \pm 0.5	470 \pm 20
1.046	0.82 \pm 0.03	2000	225	52 \pm 2	38.4 \pm 0.4	12.7 \pm 0.7	560 \pm 20

originally calculated. This means that the two materials were pumped at different rates. Not only was the pumping rate different, but the output coupler values were different. The gain in the Nd:YLF 1.047 μ m laser was so high that the Q-switch could not hold off lasing between pulses. The output coupler reflectivity was then reduced from 95% to 70% where the 1.06 μ m Q-switch could hold off the cavity and this is the point where the data was taken. When the output coupler reflectivity for the 1.06 μ m cavity was reduced from 95% to 70% in Nd:YAG, the loss was too high and the cavity would not lase at that pulse repetition rate and pump power. As a result, the reflectivity of output coupler for the Nd:YLF data was 70%, whereas the reflectivity of the output coupler for the Nd:YAG data was 95%. The results from the two sets of measurements are plotted in Figure 4.25.

Figure 4.25 again demonstrates the interdependence of the two wavelengths. As the amount of time the population is allowed to build for the 1.06 μ m pulse (the delay time) is increased, the amount of population inversion increases for the 1.06 μ m pulse at the expense of the 1.3 μ m pulse. The reason for the pulse length of the Nd:YLF $^4F_{3/2} - ^4I_{11/2}$ transition being longer than the pulse length for Nd:YAG when Nd:YLF has a greater pulse energy is not immediately obvious. One possibility is that the

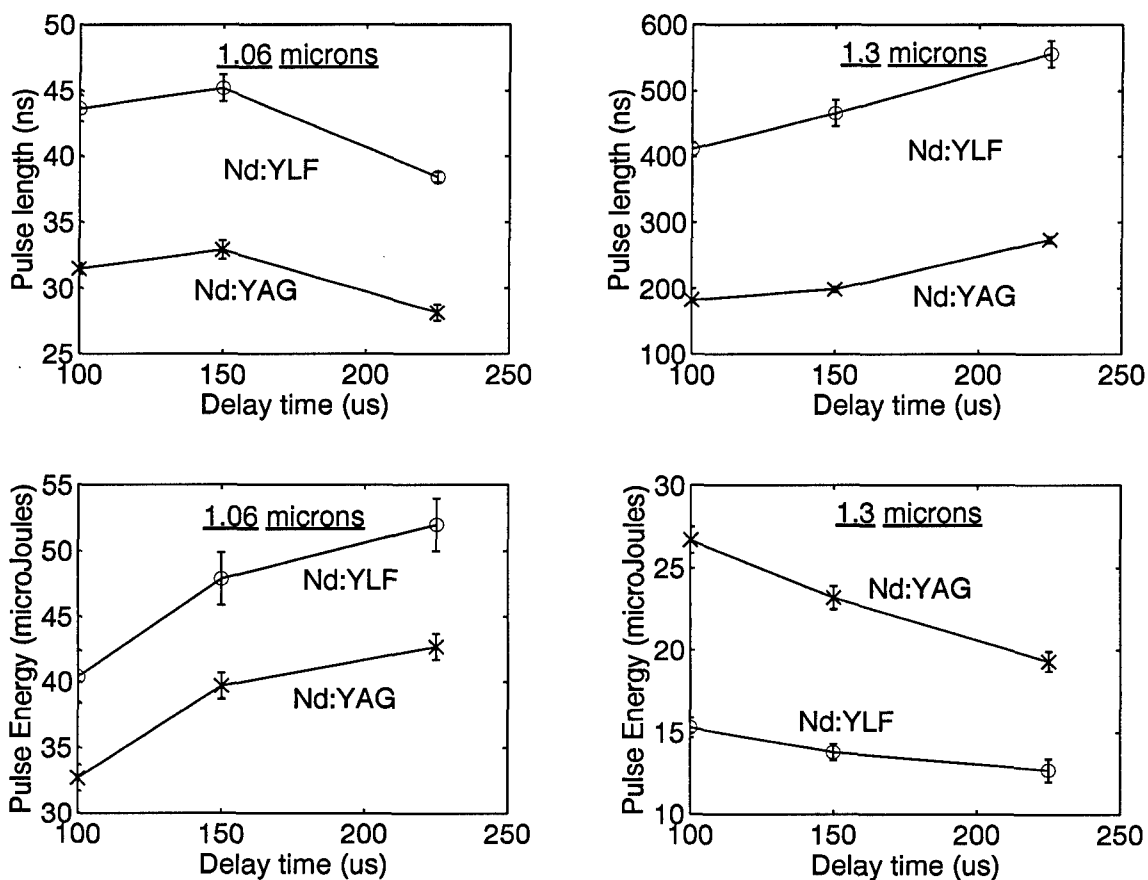


Figure 4.25 Dual wavelength operation of Nd:YLF compared with Nd:YAG. The plots on the left hand side are for the $1.06\mu\text{m}$ cavity and the plots on the right hand side are for the $1.32\mu\text{m}$ cavity. The pulse repetition frequency (for both wavelenths) is fixed at 2.0kHz.

1.06 μ m Q-switch did not have enough hold off to keep that cavity from lasing between pulses. During the measurement the Q-switch power was at its absolute maximum, and it was not clear from the amplitude of the 1.047 μ m Q-switched pulse that the Q-switch was able to fully hold off the gain in the cavity. The Q-switch was designed for unpolarized light. The relative efficiency of the device for horizontally polarized energy was never evaluated.

4.7 Error analysis

4.7.1 *Uncertainty in the pump power absorbed in the laser crystal.* The uncertainty in the amount of absorbed power results from the uncertainty in the absolute accuracy of the power meter; the fluctuation in the meter reading (which was recorded for each measurement); the uncertainty in the transmission of the high reflector; and the uncertainty in the fraction of incident energy actually absorbed by the laser crystal. The setup for this measurement is shown in Figure 4.3. The expression used to calculate the absorbed pump power from the incident pump power P_{inc} was

$$P_{Abs} = \eta_{HR}\eta_{Abs}\eta_B P_{inc} \quad (4.8)$$

The values for η_{HR} and η_{Abs} were taken from Tables 4.1 and 4.3 respectively. The value for η_B is assumed to be 1, the pump beam was focused to a spot size smaller than the spot size of the laser mode inside the laser crystal.

The accuracy of the power meters σ_{accu} used to make the power measurements was $\pm 3\%$. The meter reading for $P_{incident}$ typically fluctuated ± 5 mW during a measurement. This fluctuation is included in the uncertainty calculation. The equation used to calculate the uncertainty in the power absorbed into the laser crystal $\sigma_{P_{Abs}}$

was

$$\sigma_{P_{Abs}} = P_{Abs} \left[\left(\frac{\sigma_{acc} P_{inc}}{P_{inc}} \right)^2 + \left(\frac{\sigma_{fluct}}{P_{inc}} \right)^2 + \left(\frac{\sigma_{T_{HR}}}{T_{HR}} \right)^2 + \left(\frac{\sigma_{\eta_{Abs}}}{\eta_{Abs}} \right)^2 \right]^{\frac{1}{2}} \quad (4.9)$$

where σ_{acc} is the absolute accuracy of the power meter, σ_{fluct} is the fluctuation in the meter reading, $\sigma_{T_{HR}}$ is the uncertainty in the transmission of the high reflector, and $\sigma_{\eta_{Abs}}$ is the uncertainty in the fraction of power absorbed by the crystal.

Representative numbers for the fractions inside the expression in Eq (4.9) for Nd:YAG pumped with 1.0 Watt from the Ti:Sapphire at 808.5 nm are given below

$$\begin{aligned} \frac{\sigma_{acc} P_{inc}}{P_{inc}} &= 0.03 \\ \frac{\sigma_{fluct}}{P_{inc}} &= 0.005 \\ \frac{\sigma_{T_{HR}}}{T_{HR}} &= 0.0135 \\ \frac{\sigma_{\eta_{Abs}}}{\eta_{Abs}} &= 0.011 \end{aligned}$$

A comparison of these values indicates that the first one, from the absolute accuracy of the power meter, is by a factor of 3 the greatest source of uncertainty in the calculation of the amount of pump power absorbed in the laser crystal.

4.7.2 Uncertainty calculation for the laser pulse energy. The equation used to calculate the pulse energy from the average power measured with the Scientech model AD30 power meter was

$$W_{out} = \frac{P_{avg}}{T_{LP} \Gamma_{fold} \Gamma_{fold} (1 - \Gamma_{OC}) PRF} \quad (4.10)$$

where P_{avg} is the average power measured with the power meter, T_{LP} is the transmission of the long pass filter at the laser wavelength, Γ_{fold} is the reflectivity of the protected silver fold mirrors, Γ_{OC} is the reflection off of the back surface of the

output coupler (the output couplers were not coated on the back side), and PRF is the pulse repetition frequency.

The uncertainty in the pulse energy measurements results from the uncertainty in the absolute accuracy of the power meter; the fluctuation in the meter reading (which was recorded for each measurement); the uncertainty in the transmission of the long pass filter used to block the residual pump beam; and the uncertainty in the reflectivity of the protected silver fold mirror(s) used to direct the beam into the power meter. The reflectivity off of the back surface of the optic was not measured but assumed to be a constant 5% with no associated uncertainty. The uncertainty in the pulse repetition frequency was also disregarded since it was less than one part in one thousand, an order of magnitude less than the other sources of error. The equation used to calculate the uncertainty in the pulse energy was

$$\sigma_{W_{out}} = W_{out} \left[\left(\frac{\sigma_{acc} P_{avg}}{P_{avg}} \right)^2 + \left(\frac{\sigma_{fluct}}{P_{avg}} \right)^2 + \left(\frac{\sigma_{T_{LP}}}{T_{LP}} \right)^2 + \left(\frac{\sigma_{\Gamma_{fold}}}{\Gamma_{fold}} \right)^2 \right]^{\frac{1}{2}} \quad (4.11)$$

where P_{avg} is the average power of the pulsed laser measured with the power meter.

Representative calculations for Nd:YAG at $1.06\mu\text{m}$ associated with the top entry in Table 4.8 on page 4-22 are shown below

$$\begin{aligned} \frac{\sigma_{acc} P_{avg}}{P_{avg}} &= 0.03 \\ \frac{\sigma_{fluct}}{P_{avg}} &= 0.02 \\ \frac{\sigma_{\Gamma_{fold}}}{\Gamma_{fold}} &= 0.0052 \\ \frac{\sigma_{T_{LP}}}{T_{LP}} &= 0.0094 \end{aligned}$$

Comparing these values indicates that the first value, from the absolute accuracy of the power meter, is the greatest source of uncertainty in the calculation of the amount of pump power absorbed in the laser crystal. When the average power produced by

the laser was less than 20mW, the fluctuation in the meter reading started having a significant impact on the uncertainty values. This generally occurred at low repetition rates or low pump powers.

V. Conclusions & Recommendations

5.1 Conclusions

A figure of merit for choosing the best laser crystal from the large number of new Nd-based materials, is the sum of the stimulated emission-fluorescence lifetime product for the two transitions that produce the two wavelengths. Due to both the large variability and the gaps in the published values for these material parameters, the best method for choosing the optimum material is to evaluate their relative performance in an identical laser setup. Based on the published information available, Nd:SFAP would be the optimum material for this application because the sum of the stimulated emission cross section-fluorescence lifetime product from the two wavelengths is $23.2 \times 10^{-17} \mu\text{s cm}^2$, which is higher than any other material surveyed.

The absorption spectrum, fluorescence lifetime, and emission spectrum of Nd:YAG, Nd:SVAP, and Nd:YLF were measured. The peak absorption in the band of useful diode wavelengths between 780nm and 815nm for both Nd:YAG and Nd:SVAP was approximately 808.5nm, whereas the strongest absorption for Nd:YLF occurred at 792.1nm. The measured fluorescence lifetimes for these materials was 237 μs , 216 μs and 504 μs respectively, and all are within the range of published values.

A dual wavelength Q-switched laser cavity has been successfully designed and assembled to evaluate the different possible laser materials. The cavity design was based on a "Y" cavity designed by Tomaschke (33: 252) to achieve lasing at two wavelengths simultaneously. Initial characterization has been achieved for Nd:YAG and Nd:YLF. *The results indicate that for a fixed pulse repetition frequency, the delay time can be used to adjust the relative energy between the 1.06 μm and 1.32 μm pulses.* This ability validates using the sum of the fluorescence lifetime-stimulated emission cross section product from the two transitions as a metric for choosing the best material. Any deficiency in the performance of one transition can be made up

by performance in the other simply by changing the relative amount of time the population inversion is allowed to build up for each pulse.

The shortest pulses were achieved with both Nd:YAG and Nd:YLF using the shortest physical cavity length. When the cavity length was decreased from 18cm to 13cm, the pulse length for each wavelength decreased by a factor of 2.

Of the two materials evaluated, Nd:YLF was clearly the superior material. The gain was so high with this material that the reflectivity of the output coupler had to be decreased from 95% to 70% just so that the $1.06\mu\text{m}$ Q-switch could hold off the cavity.

The model developed using the standard differential equations was fit to the Nd:YAG data at $1.06\mu\text{m}$. The modifications which were required to make the model fit the data indicate the presence of thermal lensing in this material. An improved model would include the effects of thermal lensing as a function of pulse repetition rate and energy storage in the material. The importance of thermal lensing was also seen in the single wavelength results for Nd:YLF. The pulse energy actually started to decrease with decreasing repetition rate instead of continuing to increase as would normally be expected.

5.2 Recommendations

The first and most obvious recommendation is to obtain a sample of Nd:SFAP for evaluation. Based on the published spectroscopic information, this material should be the best out of those surveyed for this two wavelength application. Based on the information in Table 3.8 on page 3-5, Nd:YLF is the next best material to Nd:SFAP. The performance of these materials in terms of pulse energy and pulse width should be evaluated up to the pulse repetition rates necessary to achieve the needed frame rate for a dual wavelength imaging laser radar. In addition, these materials should be evaluated not only for their pulse energy and pulse width but for their absorption width at the laser diode pump wavelength (to evaluate their

suitability for laser diode pumping), thermal stability, and beam quality as well. All of these parameters have an impact on the performance of a laser radar system constructed from these materials.

The cavity element which caused the greatest loss and proved to be the greatest detriment to operation on the ${}^4F_{3/2} - {}^4I_{11/2}$ transition was the dichroic beamsplitter. This element had a transmission of 90% in the Nd:YAG cavity. One possible solution is to purchase a higher quality optic with a better design. Another solution is to modify the cavity design and use a polarization beamsplitter.

Since both of the laser transitions in all of the laser crystals have a significant stimulated emission cross section in both polarization directions, polarizing elements could be placed in each of the different legs of the cavity. The $1.3\mu\text{m}$ polarizer could be oriented to allow only the vertical to pass. This vertical polarization would be S-polarized upon incidence the dichroic beamsplitter and so its reflection would be maximized. The polarizer in the $1.06\mu\text{m}$ cavity could be oriented to allow only horizontal polarization to pass. This horizontal polarization would be P-polarized upon incidence to the dichroic beamsplitter which would maximize its transmission. If both legs then contain optics to force opposite polarizations, the dichroic beamsplitter could be replaced with a polarization beamsplitter. This polarization beamsplitter would have to be designed to operate at both wavelenths in the near IR, but a beamsplitter made from calcite would give an extinction ratio between the two polarizations of 100,000 to 1. The potential increase in performance would have to be evaluated in terms of the additional optical loss caused by having an additional intracavity element as well as the added complexity.

One characteristic of the output which was not examined here was the wavelength content of the Q-switched output. The CW measurements made with Nd:YAG and Nd:YLF indicate the presence of more than one wavelength at $1.3\mu\text{m}$. The target discrimination capability of a dual wavelength laser radar system depends not only on the wavelength of each output but also on the separation.

Temperature effects on the performance of the system need to be studied. Other researchers have found that reducing the temperature of certain crystals helps increase the gain of the laser system allowing higher energies and shorter pulses (22:886). The design of the TE cooled laser crystal mount incorporates enough capacity to make measurements down to at least 0° C. In order to make these measurements, an enclosure over the laser crystal mount would have to be fabricated and connected to a dry nitrogen purge in order to keep moisture from condensing on the mount and crystal.

The system would benefit greatly from an enclosure which could be kept in place during operation. The spot size of the laser beam in the laser crystal is on the order of 150 μ m. This is on the same order magnitude of some of the larger dust particles in the laboratory. Significant variations in the performance of the system were experienced when the optics were not clean enough and significant blocks of time were spent optimizing the performance due to this. To minimize this impact, an enclosure which is purged with dry nitrogen is necessary.

Appendix A. Laser system set up

A.1 Setup for the Ti:Sapphire Pump source

A.1.1 Ti:Sapphire laser. The experimental setup is shown in Figure 4.1, on page 4-2. A pellicle beam splitter was used to pull off a small portion of the pump beam and send it to a Burleigh Wavemeter to measure the optical wavelength of the Ti:Sapphire laser. This setup proved extremely convenient for tuning the Ti:Sapphire to the maximum absorbtion of each material.

The only purpose of the two fold mirrors was to bring the pump beam down to the elevation of the laser crystal. The alignment of the pump beam to the laser crystal was performed without the lens in place using the second fold mirror. The 30cm focal length lens used to focus the Ti:Sapphire pump beam down into the crystal had a tendency to steer and distort the pump beam if it was not aligned normal to the beam. After using the second fold mirror to align the beam to the center of the crystal, the lens was placed in the beam path and positioned so that the laser spot struck the center of the laser crystal. It was then aligned normal to the pump beam by making sure the back reflections off of the lens surfaces were headed back into the aperture of the Ti:Sapphire.

The transmission of the high reflector cavity mirror, at the pump wavelength, proved to be lower than expected. Although the back surface (the surface the pump beam strikes first) is anti-reflective coated at the pump wavelength, the second surface, the dielectric high reflector, reflects approximately 25% of the incident pump. When this surface was normal to the pump beam—which it was in most cases for the most efficient use of the pump beam in the laser mode volume—this power would reflect back into the Ti:Sapphire cavity and cause the output of the Ti:Sapphire to go into a TEM₁₀ mode and would also make the output power fluctuate. The neodymium laser output power would then start to fluctuate, sometimes by more than 50%. A more robust optical design would include both a high reflector which is

more transmissive in the region around 808nm and an optical isolator in the pump beam path.

The neutral density filter wheel has a continuous neutral density gradient and it was used to vary the Ti:Sapphire pump power. The meter used to measure the power was a Scientech model 365 with a one inch disc calorimeter.

The pump source for the dual-wavelength laser is an Argon-pumped Ti:Sapphire laser. The wavelength was fully tunable over a much wider range than the 792nm to 808.5nm range used in these experiments. The power did not vary appreciably while the wavelength was being tuned over this range making it ideal for tuning to the absorption peak of each material.

The waist size and location of the Ti:Sapphire were measured using the Coherent Modemaster. The results showed a beam waist located 10 ± 0.5 cm behind the output port of the laser with a beam waist diameter of $720 \pm 10 \mu\text{m}$. This measurement was used to calculate the placement of the 30cm focal length lens used to focus the pump beam down into the crystal. The distance between the Ti:Sapphire source beam waist and the laser crystal was fixed at 1.393 ± 0.002 m. A translation matrix was set up in the mathematical package Mathcad which had variables for translation from the Ti:Sapphire through the lens and the pump input mirror which was a 40 centimeters concave dielectric-coated mirror. The translation matrix had variables for the distance from the waist of the Ti:Sapphire laser to the lens, and for the distance from the lens to the laser crystal. The software then iterated until it found a location of the lens which produced a $147 \mu\text{m}$ spot size in the laser crystal. This location was 41.5cm from the input face of the laser crystal. The value of $147 \mu\text{m}$ was chosen in order to match the calculated spot size of the laser mode in the center of the laser crystal. After the lens was physically placed in the calculated location, the beam size was again checked with the Coherent Modemaster and found to be $146 \pm 5 \mu\text{m}$.

A.1.2 Laser crystal mount. The mounts that held the laser crystal samples were machined from solid brass. These mounts were separated from the solid copper base by three thermo-electric(TE) coolers. The coolers had a sum total of approximately 12 Watts of cooling capacity at room temperature. During the design, the most heat the TE coolers were envisioned having to dissipate, was the full 1 Watt of pump power from the Ti:Sapphire laser. The reason for the designed-in over capacity was two-fold. First, it provides very consistent, worry-free operation; and second, it provides the capability to do low (0°C) temperature measurements.

A.2 Alignment of the dual wavelength laser cavity

The first step in setting up the dual cavity was to clean all the optics. This had to be repeated later in the alignment process depending on the laser performance. Dust particles on the face of the laser crystal showed up distinctly in the laser output, causing the beam to spread and artifacts to appear outside the main beam pattern.

The first step in the alignment procedure for the dual cavity was to align the $1.06\mu\text{m}$ cavity without the dichroic or the Q-switch in the cavity. The laser output was observed on a screen at the same time as the spot due to the residual pump beam. The cavity was "walked" so that the laser output overlapped the residual pump beam. When this occurred, the pump beam's back-reflection off of the highly reflective surface of the high reflector was directed straight back into the cavity of the Ti:Sapphire, and the transverse mode of the Ti:Sapphire switched to TEM_{10} . To correct this, the angle of the high reflector was then adjusted to the point where the Ti:Sapphire switched back to TEM_{00} mode, and the output coupler was adjusted to achieve maximum $1.06\mu\text{m}$ power.

The next step was to place the dichroic in the cavity and adjust the angle to achieve maximum output at $1.06\mu\text{m}$. The angle was different between Nd:YAG and Nd:YLF, this difference most likely being caused by the difference in wavelength between the two lasers. The process of finding the optimum angle was an iterative

one consisting of finding the best angle and then adjusting the angle of the output coupler.

The next step in the process was to align the $1.3\mu\text{m}$ cavity with the dichroic but not the Q-switch in the cavity. This could be done fairly easily by letting the $1.06\mu\text{m}$ cavity lase while adjusting the $1.3\mu\text{m}$ output coupler. Alignment was achieved when the reflection of the $1.06\mu\text{m}$ beam off of the $1.3\mu\text{m}$ output coupler overlapped the $1.06\mu\text{m}$ beam reflected from the back surface of the dichroic beamsplitter.

The final step was to place the Q-switch in each cavity aligned so that the unabsorbed pump beam that passed through the laser crystal was centered on the input aperture. The Q-switches were mounted on 4-axis alignment stages so while the position of the front aperture remained fixed, the back side, away from the laser crystal, could be adjusted to achieve maximum power.

Appendix B. Model

This model was developed to configure the design of the dual wavelength laser. The primary goal in choosing the radius of curvatures for the output couplers was to match beam diameter of the pump beam and both laser modes inside the laser cavity. Using this constraint, the output coupler radii of curvature were calculated from a nominal cavity length of approximately 20cm. Once the nominal size of the mode volume had been determined by this geometry, the reflectivity of the output couplers were chosen to achieve at least twice the threshold population inversion for a constant absorbed pump power of 1 Watt.

The first step in the model is to define the terms. The following table provides a comprehensive listing of the variables and constants.

$l_1 =$	distance from the high reflector to the face of the laser crystal
$l_2 =$	distance from the laser crystal to the dichroic beamsplitter
$l_3 =$	distance from the dichroic beamsplitter to the $1.3\mu\text{m}$ Q-switch
$l_4 =$	distance from the $1.3\mu\text{m}$ Q-switch to the $1.3\mu\text{m}$ output coupler
$l_5 =$	distance from the dichroic beamsplitter to the $1.06\mu\text{m}$ Q-switch
$l_6 =$	distance from the $1.06\mu\text{m}$ Q-switch to the $1.06\mu\text{m}$ output coupler
$l_g =$	length of the gain medium
$l_q =$	length of the Q-switch ($1.06\mu\text{m}$ & $1.3\mu\text{m}$ Q-switch were the same length)
$n_g =$	index of refraction of the gain medium
$n_d =$	index of refraction of the dichroic
$n_q =$	index of refraction of the Q-switch
$l_d =$	distance the $1.06\mu\text{m}$ beam travels inside the dichroic beamsplitter
$t_d =$	thickness of the dichroic beamsplitter
$R_{out} =$	The radius of curvature of the output coupler
$R_{HR} =$	The radius of curvature of the cavity high reflector
$\Gamma_2 =$	Power reflectivity of the output coupler
$\Gamma_1 =$	Power reflectivity of the cavity high reflector

$h =$	6.626×10^{-34} Js Planck's constant
$\lambda_{1.06}$	Laser wavelength in the vicinity of $1.06\mu\text{m}$
$\lambda_{1.32}$	Laser wavelength in the vicinity of $1.32\mu\text{m}$
$c =$	$3 \times 10^{10} \frac{\text{cm}}{\text{s}}$
$\sigma_{SE} =$	Stimulated emission cross section at the laser wavelength
$\tau_f =$	Fluorescence lifetime
$\omega_p =$	radius of the pump beam
$\omega_{1.06} =$	radius of the $1.06\mu\text{m}$ beam
$\omega_{1.32} =$	radius of the $1.32\mu\text{m}$ beam
$T_q =$	Transmission of the Q-switch at the lasing wavelength
$T_g =$	Transmission of the gain medium at the lasing wavelength
$T_d =$	Transmission of the dichroic at $1.06\mu\text{m}$
$\Gamma_d =$	Reflectivity of the dichroic beamsplitter at $1.32\mu\text{m}$
rep_rate =	Pulse repetition frequency
Delay_time =	The delay time from the time the $1.32\mu\text{m}$ pulse is fired to the $1.06\mu\text{m}$ pulse
Pump_pow =	Pump power incident onto the high reflector
$\eta_{HR} =$	Transmission of the high reflector at the pump wavelength
$\eta_{Abs} =$	Absorbtion efficiency of the laser crystal at the pump wavelength
$N_{p0} =$	Initial photon density
$n =$	population inversion

Figure 4.11 provides a visual reference for the definition of the cavity dimensions.

All of the length parameters are set up in a Matlab program called "analyze.m". This program passes the material, and wavelength information to a program called "qspulse.m" which is the workhorse of the model. This program calculates and

stores the photon number and population inversion as functions of time. The first calculation is of the value for l_d , the distance the $1.06\mu\text{m}$ beam travels in the dichroic, and it is calculated from the thickness of the dichroic, t_d , the index of refraction n_d and the angle of incidence. The angle of incidence for this optic was designed to be 45° . The angle of refraction α_d , from Snell's law is

$$\alpha_d = \arcsin \left[\frac{\sin(45^\circ)}{n_d} \right]$$

and from the geometry, the distance the beam travels in the optic is

$$l_d = t_d \cos(\alpha_d)$$

The next calculation is of the effective cavity length, calculated with consideration for the indices of refraction of the various components. For the $1.06\mu\text{m}$ pulse this equation is

$$d_{eff} = l_1 + n_g l_g + l_2 + n_d l_d + l_5 + n_q l_q + l_6$$

from this, the amount of time it takes a photon to make one round trip time is calculated

$$t_{rt} = \frac{2d_{eff}}{c}$$

The total loss in the cavity is calculated from the transmission of the various components in the cavity

$$\text{loss_total} = (1 - \Gamma_1 T_g T_d T_q \Gamma_2)$$

and from the above two, the photon lifetime

$$t_{photon} = \frac{t_{rt}}{\text{loss_total}}$$

The next calculation is the Q-switch rise time. The manufacturer of the Q-switch specified the turn on time of the Q-switch to be "177ns per mm of beam diameter

inside the Q-switch". A function called "qsw_rise" calculates the size of the beam in the Q-switch from the specified cavity dimensions. A system matrix is calculated for a round trip in the cavity starting in the middle of the Q-switch. The spot size in the Q-switch is then calculated using (35:115)

$$\omega = \sqrt{\frac{\lambda}{\pi} \frac{M_{1,2}}{\sqrt{1 - \left(\frac{M_{1,1} + M_{2,2}}{2}\right)^2}}} \quad (\text{B.1})$$

where M is the system matrix. The next calculation is of the laser spot size in the laser crystal. It is calculated using the above equation except the system matrix for the round trip in the cavity begins inside the laser crystal. Using this value of the beam radius, the mode volume of the laser in the cavity is given as

$$V_{00} = \frac{\pi \omega^2 l_g}{2}$$

The pumping rate gives the number of photons absorbed per unit time in the laser gain medium and is given by

$$\text{Pump_rate} = \frac{\eta_{HR} \eta_{Abs} \lambda \text{Pump_pow}}{hc}$$

The equivalent pump time is calculated from Eq (2.24), repeated here for convenience

$$t_{equiv} = -\tau_f \ln \left(1 - \frac{n_f}{R_2 \tau_f} \right)$$

where n_f is the population inversion left over from the previous pulse. The initial population inversion is then calculated from this value and the pulse repetition rate using

$$n_0 = \text{Pump_rate} \left(1 - \exp \left(t_{equiv} + \frac{1}{\text{rep_rate}} \right) \right) \tau_f$$

The initial photon density is set at

$$N_{p0} = 6 \times 10^8$$

During actual Q-switch laser operation the power to the Q-switch is adjusted so that the Q-switch just holds off the lasing action. This is modeled by calculating the gain coefficient at the given pump rate and calculating the necessary loss required to keep the cavity from lasing. The gain coefficient is

$$\gamma_0 = \frac{\sigma_{SE} n_0}{V_{00}}$$

the Q-switch efficiency used to keep the cavity from lasing is then

$$efficiency = 1 - \frac{\sqrt{\frac{e^{-2\gamma_0 l_g}}{\Gamma_1 \Gamma_2}}}{T_g T_d T_q} + 0.03$$

where the 0.03 is added to put the threshold level above the current population inversion.

All of the above calculations are necessary to set up the calculation of the two coupled nonlinear differential equations which describe the behavior of the photon number and the population inversion. The differential equations are given in Eq 2.16 and Eq 2.17 but are repeated here (35:253)

$$\frac{dN_{phot}}{dT} = \left(\frac{n}{n_{th}} - 1 \right) N_{phot}$$

$$\frac{dn}{dT} = -2 \frac{n}{n_{th}} N_{phot}$$

The time in these equations is normalized to the photon lifetime. The maximum number of photon lifetimes is set and this value along with the chosen integration

increment h determines the total number of loops that the algorithm makes. The loop builds a picture of the time changing photon density and population inversion, one time increment at a time. The Runge-Kutta equations are

$$\begin{aligned} K_1 &= f(n, N_{phot}) \\ K_2 &= f\left(n + \frac{1}{2}h, N_{phot} + \frac{1}{2}hK_1\right) \\ K_3 &= f\left(n + \frac{1}{2}h, N_{phot} + \frac{1}{2}hK_2\right) \\ K_4 &= f(n + h, N_{phot}, hK_3) \end{aligned}$$

the model update is given by the sum

$$RK = \frac{(K_1 + 2K_2 + 2K_3 + K_4)}{6}$$

and it can be interpreted as the average slope. These equations are implemented, in Matlab, in a program called "runge.m".

The threshold inversion level was adjusted for each time step by changing the amount of Q-switch loss according to

$$Q_switch_loss(t) = 1 - \frac{efficiency}{\left(\left(\frac{1.6t}{\tau}\right)^3 + 1\right)}$$

This expression was determined empirically and gives a 90% - 10% decay rate equivalent to the value of the Q-switch switching time, τ , used in the equation. The equation for the the threshold population inversion then becomes

$$n_{th}(t) = \frac{1}{2l_g\sigma_{SE}(\nu)} \ln\left(\frac{1}{\Gamma_1(Q_switch_loss(t)T_gT_qT_d)^2\Gamma_2}\right)V_{00}$$

This expression is calculated in Matlab using a program called "threshld.m".

After the program has completed the specified number of loops the pulse energy and pulse length are calculated from the profiles of the photon number and population inversion. The pulse energy is calculated from the difference between the initial and final population inversions using the modified version of Eq (2.19) which is repeated here for convenience.

$$W_{out} = (n_i - n_f) h\nu_L \frac{\alpha_{ext}}{\alpha_{total}}$$

where, again, the factor of 1/2 has been dropped to account for small lower level lifetime, n_i and n_f are the initial and final population inversions respectively, α_{ext} is the loss associated with the output coupler, and α_{total} is the total loss in a round trip of the cavity.

B.0.1 analyze.m.

```

%                                analyze.m                                %
%                                %                                         %
% This program is the master program from which the analyses are done
%
clear;

%%%%%%%%%%%%%%%%%%%%%%%%%%%%%%%%%%%%%%%%%%%%%%%%%%%%%%%%%%%%%%%%%%%%%%%%
%%% These are the INPUT VARIABLES:      %%%
%%%%%%%%%%%%%%%%%%%%%%%%%%%%%%%%%%%%%%%%%%%%%%%%%%%%%%%%%%%%%%%%%%%%%%%%

%%% CAVITY PARAMETERS      %%%

l1=1; %cm Distance from the input flat to the laser gain medium.
l2=4.2; %cm Distance from the laser gain medium to the dichroic beamsplitter.
l3=3.5; %cm Distance from the dichroic beamsplitter to the 1.3 um Q-switch.
l4=7; %cm Distance from the 1.3 um Q-switch to the 1.3 um output coupler.
l5=1.7; %cm Distance from the dichroic beamsplitter to the 1.0 um Q-switch.
l6=8.6; %cm Distance from the 1.0 um Q-switch to the 1.0 um output coupler.

%%% OPTICS      %%%

Ref_out_10=0.95; % Reflectivity of the 1.0 micron output coupler
Ref_out_13=0.96; % Reflectivity of the 1.3 micron output coupler
rad_out_10=20; %cm Radius of curvature of the 1.0 micron output coupler
rad_out_13=20; %cm Radius of curvature of the 1.3 micron output coupler
rad_in=40; %cm Radius of curvature on the input mirror (999999=>flat).

Pump_pow=1.3 ; %W Pump power in Watts
Trans_HR=.909; % Transmission of the High Reflector at the pump wavelength
Pump_wav=808.5e-7;%cm Pump wavelength in centimeters
Pump_spot=0.016; % cm Measured spot size (radius) of the pump beam

%%% Q-SWITCH PARAMETERS      %%%

pulse_rep_rate=500; %Hz Pulse repetition frequency of
% 1.06 micron pulses.
Delay_time=200e-6; %<= Time delay between 1.06 micron
% Q-switch trigger.
% and the 1.3 micron Q-switch trigger.

%%% LASER MATERIAL WAVELENGTH AND POLARIZATION      %%%

material=1; % Laser Crystal material (1=Nd:YAG, 2=Nd:YLF, 3=SVAP)
transition=1.0; % Lasing Transition (1.0 = 1.06 microns, 1.3=1.32 microns)
polarization='pi'; % Polarization (only applies for birefringent host crystals,
% the options are 'pi' for polarization along
% the optic axis and 'sigma' for polarization
% perpendicular to the optic axis)

```

%%% PHYSICAL CONSTANTS %%%

h=6.626e-34; %J*s Planck's constant
c=3e10; %cm/s Speed of light

%%% MODEL FIT PARAMETERS %%%

%%% The following parameters help the model accurately predict the data

tau_scale_10=1; % Scales the 1.06 micron q-switch turn on time
% wo_scale_10=1; % Scales the calculated 1.06 micron beam size
% Add_loss_10=1; % adjusts the total 1.06 micron cavity loss
tau_scale_13=1; % Scales the 1.32 micron q-switch turn on time
% wo_scale_13=1; % Scales the calculated 1.32 micron beam size
% Add_loss_13=1; % Adjusts the total 1.32 micron cavity loss

%%
%XXX%
%%

%%% CALCULATIONS %%%

%%

%%% INITIAL POPULATION INVERSION %%%

n_initial=0; % For the first pulse, it is better to use the
% pulse repetition
% rate variable to achieve the initial population.

%%% INITIAL PHOTON DENSITY %%%

Np0=7e8; % photons WAG
%%
%%% %%%
%%% This is the overall system algorithm %%%
%%% %%%
%%

total_loss=1;
%%% This loop calculates the parameters for a series of pulses
for k=1:10;
wo_scale_10(k)=1+k*.1;
for i=1:16,
eta_abs(i)=.7;
pulse_rep_rate(i)=250+250*i;

Add_loss_10(i)=1;%1.066;
% Add_loss_13(i)=0.985-i*0.01 ;
% wo_scale_13(k)=1.3;

%%
%%

%%% For the first pulse the pulse build up time is set to
%%% 1/2 second in order to achieve maximum


```

%%% population inversion (this is the last entry in the call
%%% for the function qspulse.

%%% First pulse !!!!!
transition=1.0; % microns
pump_time=1/pulse_rep_rate(i);
[pk_pow,puls_energy,puls_width,profile,t_phot,n_pop,N_th]=qspulse(tau_scale_10,
wo_scale_10(k),total_loss,l1,l2,l5,l6,Ref_out_10,rad_out_10,rad_in,Pump_pow,
eta_abs(i),Pump_wav,Pump_spot,material,transition,polarization,n_initial,1/2);

n_initial=profile(2,size(profile,2)); % Leftover population inversion at the
% end of the pulse.
%%%%%%%%%%%%%%%%%%%%%%%%%%%%%%%%%%%%%%%%%%%%%%%%%%%%%%%%%%%%%%%%%%%%%%%%
%%%%%%%%%%%%%%%%%%%%%%%%%%%%%%%%%%%%%%%%%%%%%%%%%%%%%%%%%%%%%%%%%%%%%%%%
% transition=1.3;
% pump_time=(1/pulse_rep_rate)-Delay_time;

%% 1.3um PULSE 1.3um PULSE 1.3um PULSE 1.3um PULSE 1.3um PULSE %%%
% [pk_pow,puls_energy,puls_width,profile,t_phot,n_pop,N_th]=qspulse(tau_scale_13,
wo_scale_13(k),Add_loss_13(i),l1,l2,l3,l4,Ref_out_13,rad_out_13,rad_in,Pump_pow,
Trans_HR,Pump_wav,Pump_spot,material,transition,polarization,n_initial,pump_time);

% n_initial=profile(2,size(profile,2)); % Leftover population inversion at the
% end of the pulse.

%%% Now set up for 1.06 micron pulse
transition=1.0;
pump_time=1/pulse_rep_rate(i);

%% 1.06 um PULSE 1.06 um PULSE 1.06 um PULSE 1.06 um PULSE 1.06 um PULSE %%%
[pk_pow,puls_energy,puls_width,profile,t_phot,n_pop,N_th]=qspulse(tau_scale_10,
wo_scale_10(k),total_loss,l1,l2,l5,l6,Ref_out_10,rad_out_10,rad_in,
Pump_pow,eta_abs(i),Pump_wav,Pump_spot,material,transition,polarization,
n_initial,pump_time);

n_initial=profile(2,size(profile,2)); % Leftover population inversion
% at the end of the pulse.
% transition=1.3;
% pump_time=(1/pulse_rep_rate)-Delay_time;
%
%% 1.3um PULSE 1.3um PULSE 1.3um PULSE 1.3um PULSE 1.3um PULSE %%%
% [pk_pow,puls_energy,puls_width,profile,t_phot,n_pop,N_th]=qspulse(tau_scale_13,
wo_scale_13(k),Add_loss_13(i),l1,l2,l3,l4,Ref_out_13,rad_out_13,rad_in,Pump_pow,
Trans_HR,Pump_wav,Pump_spot,material,transition,polarization,n_initial,pump_time);

% profile_13=[profile(1,:);profile(2,:);profile_13];
% n_initial=profile(2,size(profile,2)); % Leftover population inversion
% at the end of the pulse
% peak_pow_13(i)=pk_pow;
% energy_13(i)=puls_energy;
% width_13(i)=puls_width;

```

```

% photon_lifetime_13(i)=t_phot;

%%%% Now set up for 1.06 micron pulse
transition=1.0;
pump_time=1/pulse_rep_rate(i);

%% 1.06 um PULSE 1.06 um PULSE 1.06 um PULSE 1.06 um PULSE 1.06 um PULSE 1.06 um PULSE %%%
%[pk_pow,puls_energy,puls_width,profile,t_phot,n_pop,N_th]=qspulse(tau_scale_10,
wo_scale_10(k),total_loss,l1,l2,l5,l6,Ref_out_10,rad_out_10,rad_in,Pump_pow,
eta_abs(i),Pump_wav,Pump_spot,material,transition,polarization,
n_initial ,pump_time);

n_initial=0; % Reset leftover population inversion
% for next loop
%
profile_10=[profile(1,:);profile(2,:);profile_10]; %Store the 1.06um pulse profile
% peak_pow_10(i)=pk_pow; % Store the 1.06 um peak power
energy_10(i)=puls_energy; % Store the 1.06 um pulse energy
width_10(i)=puls_width; % Store the 1.06 um pulse width
photon_lifetime_10(i)=t_phot; % Store the 1.06 um photon lifetime

i
end;

% Save data to a file
data_set=[pulse_rep_rate,width_10,energy_10, photon_lifetime_10' ];
fid=fopen(['mod_ft' ,num2str(k),'.dat'],'w');
fprintf(fid,'%1.5e %1.5e %1.5e %1.5e\n',data_set');
fclose(fid);
clear tau_scale width_10 energy_10 width_13 energy_13;

end;
%Save wo_scale data to a file
fid=fopen(['wo_scale.dat'],'w');
fprintf(fid,'%1.8e \n',wo_scale_10');
fclose(fid);

%%%%%%%%%%%%%%%%%%%%%%%%%%%%%%%%%%%%%%%%%%%%%%%%%%%%%%%%%%%%%%%%%%%%%%%%
%%%%%%%%%%%%%%%%%%%%%%%%%%%%%%%%%%%%%%%%%%%%%%%%%%%%%%%%%%%%%%%%%%%%%%%%

```

B.0.2 qspulse.m.

```

%                                     qspulse.m                                     %
%                                     %                                     %
% This function returns the peak power, pulse energy, pulse width, pulse profile,
% photon lifetime, final population inversion, and threshold
% inversion level profile.

function[pk_pow,puls_energy,puls_width,profile,t_photon,n0,N_th]=qspulse(
tau_scale,wo_scale,Add_loss,l1,l2,l3,l4,Ref_out,rad_out,rad_in,Pump_pow,
Trans_HR,Pump_wav,Pump_spot,mater_al,transit_n,polariz,n_initial,
pop_build_up_time);
%%%%%%%%%%%%%%%%%%%%%%%%%%%%%%%%%%%%%%%%%%%%%%%%%%%%%%%%%%%%%%%%%%%%%%%%
%%% These are the INPUT VARIABLES:      %%%%
%%%%%%%%%%%%%%%%%%%%%%%%%%%%%%%%%%%%%%%%%%%%%%%%%%%%%%%%%%%%%%%%%%%%%%%%

%l1= Distance from the input flat to the laser gain medium.
%l2= Distance from the laser gain medium to the dichroic beamsplitter.
%l3= Distance from the dichroic beamsplitter to the Q-switch.
%l4= Distance from the 1.3 micron Q-switch to the output coupler.

%Ref_out= Reflectivity of the output coupler
%rad_out_10= Radius of curvature of the output coupler
%rad_in= Radius of curvature on the input mirror (9999=inf).
%Pump_pow= Pump power in Watts
%Pump_wav= Pump wavelength in nanometers
%Pump_spot= Measured spot size (radius) of the pump beam

%pop_build_up time= time since last Q-switched pulse
%n0= Initial population inversion
%mater_al laser crystal material
%lambda lasing wavelength
%polarization pi or sigma polarization
%efficiency Q-switch efficiency
%%%%%%%%%%%%%%%%%%%%%%%%%%%%%%%%%%%%%%%%%%%%%%%%%%%%%%%%%%%%%%%%%%%%%%%%
%XXXXXXXXXXXXXXXXXXXXXXXXXXXXXXXXXXXXXXXXXXXXXXXXXXXXXXXXXXXXX%
%%%%%%%%%%%%%%%%%%%%%%%%%%%%%%%%%%%%%%%%%%%%%%%%%%%%%%%%%%%%%%%%%%%%%%%%

%%%          FIXED VARIABLES          %%%%
%%% These are the variables which are either fixed or determined by the
%%% specific material.
%%% OPTICS      %%%%

Ref_in=0.99983; % Reflectivity of the Input mirror
               % at both 1.0 and 1.3 microns

Tg=.999; % One way transmission of the gain medium (This turned out to be
         % approximately the same for all materials, they had good
         % coatings I think). (measured value)

```

%%% PHYSICAL CONSTANTS %%%

h=6.626e-34; %J*s Planck's constant
c=3e10; %cm/s Speed of light

%%% LASER MATERIALS %%%
%% %

% Nd:YAG %%

```
if mater_al==1,
up_st_lt=237.3e-6; %sec Upper state lifetime for Nd:YAG (measured)
Pump_abs=0.909; % Absorbtion of Nd:YAG at 808nm (measured)
lg=0.5; %cm Length of the Nd:YAG gain medium
ng=1.82; % Index of refraction of the gain medium at 1.0 microns
Pump_abs=0.9; % Measured absorbtion of the pump power
if transit_n==1.0,
    lambda=1.064e-4;%cm Wavelength of the 1.0 micron laser in Nd:YAG
    SE=3.4e-19; %cm2 Stimulated emission cross section at 1.0 microns
elseif transit_n==1.3,
    lambda=1.338e-4;%cm Wavelength of the 1.3 micron laser in Nd:YAG
    SE=0.9e-19; %cm2 Stimulated emission cross section at 1.3 microns
else, stop;
end;
```

% Nd:YLF %%

```
elseif mater_al==2,
lg=0.5; % cm Length of the Nd:YLF gain medium
Pump_abs=0.99; % Measured absorbtion of the pump power
if strcmp(polariz,'pi'),
    ng=1.634; % Index of refraction of the gain medium (pi
    % polarization)
elseif strcmp(polariz,'sigma'),
    ng=1.631; % Index of refraction of the gain medium (sigma
    % polarization)
else; stop;
end;

if transit_n==1.0,
    if strcmp(polariz,'pi'),
        lambda=1.047e-4; %cm Wavelength of the 1.0 micron laser in Nd:YLF.
        SE=3.7e-19; %cm2 Stimulated emission cross section at 1.0 microns.
    elseif strcmp(polariz,'sigma'),
        lambda=1.053e-4; %cm Wavelength of the 1.0 micron laser in Nd:YLF.
        SE_10=2.6e-19; %cm2 Stimulated emission cross section at 1.0 microns.
    else; stop;
end;

elseif transit_n==1.3,
```

```

        lambda=1.313e-4;      %cm Wavelength of the 1.3 micron laser in Nd:YLF.
        SE=0.6e-19;           %cm2 Stimulated emission cross section at 1.3 microns.
    else, stop;               % This else statement is here to catch errors.
    end;
    up_st_lt=503.9e-6; %sec    Upper state lifetime for Nd:YLF

end;

%%%  DICHROIC BEAMSPLITTER  %%%

nd=1.45      ;      %      Material  UV grade Fused Silica
                %      (Pg 4-13 Melles Griot 1995-1996 Catalog)
if transit_n==1.0;
    td=0.250*2.54;      %cm Thickness of Dichroic
    ang_refr=asin(sin(pi/4)/nd); % Angle of refraction of beam into dichroic
    ld=td/cos(ang_refr); % Distance the beam travels in the dichroic
    T_di=0.929;          % Transmission of the dichroic at 1.06 microns
elseif transit_n==1.3;
    ld=0.0;
    T_di=.996;           % Reflectivity of the dichroic at 1.32 microns
else; stop;
end;end;

%%%  Q-SWITCHES  %%%

lq=0.9*2.54;           %cm Thickness of Q-switches
nq=1.69;               % Dense flint glass wavelength =1.06microns
prop=.5; %<= Used to designate the distance into the
% Q-switch where the spot size is to be calculted
% for the Q-switch rise time calculation.
if transit_n==1.0;
    Tq=.975;           % Transmission of the 1.0 micron Q-switch
elseif transit_n==1.3;
    Tq=.998 ;          % Transmission of the 1.3 micron Q-switch
else; stop;
end; end;
%%%  EFFECTIVE CAVITY LENGTH  %%%

l_eff=l1+lg*ng+l2+ld*nd+l3+lq*nq+l4; % effective cavity length

%%%  PHOTON LIFETIME  %%%

t_rt=2*(l_eff)/c;      % round trip time
Add_loss=(1-Trans_HR/4.66)/(Ref_in*Ref_out*(Tg*T_di*Tq)^2)
loss_total=(1-Ref_in*Add_loss*Ref_out*(Tg*T_di*Tq)^2) % total losses

t_photon=t_rt/loss_total; % photon lifetime

%%%  Q-SWITCH RISE TIME  %%%

```

```
tau=tau_scale*qsw_rise(wo_scale,l1,l2,l3,l4,rad_out,rad_in,transit_n,
                        polariz,prop,lg,ng,lambda)/t_photon;
```

```
%%%%%%%%%%%%%%%%%%%%%%%%%%%%%%%%%%%%%%%%%%%%%%%%%%%%%%%%%%%%%%%%%%%%%%%%%
```

```
%%%    BEAM WAIST %%%
```

```
%%%    The function cr_spot returns the size of the laser
%%%    beam waist in the laser crystal.
```

```
wo=wo_scale*cr_spot(l1,l2,l3,l4,rad_out,rad_in,transit_n,
                    polariz,prop,lg,ng,lambda);
```

```
%%%%%%%%%%%%%%%%%%%%%%%%%%%%%%%%%%%%%%%%%%%%%%%%%%%%%%%%%%%%%%%%%%%%%%%%%
```

```
%XXXXXXXXXXXXXXXXXXXXXXXXXXXXXXXXXXXXXXXXXXXXXXXXXXXXXXXXXXXX%
```

```
%%%%%%%%%%%%%%%%%%%%%%%%%%%%%%%%%%%%%%%%%%%%%%%%%%%%%%%%%%%%%%%%%%%%%%%%%
```

```
%%%    CALCULATIONS    %%%
```

```
%%%%%%%%%%%%%%%%%%%%%%%%%%%%%%%%%%%%%%%%%%%%%%%%%%%%%%%%%%%%%%%%%%%%%%%%%
```

```
%%%    PUMPING RATE    %%%
```

```
Pump_rate=Trans_HR*Pump_pow*Pump_wav/(h*c);
```

```
%    Assumes 100% transference to the upper
%    laser level.
```

```
%%%    MODE VOLUME which intersects THE GAIN MEDIUM    %%%
```

```
V00=pi*(wo^2)*lg/2;
```

```
%%%    INITIAL POPULATION INVERSION    %%%
```

```
t_equivalent=-up_st_lt*log(1-(n_initial/(Pump_rate*up_st_lt)));
```

```
%    This accounts for the
%    leftover population
%    after the last pulse.
```

```
n0=Pump_rate*up_st_lt*(1-exp(-(t_equivalent+pop_build_up_time)/up_st_lt));
```

```
%%%    INITIAL PHOTON DENSITY    %%%
```

```
Np0=6.383e8;    % photons/cm^3    If this number is too
%                                high then the pulse starts to form
%    while the Q-switch is turning off.
```

```
%%%    Q-SWITCH EFFICIENCY CALCULATION    %%%
```

```
gamma_0=SE*n0/V00;
```

```
gamma_th=(1/(2*lg))*log(1/((Ref_in*Add_loss*Ref_out)*(Tg*T_di*Tq)^2));
```

```
efficiency=1-sqrt(exp(-gamma_0*2*lg)/(Ref_in*Add_loss*Ref_out))
/(Tg*T_di*Tq)+.03;
```

```
gamma_th=(1/(2*lg))*log(1/((Ref_in*Add_loss*Ref_out)*((1-efficiency)
*Tg*T_di*Tq)^2));
```

```
%%%      Q-SWITCH PULSE CALCULATION      %%%
```

```
t_initial=0;%    Time is in normalized units of Photon lifetime.
t_final=75;%    Choose t_final to be after the pulse leaves.
incr=0.1;%    Size of the differential step increment (too large and the
              %    whole thing becomes unstable).
```

```
num_increments=(t_final-t_initial)/incr;%    Total number of differential
                                           %    steps to be calculated.
```

```
profile(:,1)=[Np0;n0];    % Row 1 of profile contains the photon #.
                        % Row 2 of profile contains the
                        % population inversion
```

```
for count=2:num_increments;
t=(count-1)*incr;%    Time increment in units
                  % normalized to photon lifetime.
N_th(1,count-1)=(count-1)*incr*t_photon;%    build time axis
N_th(2,count-1)= threshld(t,Ref_out,Ref_in,Tg,T_di,Tq,tau,SE,lg,V00,
                        efficiency,Add_loss);
%% The above line calculates the threshold as a function
%% of time. It changes because of the Q-Switch loss.
```

```
profile(:,count)=profile(:,count-1)+ runge(profile(:,count-1),incr, t, Ref_out,
      Ref_in,Tg, T_di, Tq,tau,SE,lg,V00,efficiency,Add_loss);
end;
```

```
profile(3,:)= [0:num_increments-1].*(incr*t_photon);%    build time axis
```

```
loss_out=(1-Ref_out);    %    Calculate losses due to output
%    coupling
```

```
%%%% Calculate the pulse width (FWHM) %%%%%%%%%
pk=max(profile(1,:))/2;%<= Find the maximum
puls_width=sum(profile(1,:)>pk)*incr*t_photon;%<= Full Width
```

```
%%%% Calculate the peak power %%%%%%%%%
pk_pow=max(profile(1,:))*(loss_out/loss_total)*h*c/(lambda*t_rt);
```

```
%%%% Calculate the pulse energy %%%%%%%%%
```

```
%%%% The pulse energy is equal to the change in the upper state population
```

```
puls_energy=(profile(2,1)-profile(2,size(profile,2)))  
             *h*c*loss_out/(loss_total*lambda);
```

```
return;
```


B.0.3 *runge.m.*

```
%                                     runge.m                                     %
%                                     %                                     %
% This function calculates an update for one time step

function[RK]=runge(A,h,t,Ref_out,Ref_in,Tg,T_dich,T_Q,tau,SE,lg,V00,
                  efficiency,Add_loss)

nth_full= threshld(t,Ref_out,Ref_in,Tg,T_dich,T_Q,tau,SE,lg,V00,
                  efficiency,Add_loss);
nth_half= threshld(t+h/2,Ref_out,Ref_in,Tg,T_dich,T_Q,tau,SE,lg,
                  V00,efficiency,Add_loss);
K1=coup_dif(A,nth_full);
K2=coup_dif(A+(h/2).*K1,nth_half);
K3=coup_dif(A+(h/2).*K2,nth_half);
K4=coup_dif(A+h.*K3,nth_full);
RK=(h/6)*(K1+2*K2+2*K3+K4);

return;
```

B.0.4 coup_dif.m.

```
%                                coup_dif.m                                %
%                                %                                         %
% This function calculates the instantaneous value of the coupled
% differential equations for a Q-Switched laser

function [differentials]=coup_dif(A,nth)

%%%%%%%%%%%%%%%%%%%%%%%%%%%%%%%%%%%%%%%%%%%%%%%%%%%%%%%%%%%%%%%%%%%%%%%%%%%%%%
Np=A(1);
n=A(2);
d_Photons=((n/nth)-1)*Np;
d_Pop_inv=-n*Np/nth;
differentials=[d_Photons;d_Pop_inv];
return;
```

B.0.5 cr_spot.m.

```

%%%%%%%%%%%%%%%%%%%%%%%%%%%%%%%%%%%%%%%%%%%%%%%%%%%%%%%%%%%%%%%%%%%%%%%%%%%%%%
%                               cr_spot.m                               %
%%%%%%%%%%%%%%%%%%%%%%%%%%%%%%%%%%%%%%%%%%%%%%%%%%%%%%%%%%%%%%%%%%%%%%%%%%%%%%
% This function calculates the spot size of the laser beam in the crystal
% function[spot]=cr_spot(l1,l2,l3,l4,rad_out,rad_in,transition,
%                        polarization,prop,lg,ng,lambda);

%%%%%%%%%%%%%%%%%%%%%%%%%%%%%%%%%%%%%%%%%%%%%%%%%%%%%%%%%%%%%%%%%%%%%%%%%%%%%%
%%% These are the INPUT VARIABLES:  %%%
%%%%%%%%%%%%%%%%%%%%%%%%%%%%%%%%%%%%%%%%%%%%%%%%%%%%%%%%%%%%%%%%%%%%%%%%%%%%%%

%l1= Distance from the input flat to the laser gain medium.
%l2= Distance from the laser gain medium to the dichroic beamsplitter.
%l3= Distance from the dichroic beamsplitter to the Q-switch.
%l4= Distance from the 1.3 micron Q-switch to the output coupler.
%prop= Proportion of the distance into the
%      laser crystal where the spot size is desired
%Ref_out= Reflectivity of the output coupler
%rad_out_10= Radius of curvature of the output coupler
%rad_in= Radius of curvature on the input mirror (9999=inf).
%Pump_pow= Pump power in Watts
%Pump_wav= Pump wavelength in nanometers
%Pump_spot= Measured spot size (radius) of the pump beam

%Pulse_rep_rate Pulse repetition frequency
%n0 Initial population inversion
%tau Q-switch time constant
%material laser crystal material
%lambda lasing wavelength
%lg length of the gain medium
%ng index of refraction of the gain medium
%polarization pi or sigma polarization
%efficiency Q-switch efficiency
%%%%%%%%%%%%%%%%%%%%%%%%%%%%%%%%%%%%%%%%%%%%%%%%%%%%%%%%%%%%%%%%%%%%%%%%%%%%%%
%%%%%%%%%%%%%%%%%%%%%%%%%%%%%%%%%%%%%%%%%%%%%%%%%%%%%%%%%%%%%%%%%%%%%%%%%%%%%%
%%%%%%%%%%%%%%%%%%%%%%%%%%%%%%%%%%%%%%%%%%%%%%%%%%%%%%%%%%%%%%%%%%%%%%%%%%%%%%
%%% DICHROIC BEAMSPLITTER %%%

nd=1.45;% Material UV grade Fused Silica
% (Pg 4-13 Melles Griot 1995-1996 Catalog)
if transition==1.0,
    td=.250*2.54;%cm Thickness of Dichroic
    ang_refr=asin(sin(pi/4)/nd); % Angle of refraction of beam into dichroic
    ld=td/cos(ang_refr); % Distance the beam travels in the dichroic
elseif transition==1.3,
    ld=0.0;
else; stop;

```

```

end;
end;
%%%      Q-SWITCHES      %%%%

lq=0.9*2.54;%cm      Thickness of Q-switches
nq=1.69; %Dense flint glass wavelength ???

T1=[ 1  11;
     0 1];

T2=[ 1  12;
     0 1];

T3=[ 1  13;
     0 1];

T4=[ 1  14;
     0 1];

T_las_cry_1=[ 1 prop*lg/(ng);
              0 1];

T_las_cry_2=[ 1 (1-prop)*lg/(ng);
              0 1];

T_dich=[ 1  ld/nd;
          0  1 ];

T_Q=[ 1  lq/nq;
      0  1 ];

Ref_HR=[1 0;
        -2/rad_in 1];
Ref_out=[1 0;
         -2/rad_out 1];

M=T_las_cry_1*T1*Ref_HR*T1*T_las_cry_1*T_las_cry_2*T2*T_dich*T3*T_Q*
T4*Ref_out*T4*T_Q*T3*T_dich*T2*T_las_cry_2;

% The size of the beam at this point is given by
spot=sqrt((lambda/pi)*M(1,2)/sqrt(1-((M(1,1)+M(2,2))/2)^2));

```

B.0.6 qsw_rise.m.

```

%%%%%%%%%%%%%%%%%%%%%%%%%%%%%%%%%%%%%%%%%%%%%%%%%%%%%%%%%%%%%%%%%%%%%%%%
%
%                               qsw_rise.m
%
%%%%%%%%%%%%%%%%%%%%%%%%%%%%%%%%%%%%%%%%%%%%%%%%%%%%%%%%%%%%%%%%%%%%%%%%
%
%   This function calculates the Q-switch rise time given the cavity parameters.
function[rise_time]=qsw_rise(wo_scale,l1,l2,l3,l4,rad_out,rad_in,
    transition,polarization,prop,lg,ng,lambda);

```

```

%%%%%%%%%%%%%%%%%%%%%%%%%%%%%%%%%%%%%%%%%%%%%%%%%%%%%%%%%%%%%%%%%%%%%%%%
%%%   These are the INPUT VARIABLES:   %%%
%%%%%%%%%%%%%%%%%%%%%%%%%%%%%%%%%%%%%%%%%%%%%%%%%%%%%%%%%%%%%%%%%%%%%%%%

```

```

%l1= Distance from the input flat to the laser gain medium.
%l2= Distance from the laser gain medium to the dichroic beamsplitter.
%l3= Distance from the dichroic beamsplitter to the Q-switch.
%l4= Distance from the 1.3 micron Q-switch to the output coupler.
%prop= Proportion of the distance into the laser crystal where
%      the spot size is desired.

```

```

%Ref_out= Reflectivity of the output coupler
%rad_out_10= Radius of curvature of the output coupler
%rad_in= Radius of curvature on the input mirror (9999=inf).
%Pump_pow= Pump power in Watts
%Pump_wav= Pump wavelength in nanometers
%Pump_spot= Measured spot size (radius) of the pump beam

```

```

%Pulse_rep_rate= Pulse repetition frequency
%n0= Initial population inversion
%tau= Q-switch time constant
%material laser crystal material
%lambda lasing wavelength
%lg=                               length of the gain medium
%ng                               index of refraction of the gain medium
%polarization pi or sigma polarization
%efficiency Q-switch efficiency
%%%%%%%%%%%%%%%%%%%%%%%%%%%%%%%%%%%%%%%%%%%%%%%%%%%%%%%%%%%%%%%%%%%%%%%%
%XXXXXXXXXXXXXXXXXXXXXXXXXXXXXXXXXXXXXXXXXXXXXXXXXXXXXXXXXXXX%
%%%%%%%%%%%%%%%%%%%%%%%%%%%%%%%%%%%%%%%%%%%%%%%%%%%%%%%%%%%%%%%%%%%%%%%%

```

%%% DICHROIC BEAMSPLITTER %%%

```

nd=1.45      ;      %      Material UV grade Fused Silica
              %      Pg 4-13 Melles Griot 1995-1996 Catalog
if transition==1.0,
    td=.250*2.54;%cm      Thickness of Dichroic

```

```

    ang_refr=asin(sin(pi/4)/nd); %    Angle of refraction of beam into dichroic
    ld=td/cos(ang_refr);           %    Distance the beam travels in the dichroic
elseif transition==1.3,
    ld=0.0;
else; stop;
end;
end;
%%%    Q-SWITCHES    %%%

lq=0.9*2.54;%cm    Thickness of Q-switches
nq=1.69; %Dense flint glass wavelength

T1=[ 1  11;
     0 1];

T2=[ 1  12;
     0 1];

T3=[ 1  13;
     0 1];

T4=[ 1  14;
     0 1];

T_las_cry=[ 1 lg/(ng);
            0 1];

T_Q_2=[ 1 (1-prop)*lq/(nq);
        0 1];

T_Q=[ 1 lq/(nq);
      0 1];

T_dich=[ 1  ld/nd;
          0  1 ];

T_Q_1=[ 1 prop*lq/nq;
        0  1 ];

Ref_HR=[1 0;
        -2/rad_in 1];

Ref_out=[1 0;
         -2/rad_out 1];

M=T_Q_1*T3*T_dich*T2*T_las_cry *T1*Ref_HR*T1*T_las_cry*
T2*T_dich*T3*T_Q*T4*Ref_out*T4*T_Q_2;

% The size of the beam at this point (in centimeters) is given by
spot=wo_scale*sqrt((lambda/pi)*M(1,2)/sqrt(1-((M(1,1)+M(2,2))/2)^2));

```

```
% The rise time is given by  
rise_time=2*spot*177*1e-9*10; % See Manufacturer specifications  
return;
```

B.0.7 threshld.m.

```

%%%%%%%%%%%%%%%%%%%%%%%%%%%%%%%%%%%%%%%%%%%%%%%%%%%%%%%%%%%%%%%%%%%%%%%%%%%%%%
% This function calculates the value of the threshold inversion
% from the cavity parameters.
function[nth]=threshld(t,Ref_out,Ref_in,Tg,T_dich,
                        T_Q,tau,SE,lg,V00,efficiency,Add_loss)
%%%%%%%%%%%%%%%%%%%%%%%%%%%%%%%%%%%%%%%%%%%%%%%%%%%%%%%%%%%%%%%%%%%%%%%%%%%%%%
%% t                Time into the pulse (from zero)
%% Ref_out          Reflectivity of the output coupler
%% Ref_in           Reflectivity of the input mirror
%% Tg               One way transmission of the gain medium
%% T_dich           One way transmission (reflection) of the dichroic @45 degrees
%% T_Q              One way transmission of the Q-switch
%% tau              Q-switch turn on time for the particular beam size
%% SE               Stimulated emission cross section at the lasing wavelength
%% lg               Length of the gain medium
%% V00              Mode volume which intersects the lasing medium
%% efficiency       Q-switch diffraction efficiency at the lasing wavelength
%%%%%%%%%%%%%%%%%%%%%%%%%%%%%%%%%%%%%%%%%%%%%%%%%%%%%%%%%%%%%%%%%%%%%%%%%%%%%%

Q_switch=1-efficiency/(((t*1.6/tau)^3)+1);
gamma_thresh=log(1/( Add_loss*Ref_out*Ref_in*( Q_switch*
                        Tg*T_dich*T_Q)^2))/(2*lg);
nth=gamma_thresh* V00/SE;
return;

```


BIBLIOGRAPHY

1. Fox, Clifton, S. Ed. , *The Infrared & Electro-Optical Systems Handbook, Vol. 6 Active Electro-Optical Systems* ERIM, Infrared Information Analysis Center, Ann Arbor, Michigan and SPIE Optical Engineering Press, Bellingham, Washington 1993.
2. Pollock, David H. Ed. , *The Infrared & Electro-Optical Systems Handbook, Vol. 7 Countermeasure Systems* ERIM, Infrared Information Analysis Center, Ann Arbor, Michigan and SPIE Optical Engineering Press, Bellingham, Washington 1993.
3. Grossman, William M., Martin Gifford, and Richard Wallace. "Short- pulse Q-switched 1.3- and 1- μ m diode-pumped lasers," *Optics Letters*, 15: 622-624 (June 1990).
4. Zayhowski, J. J., and C. Dill III. "Coupled-cavity electro-optically Q-switched Nd:YVO₄ microchip lasers," *Optics Letters*, 20: 716-718 (April 1995).
5. DeShazer, L. " Vanadate crystals exploit diode-pump technology," *Laser Focus World* 88-93 PennWell Publishing Co. 1994
6. Koechner, W. *Solid-State Laser Engineering*: Berlin: Springer-Verlag 1992.
7. Bibeau, C., S. A. Payne, and H. T. Powell, "Direct measurements of the terminal laser level lifetime in neodymium-doped crystals and glasses," *Journal of the Optical Society of America B*, : 1981-1992. (October 1995).
8. Hughes, D. W. , and J. R. M. Barr, "Laser Diode pumped solid state lasers," *Journal of Physics B*, : 563-586. Journal of Physics 1992.
9. Dinndorf, K. , private conversations.
10. Zagumennyi, A. I., M. Yu. Nikol'skii, A. M. Prokhorov, and I. A. Shcherbakov. "Laser based on a Nd:GdVO₄ with crystal semiconductor pumping," *Quantum Electronics*, 23: 999-1000 (December 1993).
11. Barnes, Norman P., Donald J. Gettemy, Leon Esterowitz, and Roger E. Allen, "Comparison of Nd 1.06 and 1.33 μ m Operation in Various Hosts," *IEEE Journal of Quantum Electronics*, 23: 1434-1450 (September 1987).
12. Chai, B. H. T. "Crystal growth trends in solid-state lasers," *Conference on Lasers and Electro-Optics*: 387 New York: IEEE Press, 1994.
13. Chai, B. H. T., G. Loutts, J. Lefaucher, X. X. Zhang, P. Hong, M. Bass, I.A. Shcherbakov and A. I. Zagurnennyi, "Comparison of Laser Performance of Nd-Doped YVO₄, GdVO₄, Ca₅(PO₄)₃F, Sr₅(PO₄)₃F and Sr₅(PO₄)₃F, " *Advanced Solid State Lasers*: 20 Bellingham Washington, Optical Society of America, 1994. (preprint)

14. Scheeps, Richard, Joseph F. Myers, and Greg Mizell. "High-efficiency 1.06 μm output in a monolithic Nd:YVO₄ laser," *Applied Optics*, 33: 5546-5549 (August 1994).
15. Jain, R. K., D. L. Sipes, T. J. Pier, G. R. Hulse. "Diode-pumped 1.3 μm Nd:YVO₄ laser," *Conference on Lasers and Electro-Optics*: 298. New York: IEEE Press 1988.
16. Zagumennyi, A. I., V.G. Ostroumov, I. A. Shcherbakov, T. Jensen, J. P. Meyen, and G. Huber. "The Nd:GdVO₄ crystal: a new material for diode-pumped lasers," *Soviet Journal of Quantum Electronics*, 22: 1071-1072 (December 1992).
17. Jensen, T., V. G. Ostroumov, J. P. Meyn, G. Huber, A. I. Zagumennyi, I. A. Shcherbakov. "Spectroscopic Characterization and Laser Performance of Diode-Laser-Pumped Nd:GdVO₄," *Applied Physics B*, 58: 373-379 (1994).
18. Barnes, Norman P., Mark E. Storm, Patricia L. Cross, and Milton W. Skolaut, Jr. "Efficiency of Nd Laser Materials with Laser Diode Pumping," *IEEE Journal of Quantum Electronics*, 26: 558-568 (March 1990).
19. Zhang, X. X., P. Hong, G. G. Loutts, J. Lefaucher, M. Bass, and B. H. T. Chai. "Efficient laser performance of Nd³⁺:SR₅(PO₄)₃F at 1.059 and 1.328 μm ," *Applied Physics Letters*, 64: 3205-3207 (June 1994).
20. Baer, Thomas M., David F. Head, Phillip Gooding, Gregory J. Kintz, and Sheldon Hutchison. "Performance of Diode-Pumped Nd:YAG and Nd:YLF Lasers in a Tightly Folded Resonator Configuration," *IEEE Journal of Quantum Electronics* 28: 1131-1138 (April 1992).
21. Plaessmann, Henry, Kevin S. Yamada, Charles E. Rich, and William Grossman. "Subnanosecond pulse generation from diode-pumped acousto-optically Q-switched solid-state lasers," *Applied Optics*, 32: 6616-6619 (November 1993).
22. Plaessmann, Henry, Fritz Stahr, and William M. Grossman. "Reducing Pulse Durations in Diode Pumped Q-Switched Solid-State Lasers," *IEEE Photonics Technology Letters*, 3: 885-887 (October 1991).
23. Wagner, William G. and Bela A. Lengyel. "Evolution of the Giant Pulse in a Laser," *Journal of Applied Physics*, 34: 2040-2046 (July 1963).
24. Shen, Hong-Yuan, R. R. Zeng, Yu-Ping Zhou, G. F. Yu, Cheng-Hui Huang, Zheng-Dong Zeng, W. J. Zhang, and Q. J. Ye. "Simultaneous Multiple Wavelength Laser Action in Various Neodymium Host Crystals," *IEEE Journal of Quantum Electronics*, 27: 2315-2318 (October 1991).
25. Danailov, M. B. and I.Y. Milev. "Simultaneous multiwavelength operation of Nd:YAG laser," *Applied Physics Letters*, 61: 746-748 (August 1992).

26. Jeys, Thomas H., A. A. Brailove, and Aram Mooradian. "Sum frequency generation of sodium resonance radiation," *Applied Optics*, 28: 2588-2591 (July 1989).
27. Nadtocheev and O.E. Nanii. "Two-wave emission from a cw solid-state YAG:Nd³⁺ laser," *Soviet Journal of Quantum Electronics*, 19: 444-446 (April 1989).
28. Dallas, J. L. "Frequency-modulation mode-locking performance of four Nd³⁺-doped laser crystals," *Applied Optics*, 33: 6373-6376 (September 1994).
29. Tucker, Armin W., Milton Birnbaum, and Curtis L. Fincher "Stimulated emission cross sections of Nd:YVO₄ and Nd:La₂Be₂O₅(BEL)," *Journal of Applied Physics*, 52: 3067-3068 (April 1981).
30. Devor, D. P., L. G. DeShazer, and R. C. Pastor. "Nd:YAG Quantum Efficiency and Related Radiative Properties," *IEEE Journal of Quantum Electronics*, 25: 1863-1873 (August 1989).
31. Machan J., R. Kurtz, M. Bass, and M. Birnbaum, " Simultaneous, multiple wavelength lasing of (Ho, Nd):Y₃Al₅O₁₂," *Applied Physics Letters*, 51: 1313-1315 (October 1987).
32. Zhang, X. X., M. Bass, and B. H. T. Chai. "Flashlamp-pumped Neodymium Doped Strontium Fluorapatite," *Advanced Solid State Lasers*: (April 1995).
33. Tomaschke, Harry E., George A. Henderson, Donald A. Thompson, James S. Brookman, Roland E. Juhala, "Experimental and theoretical study of a pulsed dual frequency Nd:YAG laser with intracavity sum frequency mixing," *Conference on Lasers and Electro-Optics, Vol. 7, 1990 OSA Technical Digest Series*: 252-253. Optical Society of America, Washington, D.C. 1990.
34. Anthon, D. W., A. T. Eggleston, G. R. Ristau, " Angle-cut Nd:YLF as a polarized laser medium at 1313nm," *Conference on Lasers and Electro-Optics, Vol. 12, 1992 OSA Technical Digest Series*: 52. Optical Society of America, Washington, D.C. 1992.
35. Verdeyen, Joseph T., *Laser Electronics 2nd ed.*: Englewood Cliffs, New Jersey: Prentice-Hall.
36. Hovis, F. E., M. Stuff, C. J. Kennedy, and B. Vivian. "Lower Level Relaxation of Nd:YAG," *IEEE Journal of Quantum Electronics*, 28: 39-42 (January 1992).
37. Fan, Tso Yee. "Effect of Finite Lower Level Lifetime on Q-Switched Lasers," *IEEE Journal of Quantum Electronics*, 24: 2345-2349 (December 1988).

Vita

Captain Scott McCracken ~~was born [redacted] 1964 in [redacted], NY.~~
He graduated from Northstar Christian Academy in Greece, NY in 1982 and attended SUNY Brockport during the 1982-1983 school year. In the fall of 1983 he entered the Microelectronic Engineering program at Rochester Institute of Technology, Rochester, NY. As a co-op student he had the opportunity to work in several semiconductor manufacturing plants including IBM's facilities in East Fishkill, NY and Manassas, VA and Hughes Aircraft Co.'s facilities in Carlsbad, CA. He graduated from Rochester Institute of Technology in 1988 with Highest Honors. His first tour of duty was at Wright-Patterson AFB as part of the Electro-Optics branch of Wright Laboratory's Avionics Directorate. There he was involved with several in-house experiments including the construction of a 2.09 μ m coherent lidar system, and the start of a program to develop an airborne wind profiling system for the C-141. He was also involved with the start up of a program to develop an on-board lidar wind measuring system for the AC-130 gunship. He entered the Air Force Institute of Technology in May 1994.

~~Permanent address [redacted]
[redacted]~~

VITA-1

REPORT DOCUMENTATION PAGE

Form Approved
OMB No. 0704-0188

Public reporting burden for this collection of information is estimated to average 1 hour per response, including the time for reviewing instructions, searching existing data sources, gathering and maintaining the data needed, and completing and reviewing the collection of information. Send comments regarding this burden estimate or any other aspect of this collection of information, including suggestions for reducing this burden, to Washington Headquarters Services, Directorate for Information Operations and Reports, 1215 Jefferson Davis Highway, Suite 1204, Arlington, VA 22202-4302, and to the Office of Management and Budget, Paperwork Reduction Project (0704-0188), Washington, DC 20503.

1. AGENCY USE ONLY (Leave blank)		2. REPORT DATE December 1995	3. REPORT TYPE AND DATES COVERED Master's Thesis
4. TITLE AND SUBTITLE TWO-WAVELENGTH NEODYMIUM BASED LASERS			5. FUNDING NUMBERS
6. AUTHOR(S) Scott H. McCracken Captain, USAF			
7. PERFORMING ORGANIZATION NAME(S) AND ADDRESS(ES) Air Force Institute of Technology, WPAFB OH 45433-6583			8. PERFORMING ORGANIZATION REPORT NUMBER AFIT/GEO/ENP/95D-02
9. SPONSORING / MONITORING AGENCY NAME(S) AND ADDRESS(ES) WL/MNGS Eglin AFB FL 32542-5434 Capt Ken Dinndorf			10. SPONSORING / MONITORING AGENCY REPORT NUMBER
11. SUPPLEMENTARY NOTES			
12a. DISTRIBUTION / AVAILABILITY STATEMENT Approved for public release; Distribution Unlimited			12b. DISTRIBUTION CODE A
13. ABSTRACT (Maximum 200 words) A dual wavelength Q-switched laser cavity has been successfully designed and assembled to evaluate the new neodymium (Nd) based materials. Initial characterization has been achieved for Nd:YAG and Nd:YLF. The results indicate that for a fixed pulse repetition frequency, the delay time can be used to adjust the relative energy between the 1.06 μ m and 1.32 μ m pulses. Any deficiency in the performance of one transition can be made up by performance in the other simply by changing the relative amount of time the population inversion is allowed to build up for each pulse. The best performance was obtained using a 13cm cavity length, the shortest possible cavity with the available equipment. The gain in the Nd:YLF 1.047 μ m cavity was so high, the diffraction efficiency of the acousto-optic Q-switch was insufficient to hold off lasing with a 5% output coupler. The transmission of the 1.047 μ m output coupler used for dual wavelength operation of Nd:YLF was 30% whereas the transmission of the 1.06 μ m output coupler necessary to achieve dual wavelength operation in Nd:YAG was 5%. At a pulse repetition frequency for each wavelength of 2kHz, and with 820mW of absorbed pump power, Nd:YLF produced pulse energies of 40 \pm 2 μ J and 15.3 \pm 0.6 μ J, and pulse lengths of 44 \pm 1ns, and 410 \pm 10ns at the wavelengths of 1.047 μ m and 1.32 μ m respectively. Nd:YAG produced pulse energies of 33 \pm 1 μ J and 27 \pm 1 μ J, and pulse widths of 32 \pm 0.4ns and 183 \pm 1ns at the wavelengths of 1.06 μ m and 1.34 μ m respectively.			
14. SUBJECT TERMS Nd:YAG, Nd:YLF, DUAL WAVELENGTH LASER, Q-SWITCHED, LASER RADAR			15. NUMBER OF PAGES 141
			16. PRICE CODE
17. SECURITY CLASSIFICATION OF REPORT UNCLASSIFIED	18. SECURITY CLASSIFICATION OF THIS PAGE UNCLASSIFIED	19. SECURITY CLASSIFICATION OF ABSTRACT UNCLASSIFIED	20. LIMITATION OF ABSTRACT UL